Rajeev Shrestha

2D Numerical Modeling of Sediment Diversion in a River Bend

Master's thesis in Hydropower Development
Supervisor: Nils Rüther
Co-supervisor: Diwash Lal Maskey

June 2022

Master's thesis

NTNU
Norwegian University of Science and Technology
Faculty of Engineering
Department of Civil and Environmental Engineering

NTNU
Kunnskap for en bedre verden

Rajeev Shrestha

2D Numerical Modeling of Sediment Diversion in a River Bend

Master's thesis in Hydropower Development
Supervisor: Nils Rüther
Co-supervisor: Diwash Lal Maskey
June 2022

Norwegian University of Science and Technology
Faculty of Engineering
Department of Civil and Environmental Engineering

■ NTNU

Norwegian University of
Science and Technology

Acknowledgement

Abstract

Sedimentation has been one of the existing challenges in the sustainability of hydraulic structures. Proper modelling of sediment transport is, therefore, an important task for a designer or a project planner. Research has shown the complexity of using a 3D model because of data and knowledge requirements, computing demand, time and cost associated to it etc. At the same time, there are some limitations to a 1D model which demands the optimum use of 2D softwares for modelling. This study investigates sediment transport capability of HEC-RAS 2D 6.2 and the possibility of using 2D modelling tools for bed load transport. With the proper study of newly added feature in HEC-RAS 2D, the study asks: to what extent can the software represent transport and bed changes that occurs in a river channel and its bends?

A physical model was set up at Norsk Hydroteknisk Laboratorium, NTNU to evaluate the pattern of bed changes, efficiency of sediment bypass channel and the change in efficiency with the installation of guide walls. Several tests were made at varied flow conditions through inlet and through the bypass channel. Observations were made for proper evaluation and comparison.

Based on the observations made in physical model, a calibrated hydraulic model was set up. Using the calibrated model, sediment transport modelling was done for three different cases. An extra simulation was performed to check the effect of increased discharge through the sediment bypass channel. Analyses indicate that the simulations show a good agreement with observed model in case of transport through river channel without any structures. It also demonstrates how the efficiency of a bypass channel can be increased using structures like inlet gate and guide walls. On this basis, proper transport modelling can be done with HEC-RAS for design and planning purposes. Improvements in limitations mentioned in the study could result in better simulations. Further research is needed to identify parameters and methods to strengthen the effectiveness and reduce uncertainties in modelling.

Contents

List of Figures

List of Tables

List of Abbreviations

1D :- One Dimensional

2D :- Two Dimensional

3D :- Three Dimensional

DEM :- Digital Elevation Model

DWE :- Diffusion Wave Equation

GIS :- Geographic Information System

HEC-RAS :- Hydrologic Engineering Center's River Analysis System

HPP :- Hydropower Plants

MAE :- Mean Absolute Error

MPM :- Meyer Peter and Müller

NTNU :- Norwegian Institute of Science and Technology

ROR :- Run of River

SA :- Storage Area

SBT :- Sediment Bypass Tunnel

SWE :- Shallow Water Equation

SWE-ELM :- Shallow Water Equations Eulerian - Lagrangian Method

SWE-EM :- Shallow Water Equations Eulerian Method

WSE :- Water Surface Elevation

ppm :- parts per million

1   Introduction

1.1   Background

Water is one of the major natural resources that has a variety of uses. Most of the infrastructure of development depends on the use of water. One such example is the use in the hydropower sector. Hydropower is one of the primary renewable sources of energy. It is considered a green battery that can be utilized without over-exploiting the nonrenewable components of the environment. However, there are many problems that require proper planning and attention for the efficient operation of hydropower plants (HPP). One of such problems is sedimentation. Sediment influx and outflow in most natural river reaches are more or less balanced. Any change in the natural condition of the channel alters this balance dramatically (Morris and Fan, 1998). For the completion of a hydropower plant, various hydraulic structures have to be constructed. These structures alter the balance one way or another. For example, the construction of a dam leads to decrease in velocity of water leading to the deposition of flowing sediment. (Morris and Fan, 1998).

However, there could be various reasons for the presence of sediment in river networks apart from dam construction. Soil erosion is one of the major causes. As an example in China, the highest sediment load in the world is observed in the Yellow River with about $11 * 10^8$ tons of suspended sediments every year (Ren and Shi, 1986). While some Himalayan rivers have recorded a maximum suspended sediment concentration of around 40,000 ppm (Ghimire et al., 2021). Sediments carried by river channels pose problems to both run of river as well as storage type hydropower schemes. Excess sediments result in instability of channel, reduction in flood capacity due to infilling, channel aggradation, bank erosion, reduction in power generation from hydropower plants, etc. If the effectiveness of a bypass is known before it reaches the reservoir, it can be helpful to adopt countermeasures to tackle many technical and economic problems.

Some of the major reasons why channel bed sediment should be studied are engineering design, environmental and eco-hydrological reasons (Song et al., 2015). A laboratory experiment has been conducted at Norsk Hydroteknisk Laboratorium, NTNU to see the bed changes and the efficiency of a sediment bypass tunnel in a river bend. Flushing operations can be very expensive, and it is therefore important to know the efficiency beforehand. Hence, the physical model has been operated at different discharges with varying flow passing through the sediment bypass tunnel. A problem with a physical model is that it is expensive to construct and operate or to introduce any major modifications. Some changes have been made in the physical model like modification in the channel and installation of guide walls which was expensive as well as time consuming. A numerical model is faster and cheaper to set up and to simulate for the same changes. Hence, the purpose of the current work is to set up a numerical model with an aim to replicate the physical model, any changes made to it and the results obtained from it.

1.2   Objectives

The three main objectives of this study are:

- To demonstrate the capabilities of HEC-RAS as 2D sediment modelling tool. Determine whether HEC-RAS 2D can properly simulate the sediment transport and bed changes in the river channel and its bend.

- Numerical verification of results obtained from physical model.

- To properly evaluate the pros of using free 2D Modelling softwares like HEC- RAS for sediment study and why it could be better than a 3D model.

Additionally, there will be two secondary objectives.

- Study the best practice for the development of a proper 2D grid for model setup.

- Study how different features of HEC-RAS can be used as per the requirement of the user.

1.3   Dissertation Outline

The thesis contains some theoretical and practical information about the project and the analysis. It is divided into nine main chapters. Chapter 1 provides some background information about why the thesis is carried out, the main objective of the work and how the thesis is structured. Chapter 2 focuses mainly on the theoretical aspect, processes of sediment transport and prior studies done in numerical modelling. It also shows the relevance of this thesis with previous studies. Chapter 3 presents the underlying equations used in HEC-RAS, the different features that can be used and some practices for a good model. Chapter 4 gives a brief description of the working structure of thesis, data available from physical model and how the study is planned. Chapter 5 describes how the model was set up to start the simulations. Chapter 6 shows how hydraulic calibration was done, a very important process in sediment modelling. Chapter 7 presents results obtained from the 2D sediment modelling done in different cases and some additional simulations. Chapter 8 evaluates and discusses the results obtained in chapter 7, describes the limitation of the software and the study and suggests paths for further research. Chapter 9 presents the conclusion of the study.

2 Basic Theory and Literature Review

2.1 Erosion and Sedimentation

The term sediment may represent tiny particles such as gravel, sand, silt and clay. When the stream is able to move more material out from an area than is brought into it, erosion occurs (Lysne et al., 2003). The process of deposition of these carried away sediments in a different location is known as sedimentation. Composedly the term "Erosion and Sedimentation" refers to the motion of solid particles in a channel. Human activities such as plowing, vegetation, construction activities, mining etc trigger erosion and movement of sediments (Julien, 2010). Basically, sediments can be divided into four main categories: bed load, suspended load, wash load and floating load. The particles that are carried along the channel bed through the process of rolling, sliding and saltation are known as bed loads. Fine particles conveyed in the stream without touching the bed and remains suspended for an adequate period of time are known as suspended sediments. Wash loads are composed of suspended sediments that do not come into contact with the riverbed (Tigrek and Aras, 2011). The materials such as woods, logs, wastes etc that float on the surface of water are known as the floating load.

2.1.1 Sediment Transport

The geometric and plan form shape of a river is determined by the hydraulics of flow and the sediment transport characteristics of the river. The hydraulics of flow and the nature of sediment movement in a natural stream are influenced by a number of factors (Hassanzadeh, 2012). Many researchers have contributed for the study of sediment transport in natural channels. There are many factors that influence the movement of sediment by water like water discharge, average flow velocity, energy slope, shear stress, bed structure, turbulence intensity, particle size and water temperature. Before analysing the transport of sediment, one should always be sure about the relative importance of these variables and the selection of one or more as the primary factors regulating sediment transport (Yang and Stall, 1974).

Verified in both laboratory flume and natural river, Yang and Stall (1974) related the stream power to the transport rate of sediment. Similarly, Van Rijn (1984) proposed a method to determine the bed load transport relating it to the product of the saltation height, the particle velocity and the bed load concentration. So, it is necessary to understand the basic parameters and factors that influence the sediment transport.

The average bed shear stress τ in a cross section is given by Equation 1.

$$\tau = \rho g R I_f \tag{1}$$

where τ is the bed shear stress, ρ is the density of water, g is the acceleration due to gravity, R is hydraulic radius and I_f is the energy slope. However, if the width of channel is more than 30 times the depth of water, hydraulic radius (R) shall be replaced with depth of water (h). The equation then becomes:

$$\tau = \rho g h I_f \tag{2}$$

In 2D numerical models, this equation is still used because the hydraulic information is still stored in the computational nodes. Friction slope I_f is expressed by Strickler - equation as shown in Equation 3

$$I_f = \frac{v^2}{k_{st}^2 R^{4/3}} \tag{3}$$

Most rivers with steady flows and uniform equilibrium flow condition has the average flow velocity V of:

$$V = \sqrt{\frac{8g}{f}} \sqrt{\frac{D_H}{4}} sin\theta \tag{4}$$

where f is the Darcy friction factor, θ is the bed slope and D_H is the hydraulic diameter. However, proper knowledge of velocity profile is required for the flow in alluvial streams. (Chanson, 2004)
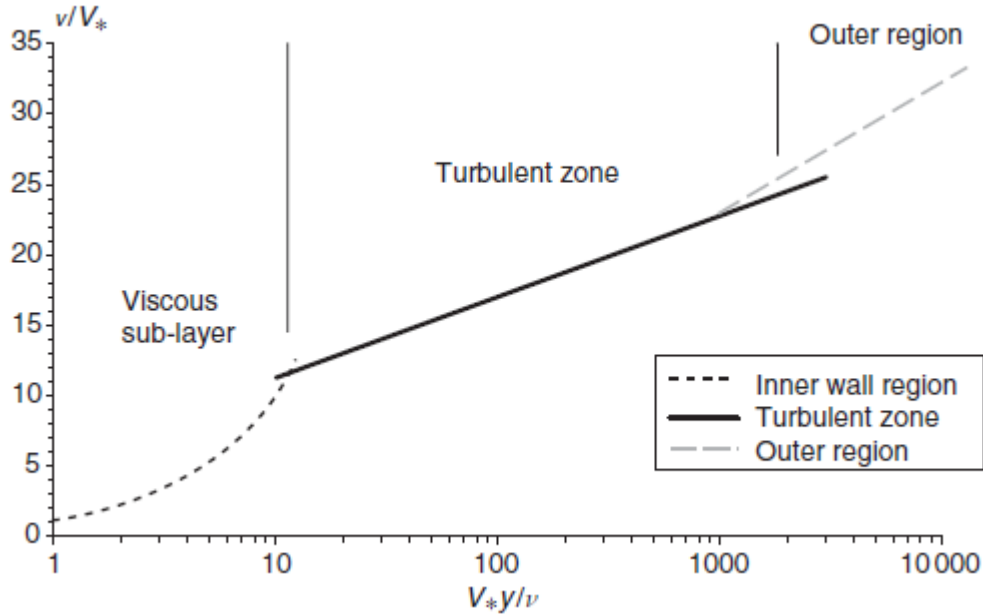
Figure 2.1: Velocity distribution in turbulent flows (Chanson, 2004)

A flow through a smooth boundary can be divided into three different layers.

A Viscous sub- layer where turbulent stress is minimum and viscous stress is maximum, the velocity distribution follows Equation 5.

$$\frac{v}{V_*} = \frac{V_* y}{v}; \frac{V_* y}{v} < 5 \tag{5}$$

The outer region where turbulent stress is maximum and viscous stress is minimum, the

velocity distribution follows Equation 6.

$$\frac{V_{max} - v}{V_*} = -\frac{1}{K}ln(\frac{y}{\delta}); \frac{y}{\delta} > 0.1 - 0.15 \tag{6}$$

The region in between inner viscous sub layer and outer region is known as turbulent region and the velocity distribution follows Equation 7.

$$\frac{v}{V_*} = \frac{1}{k}ln\frac{V_*y}{v} + D; 30 - 70 < \frac{V_*y}{v} and \frac{y}{\delta} < 0.1 - 0.15 \tag{7}$$

where v is the velocity at y distance normal to boundary, δ is the thickness of boundary layer, *Vmax* is the free stream velocity, K is the Karman constant (0.4) and D_1 is the constant (5.5). V_* is shear velocity given by Equation 8.

$$V_* = \sqrt{\frac{\tau_o}{\rho}} \tag{8}$$

where τ_o is the mean bed shear stress and ρ is the density of fluid.

One of the important parameters in sediment hydraulics is the fall velocity of particles. Fall velocity of particles with diameter greater than 2mm can be approximated using Equation 9.

$$\omega = 3.32\sqrt{d(mm)} \tag{9}$$

When particle falls under the influence of gravity, it reaches a constant velocity called as terminal velocity. When the drag is equal to the terminal velocity, Equation 10 is obtained.

$$\omega^2 = \frac{4}{3}\frac{1}{C_D}gd\left(\frac{\rho_s - \rho}{\rho}\right) \tag{10}$$

where C_D = drag coefficient, d= grain diameter, ρ_s and ρ are the density of sediment and water respectively. In the equation (10), the only unknown is drag coefficient. Many researchers have suggested various methods to determine the value of coefficient. A general approximation is provided by Stoke. If the Reynold's number (Re) < 0.5 to 1 and if the particle size is very small, drag coefficient is given by Equation 11.

$$C_d = \frac{24}{Re} \tag{11}$$

2.1.2 Erosion Mechanism

Usually, movement of bed load occurs near to the channel bed by rolling, sliding or saltation. Saltation refers to the random irregular jumping movement of particles. When the balance in equilibrium is disturbed due to several reasons such as increase in flow velocity, the bed load particles start to move. The movement occurs when the bed shear stress exceeds a critical value. In short,

$$\tau_* = (\tau_*)_c \tag{12}$$

where τ_* is the Shield's parameter and $(\tau_*)_c$ is the critical shields parameter for the initiation of bed load motion (Chanson, 2004). According to Shields (1936), while considering the bed load movement, the force acting on the particles on the uppermost layer should be considered. Because only the upper layer of the bed is being transported. This force does not necessarily equal to the total shear because the layers below the uppermost layer also contribute to the the shear strength of the bed.

The Shields diagram provides a visual representation of the condition of incipient motion based on bed shear stress. If the point lies below the curve, there is no motion of particles. If the point lies above the curve, it represents the particles are in motion. It requires the calculation of boundary Reynolds number and critical shields stress. The visual representation is presented in Figure 2.2.
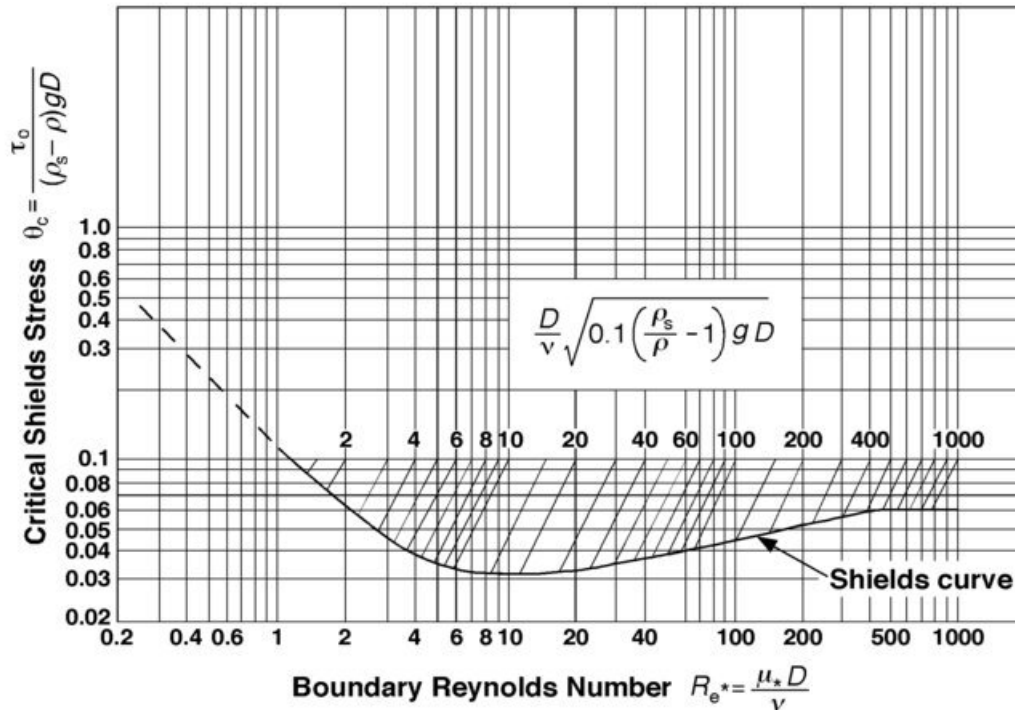
Figure 2.2: Shield's Diagram (Shields, 1936)

Shield's diagram provides the condition for start of movement of sediments. The type of sediment that is being transported can be determined using Rouse number. Rouse number is given by Equation 13.

$$Z = \frac{v_s}{\kappa u_*} \qquad (13)$$

where Z is Rouse number, v_s is settling velocity, κ is Von Karman constant and u_* is the shear velocity. The particles can be divided into wash load and bed material load. The bed material load can be further divided into bed load and suspended load. The sediment particles are said to be wash load if Z < 0.06. The sediment particles are bed material load if Z > 0.1. If 0.1 < Z < 3, the particles are suspended load and if 3 < Z < 5, the particles are in transition phase between bed and suspended load. If Z > 5, it is bed load.

2.1.3 Sediment Problems in Channel

Soil is considered to be a non renewable source. The natural rate of formation of soil is very low with about few millimeters per century. However, the rate of erosion is very high which can be in the range of several centimeters of soil per storm event (Woodward and Foster, 1997). Erosion is one of the major threats to the fertile land for agriculture (Brown and Wolf, 1984). This soil is eroded from agricultural land and is deposited into areas such as rivers and reservoir rendering it useless.

Hydropower plants are also affected by sedimentation. Sedimentation problems are observed in rivers which directly affects the run-of-river hydro power plants starting early during the construction phase. The deposition of sediment right in front of intake can clog the opening, reducing the flow through it or rendering it useless. Also, deposition of sediment in canals pose various problems. It does not only increase the operation and maintenance cost but also reduces the reliability of the service offered by the canal (Paudel, 2010). Flow of sediment through these canal or water conveyance structures directly hampers hydraulic machines like hydro turbines. When fine sediments hit the blades of runner, it starts eroding. Induction of material erosion in turbines lead to changes in flow pattern, vibrations, losses in efficiency, increase in maintenance cost and final breakdown of the structure (Thapa et al., 2015).

When the natural flow of sediment in river channel is disturbed by a structure for the purpose of storage, equilibrium in the channel is altered. The storage loses its capacity to store water. With time, the reservoir volume gets filled up by sediment. Loss of storage capacity is one of the major effects of sedimentation. Reduction in storage means it cannot provide enough water during the time of less inflow and high demand. It can result in a high impact in hydro power production, water supply distribution, irrigation supply and the effectiveness of flood control (Wong and Parker, 2006). Suspended sediments as well as the sediment at the bottom results in degradation of water quality. The storage acts as both source and the sink for organic constituents of reservoir (Ammar et al., 2015). Construction of dam has a great impact in the sediment delivery to both upstream and downstream reach. Deposition of sediment in the upstream leads to increased flood levels exposing downstream to high flood effects (Chanson, 2004).

2.1.4   Sediment Handling Mechanisms

Proper sediment handling mechanism is required for a sustainable development of river infrastructure system. For example, the hydropower plant can last much longer if the sediment passing through is handled properly. In the case of a simple Run of River (ROR) Hydropower Plant, some of the methods of sediment management are selecting a suitable intake location, modification of flow in front of the intake, upstream sediment trapping, removal of dam, sediment pass through by draw down, sediment bypass tunnel or channel etc.

Extraction of clear water from channel can be done with a side intake placed at the outer bend. The inner bend has higher sediment concentration than the outer bend. When water hits the outer bend, rotational current erodes the toe in the bend that keeps sediment away from the intake. If this is not possible in the channel, flow modifications can be done by adjusting intake alignment, operating gates or by river training structures. Settling basin can also be installed right after the intake to remove sediment from the system before it reaches conveyance channel (Annandale, 2016).

Sediment routing is another technique to divert sediment from the channel section to downstream. It requires a portion of channel discharge to be diverted along with the sediment load. It is applicable in both channel section as well as reservoirs. One of the long term and best methods of sediment routing is the use of Sediment Bypass Tunnel (SBT) (Wang et al., 2018). SBT is ideal where the channel makes a sharp turn between the point of sediment collection and reintroduction, minimizing conveyance length and allowing gravity flow to take advantage of a steeper gradient (Kondolf et al., 2014).

According to Auel and Boes (2011), a sediment bypass tunnel usually consists of a guiding structure, an intake structure, gate, steep sloping acceleration section, a long sloping bypass tunnel section and an outlet structure. It has several advantages over other measures of sediment removal. It has positive impacts on ecology because it increases the morphological variability downstream. Hence the tailwater sediment concentration is less affected by the reservoir. However, the design of outlet structure should be such that there is no sedimentation in immediate downstream of the opening. It is also effective in diverting the bed load. One disadvantage of SBT is that it is economically expensive to construct and maintain regularly.

2.2   Numerical Modelling

2.2.1   1D vs 2D vs 3D Numerical Models

One dimensional modelling assumes the forces in water predominant in only one direction usually in the direction of flow. Similarly, two and three dimensional modelling assumes the forces predominant in two and three directions respectively. The equations used in these modelling are respective of the assumptions of direction of flow. There are situations where a 2D model gives better results compared to a 1D model. Also, there are situations when a 1D model gives a good result compared to a 2D model.

1D model computes same water surface elevation over the entire cross section whereas 2D and 3D models compute unique values of water surface elevation for each cell face. It allows for the better hydraulics representation. Modelling of ineffective flow area is easier in 2D models whereas it is difficult and needs user judgement in 1D models. The horizontal flow direction in 2D and three dimensional flow directions in 3D model are computed automatically while it must be defined by the modeler in 1D model. There lies many differences between 1D, 2D and 3D models in how the equations are used and how outputs are generated.

Apart from this, time and cost for the development of these models is one of the important differences between them. A rough hydraulic model can be easily prepared in a 2D model compared to 1D and a 3D model. But if a detailed analysis needs to be done, all of these models take significant amount of time depending on the type and purpose of model. However, the computation time for a detailed 3D model is much higher than 1D and 2D model. Hardware requirement for a 3D model is more compared to a 2D and 1D model. So the possibilities of using 2D for reasonable solution should be explored instead of 3D to save time and cost for modelling. (Brunner et al., 2020)

Advantages of a 2D model
Though there are some limitations of 2D models, it has many advantages over 1D and 3D models. Some of the advantages are highlighted below:

- In any case,unlike a 3D model, the water flow path does not have to be known in order to create the model. The domain's scope, on the other hand, must be properly defined.

- Mesh development is much faster in 2D compared to a 3D model which requires an initial description of 2d domain.

- The computation time as well as cost is higher than that of 1D models but much lower than a 3D model.

- Outputs can be visualized without dedicated training and knowledge of post-processing software.

- A rough 2D model can be prepared faster than a 3D model and sometimes even faster than a 1D model.

- The complexity of modelling a 3D model is much higher so an in depth knowledge of code is required to avoid instabilities in the model.

2.2.2   Sediment Transport 1D, 2D and 3D

Modelling of sediments can be done numerically in one, two or three dimensions depending on various factors. Papanicolaou et al. (2008) has some detailed explanation of the use of these modelling softwares used in past. One dimensional models have been in use since early 1980s. Usually, one dimensional models are formulated in rectilinear coordinate system that solves sediment mass continuity equation along with differential conservation equations of mass and momentum of flow. Some examples of 1D sediment transport modelling tools are HEC-6 by Thomas and Prasuhn (1977), IALLUVIAL by Karim and Kennedy (1982), MOBED by Krishnappan (1981), CHARIMA by Holly et al. (1990), SEDI-COUP by Holly Jr and Rahuel (1990), 3STID by Papanicolaou et al. (2004), FLUVIAL 11 by Chang (1984), GSTARS by Molinas and Yang (1986), HEC-RAS developed by US Department of Defense Army Corps of Engineers. Icold (2021) shows the examples of models such as MIKE 11, RESSASS, GSTARS. Most of these tools are able to predict basic parameters such as water surface elevation, sediment transport load, bed variation or the bulk velocity and some are capable of more advanced computations.

2D numerical models for sediment transport provides better data input interface and result visualization which made it more user friendly compared to 1D models. These are depth average models that can compute the information on water depth and bed elevations (Chaudhary et al., 2019). Papanicolaou et al. (2008) provides some detailed lists of 2D sediment transport modelling tools such as SUTRENCH -2D developed by Van Rijn and Tan (1985), MOBED2 by Spasojevic and Holly (1990), FLUVIAL 12 by Chang (1998), DELFT-2D, CCHE2D by Jia and Wang (1999), HEC-RAS by Alex Sanchez and Stanford Gibson (Brunner, 2022a) etc.

With the advancement in computing technology, 3D models have become much more attractive today. It can provide better results when it comes to complex flow patterns and flows near the vicinity of piers and hydraulic structures. Most of the 3D models solve sediment mass balance equation using the methods of finite element, finite difference or finite volume. Examples of different 3D modelling tools are listed in Papanicolaou et al. (2008) which includes EFDC3D in Hamrick (1992), ROMS used by Song and Haidvogel (1994), CH3D-SED in Spasojevic and Holly (1994), SSIIM developed by Olsen and Skoglund (1994), MIKE 3 developed by Danish Hydraulic Institute, DELFT3D developed by Delft Hydraulic Laboratory team, TELEMAC-3D etc.

2.2.3   Grid Independence Test

It is the procedure used to discover the ideal grid size that has fewest number of grids without causing a significant difference in the simulated results because the entire computational cost and accuracy of the simulation results are influenced by the number of grids (Lee et al., 2020). Also, use of a coarse mesh can lead to larger spatial discretization error whereas very fine grids can lead to round off error which could be more than the truncation error. It can result in poor accuracy in the fine grid. Using very fine or coarse grid may both lead to poor

result (J.Tu and C.Liu, 2007). Hence it is necessary to get a result which is independent of the change in grid. One of the techniques to achieve this is the method of grid convergence. It involves both grid refinement as well as grid coarsening. Whether to refine or coarsen depends on the size of grid that was used for initial computation (Roache, 1997). However, the selection of grid size also depends on the experience and subjective judgement of the researcher (Lee et al., 2020).

2.3   Uses of HEC-RAS in Modelling

HEC-RAS has been used for many years for various purposes. It was first released to the public in 1995 A.D (Brunner and Gibson, 2005). It included design of hydraulic structures (bridges, culvert, inline and lateral weirs, spillways etc), flood zone mapping, dam break analysis, 1D sediment transport modelling etc. Bhandari et al. (2017) shows the use of HEC-RAS to determine the extent of flooding or flood inundation. The study can be used for the purpose of planning infrastructures and land development. Nyaupane et al. (2018) and Thakur et al. (2017) demonstrates the combination of hydrological scenarios to determine the flood events under different condition using the software. It shows how HEC-RAS can be used to estimate the future flood inundation conditions based on climate data.

Brunner and Gibson (2005) summarizes the capabilities of HEC-RAS to model sediment transport in one dimension. This version of hecras was limited to quasi-unsteady flow and vertical bed change. But the new version of HEC-RAS 5.0 was developed over this limitation including the unsteady flow, lateral cross section changes with USDA-ARS Bank Stability and Toe Erosion Model (BSTEM) and many other features (Gibson et al., 2017). Shelley et al. (2015) demonstrates the sediment transport modelling features in HEC-RAS 5.0 to analyse the sedimentation in large reservoirs. Hussain and Shahab (2020) shows how HEC-RAS sediment transport can be used in the planning and study of flushing of reservoirs. Damte et al. (2021) discusses how HEC-RAS was used to determine the inundation level, temporary morphological change in river due to flood and its effects such as aggradataion and degradation of the bed in Kulfo river in Ethiopia.

3   HEC-RAS 2D

HEC-RAS is an integrated system of softwares developed by Hydrologic Engineering Center of the US Army Corps of Engineers to perform 1D or 2D modelling of river networks. It can be used for one dimensional (1D) and two dimensional (2D) unsteady flow modelling.New version of the software allows 2D sediment transport modelling offering a user-friendly graphical user interface for data management and model visualization. HEC-RAS uses three different equation sets to solve the flow over mesh. They are Diffusion Wave Equation (DWE), Shallow Water Equations Eulerian-Lagrangian method (SWE-ELM), Shallow Water Equation Eulerian Method (SWE-EM). (Brunner, 2022b)

3.1   Hydraulic Equations in HEC-RAS 2D

Shallow Water Equations (SWE) are a collection of equations that describe a shallow layer of fluid in hydrostatic balance and enable for three-dimensional analysis to be simplified while yet retaining a reasonable description of the real phenomenon. SWE assumes that the vertical length scale is much smaller than the horizontal scale. Other assumptions include incompressible flow, uniform density and hydrostatic pressure. (Brunner, 2022b)

If the flow is considered incompressible, the continuity equation can be expressed by Equation 14.

$$\frac{\partial h}{\partial t} + \frac{\partial (hu)}{\partial x} + \frac{\partial (hv)}{\partial y} = q \tag{14}$$

where, t= time(T), h=water depth(L), u and v = velocity components in the x and y direction respectively. q=source/sink flux term. Subgrid bathymetry approach can be used to improve the computation time where detailed information about the terrain is given with coarse grid. (Brunner, 2022b)

Navier stokes vertical momentum equation can be used when the pressure is hydrostatic and horizontal scale is larger than the vertical scale. In absense of pressure gradient and strong wind, the shallow water equation can be expressed by Equation 15 and 16.

$$\frac{\partial u}{\partial t} + u\frac{\partial u}{\partial x} + v\frac{\partial u}{\partial y} - f_c v = -g\frac{\partial z_s}{\partial x} + \frac{1}{h}\frac{\partial (v_{t,xx}h\frac{\partial u}{\partial x})}{\partial x} + \frac{1}{h}\frac{\partial (v_{t,yy}h\frac{\partial u}{\partial y})}{\partial y} - \frac{\tau_{b,x}}{pR} + \frac{\tau_{s,x}}{ph} \tag{15}$$

$$\frac{\partial v}{\partial t} + u\frac{\partial v}{\partial x} + v\frac{\partial v}{\partial y} - f_c u = -g\frac{\partial z_s}{\partial x} + \frac{1}{h}\frac{\partial (v_{t,xx}h\frac{\partial v}{\partial x})}{\partial x} + \frac{1}{h}\frac{\partial (v_{t,yy}h\frac{\partial v}{\partial y})}{\partial y} - \frac{\tau_{b,y}}{pR} + \frac{\tau_{s,y}}{ph} \tag{16}$$

where, u and v = velocities in the cartesian directions, g = gravitational acceleration, zx = water surface elevation, vt,xx and vtyy = horizontal eddy viscosity coefficients in the x and y directions, Tb,x and Tb,y = bottom shear stresses on the x and y directions, Ts,x and Ts,y are the surface wind stress directions, R = hydraulic radius, h= water depth, fc = cariolis

parameter.The acceleration terms are found on the left side of the equation. The internal or external forces acting on the fluid are represented on the right hand side.

The bed friction coefficient, using Manning's formula is given by Equation 17.

$$c_f = \frac{n^2 g |V|}{R^{\frac{4}{3}}} \tag{17}$$

where, n= manning's roughness coefficient $[s/m^{1/3}]$
R= hydraulic radius [m]
g = gravitational acceleration $[m/s^2]$

3.2   Subgrid Bathymetry

Sometimes, even when the data available is detailed, a coarser grid is to be used for computation. However, all the features needs to be addressed in the calculation. HEC-RAS uses the subgrid bathymetry approach to tackle this problem. The extra information in the computational grid cells, such as hydraulic radius, volume, and cross sectional area, can be pre-computed using the fine bathymetry data. Because the free water surface is smoother than the bathymetry, a coarser grid can be utilized to calculate the spatial variability in free surface elevation more effectively (Brunner, 2022b). The high resolution bathymetric data can be used at a subgrid level.The model used for this is efficient, produces quite accurate results with relatively coarser mesh dimensions and large time step sizes. It does not require a minimum water depth threshold and does not cause physically negative water depths. (Vincenzo Casulli, 2008)

3.3   Computational Mesh

HEC-RAS 2D is capable of both structured and unstructured meshes. The computational cells can be triangles, squares, rectangles, pentagons, hexagons, heptagons or even octagons. Each cell represents a detailed elevation volume relationship to represent the underlying terrain. The cell faces are processed into detailed elevation vs area, wetted perimeter and roughness relationships. One thing a modeler should keep in his mind is to ensure that the faces captures high points of flow barriers. Single water surface elevation is calculated at the center of each cell meaning with the increase in cell size, the slope of water surface is averaged over a longer length. If the water surface is not varying over the large area, larger computational mesh can be used. However, if the velocity and the water surface slope is varying rapidly, smaller cell size should be used. One advantage of HEC-RAS is that it allows the users to define different sizes of cells at different location using breaklines or refinement regions. A polygon is used to define the computational mesh's outer boundary. Though structured mesh is faster and efficient to solve, unstructured mesh is more flexible in the sense it can represent the complex terrain properly.

It uses a dual grid approach to solve the second order derivative numerically. The dual grid spans the domain as well, and is distinguished by the existence of a correlation between dual nodes and regular grid cells, as well as between dual cells and regular grid nodes (Brunner, 2022b).

3.4 Shallow water vs Diffusion wave equation

The shallow water equation is mainly used to obtain the high resolution and detailed flows with dynamic changes in acceleration and important wave effects and tidal flows. It is used for the detailed solution of flows around obstacles, bridges or bends. SWE simulations are influenced by Coriolis, mixing or wind. However, diffusive wave equation is mainly used for the quick estimations or preliminary runs when fluid acceleration is monotonic or smooth. It is used for the global estimates like flooding event rather than detailed flows. DWE flow is mainly driven by gravity and friction. (Brunner, 2022a)

It is usually a good idea to initially run the model with DWE. Once the model runs properly, new plan shall be created to run the model with SWE. On comparing the two, if the difference is too significant, it is assumed that the SWE is more accurate and shall be used for calibration and further simulations. (Brunner, 2022a)

3.5 Terrain Modification

Terrain modification can be done in HEC-RAS to change the terrain surface elevation. It is used to represent the correct river channel or to incorporate important features that control the flow of water. With a correct intial terrain, different tools in HEC-RAS can be used to modify it. According to HEC-RAS mapper user's manual, the software currently provides two methods to modify the terrain.

3.5.1 Cross Section Interpolation

In this method, a simple 1D model can be used to create or modify the terrain as the user wants. One needs to create a river channel and multiple cross sections with or without overbanks. The created geometry is then interpolated to form a new terrain. Users can even define the cell size for new terrain. This terrain can then be combined with existing terrain with modifications in it.

3.5.2 Terrain Modification Tools

Vector editing tools in RAS Mapper can be used to create points, lines and polygons to create vector modification to the terrain. It allows users to add simple to complex shapes with same or varying elevations. A clone terrain can be created so that it is easier for the users to use vector modification tools without having to save enormous data on disk. Under clone terrain, a modification layer can be added where all the editings can be done. This layer can then be easily edited and copied to other terrain files.

3.6   Variable Time Step

Time step or the computational time in HEC-RAS can be defined as the incremental change in time when the governing equations are solved. It can also be defined as a rule or a guide to determine the time step. It is possible to use a variable time step in HEC-RAS. This capability can be used to set a varying computational time step to improve the model stability and reduce computational time. However, faster computation of the models is not guaranteed for all the cases. It depends on the mesh as well as the size of geometry. Courant number method is one of the options in variable time step control. Selecting an appropriate time step is the function of cell size and velocity of flow through the cells. HEC-RAS uses three different equations to solve the flow over mesh (Brunner, 2022a).

Shallow Water Equations, Eulerian-Lagrangian Method (SWE-ELM)

It is the original shallow water equation where courant number is calculated as expressed by Equation 18.

$$C = \frac{V\Delta T}{\Delta X} \leq 1.0 \ (with \ a \ max \ C = 3.0) \tag{18}$$

$$\Delta T \leq \frac{\Delta X}{V}; (with \ C = 1.0) \tag{19}$$

Shallow Water Equations, Eulerian Method (SWE-EM)

It uses an explicit solution scheme to solve equations. It requires small computational time steps and is more momentum conservative. In this method, the time step is selected in such a way that the Courant number is less than 1. It is expressed by Equation 20.

$$C = \frac{V\Delta T}{\Delta X} \leq 1.0 \ (with \ a \ max \ C = 1.0) \tag{20}$$

$$\Delta T \leq \frac{\Delta X}{V}; (with \ C = 1.0) \tag{21}$$

Diffusion Wave Equations(DWE)

Compared to SWE, larger time steps can be used in DWE and at the same time get numerically stable result. The courant condition for DWE is shown by Equation 22.

$$C = \frac{V\Delta T}{\Delta X} \leq 2.0 \ (with \ a \ max \ C = 5.0) \tag{22}$$

$$2\Delta T \leq \frac{\Delta X}{V}; (with \ C = 1.0) \tag{23}$$

3.7 Sediment Equations Concepts in HEC-RAS 2D

Total load consists of the combination of bed load and suspended load i.e all the transported particles. One of the advantages of using this is reduced computational time as only one equation is being used. The total load transport equations is given by Equation 24.

$$\frac{\partial}{\partial t}\left(\frac{hC_{tk}}{\beta_{tk}}\right) + \nabla.(hUC_{tk}) = \nabla(\varepsilon_{tk}h\nabla C_{tk}) + E_{tk}^{HF} - D_{tk}^{HF} + S_{tk} \tag{24}$$

where,

C_{tk} = Total load sediment concentration
β_{tk} = Total load correction factor
U = depth averaged current velocity in jth direction
h = depth of water
ε_{tk} = mixing coefficient corresponding to $k^t h grainclass$
E_{tk}^{HF} = total load erosion rate in hydraulic flow
D_{tk}^{HF} = total load deposition rate in flow
S_{tk} = total load source/sink term (F)

The fractional bed change is given by Equation 25.

$$\rho_{sk}(1-\phi_b)\left(\frac{\partial z_b}{\partial t}\right)_k = D_{tk} - E_{tk} + \nabla.(\kappa_{bk}|q_{bk}|\nabla z_b) \tag{25}$$

Sum of the fractional bed changes gives total bed change and is given by Equation 26:

$$\frac{\partial z_b}{\partial t} = \sum_k \left(\frac{\partial z_b}{\partial t}\right)_k \tag{26}$$

where,

rho_{sk} = particle density of grain class
phi_b = porosity of eroded and deposited material
z_b = elevation of bed with respect to vertical datum
κ_{bk} = empirical bed slope coefficient for grain class k
q_{bk} = magnitude of bed load mass transport rate

The value of bed slope coefficient for grain class k can be determined using Equation 27 (Koch and Flokstra, 1981; Kovacs and Parker, 1994; Parker et al., 2003)

$$\kappa_{bk} = \kappa_{b0}\sqrt{\frac{\tau_{crk0}}{max(\tau_b', \tau_{crk0})}} \tag{27}$$

where,

κ_{b0} = empirical parameter
τ_{crk0} = critical shear stress
τ_b' = bed skin shear stress

3.8   Transport Functions

There are eleven different transport functions available in HEC-RAS. Each of the functions were developed considering different scenarios, assumptions and conditions. So, the functions that represent the model shall be adopted for simulation and actual bed changes shall be used for calibration of the model. Brunner (2022b) provides a list of functions including the condition of how transport functions were developed and the basis for the use of these functions. A preliminary selection can be made using the conditions such as the particle diameters, water temperature, energy gradient etc. It is presented in Table 3.1.

Table 3.1: Range of input values for sediment transport functions (SAM User's Manual, 1998)

Function	d	dm	s	V	D	S	W	T
Ackers-White (flume)	0.04 - 7.0	NA	1.0 - 2.7	0.07 - 7.1	0.01 - 1.4	0.00006 - 0.037	0.23 - 4.0	46 - 89
Englund-Hansen (flume)	NA	0.19 - 0.93	NA	0.65 – 6.34	0.19 – 1.33	0.000055 – 0.019	NA	45 - 93
Laursen (flume)	NA	0.011 -29	NA	0.7 - 9.4	0.03 – 3.6	0.00025 – 0.025	0.25 – 6.6	46 - 83
Meyer-Peter Muller (flume)	0.4 – 29	NA	1.25 – 4.0	1.2 – 9.4	0.03 – 3.9	0.0004 – 0.02	0.5 – 6.6	NA
Tofaletti (field)	0.062 – 4.0	0.095 – 0.76	NA	0.7 - 7.8	0.07 – 56.7 (R)	0.000002 – 0.0011	63 - 3640	32 – 93
Tofaletti (flume)	0.062 – 4.0	0.45 – 0.91	NA	0.7 - 6.3	0.07 – 1.1 (R)	0.00014 – 0.019	0.8 – 8	40 - 93
Yang (field-sand) (field-sand)	0.15 – 1.7	NA	NA	0.8 - 6.4	0.04 – 50	0.000043 – 0.028	0.44 – 1750	32 - 94
Yang (field-gravel)	2.5 – 7.0	NA	NA	1.4 - 5.1	0.08 – 0.72	0.0012 – 0.029	0.44 – 1750	32 - 94

where,

d = Overall diameter of particles (mm)
d_m = Median particle diameter (mm)
s = Specific gravity of sediment
V = Average velocity of channel (fps)
D = Depth of channel
S = Energy gradient
W = Width of channel (ft)
T = Temperature of water (F)
R = Hydraulic Radius (ft)
NA = Data not available

Brief description for some of the transport functions applicable in the model is done in this section.

3.8.1   Meyer Peter and Müller (MPM)

The empirical relation proposed by Meyer- Peter and Müller (Meyer-Peter and Müller, 1948) is one of the most used formulas for bed load transport in field as well as laboratory. Here, the bed load is estimated as a function of excess shear stress applied by flowing water. One

of the common cases where MPM equation is applied is when the slope of bed is less than
0.02 (Wong and Parker, 2006). Meyer-Peter and Müller (1948) gives the MPM formula as
in Equation 28.

$$\gamma_w \cdot \frac{Q_s}{Q} \cdot \left(\frac{k_s}{k_r}\right)^{3/2} . h.J = 0.047 . \gamma_s'' . d_m + 0.25 \left(\frac{\gamma_w}{g}\right)^{1/3} . g_s''^{2/3} \tag{28}$$

where,

$Q_s = q_s.B$
q_s = specific discharge
B = the width of channel
Q = the total discharge
k_s = the coefficient of roughness for the bed
k_γ = the coefficient of particle friction with smooth bed
h = the water depth,
J = the slope of energy line
γ_s'' = the specific gravity of bed load under water
d_m = the effective diameter
γ_w = the specific gravity of water
g = the acceleration due to gravity
g_s'' = the specific bed load transport under water

According to Hunziker and Jaeggi (2002), the simple approach of bed load transport over
predicts the transport rates. Chien (1954) suggested the dimensionless form of Equation 28
as:

$$q^* = 8 \left[\frac{q_w'}{q_w} \left(\frac{K_b}{K_r}\right)^{3/2} \tau^* - 0.047\right]^{3/2} \tag{29}$$

where,

q^* = the dimensionless volume bed-load transport rate per unit channel width
q_w' = the volume discharge of water per unit channel width after correcting sidewall effects
K_b = Manning - Strickler coefficient of roughness for the bed region
K_r = Manning- Strickler coefficient of bed roughness associated with skin friction only
τ^* = dimensionless boundary shear stress (Shield's number)

HEC-RAs uses the Meyer Peter and Müller formula as presented by Wong and Parker (2006)
in Equation 30.

$$q_b^* = 8(\tau^* - \tau_c^*)^{3/2} \tag{30}$$

where,

q_b^* = the dimensionless transport parameter
τ^* = the dimensionless mobility parameter
τ_c^* = the critical Shields stress whose value is 0.047

Wong and Parker (2006) mentioned that absence of form drag coefficient over predicts the bed load transport. The equation was modified a little for lower regime plant bed conditions and Equation 31 was proposed.

$$q_b^* = 3.97(\tau^* - \tau_c^*)^{3/2} \tag{31}$$

where the value of critical shields stress is 0.0495. This correction can easily be applied in HEC-RAS with the built in function.

3.8.2   Yang

Yang formulated a total load transport equation based on stream power, which is the product of shear stress and the velocity. This function was tested over a number of flume and field conditions. This function is more sensitive to the stream velocity and fall velocity. According to Yang (1973), for the particles with diameter less than 2mm, concentration is given by Equation 32.

$$
\begin{aligned}
logC_t = {}& 5.435 - 0.286log\left(\frac{\omega d_m}{v}\right) - 0.457log\frac{u_*}{\omega} + 1.799 - 0.409\left(\frac{\omega d_m}{v}\right) \\
& -0.314log\frac{u_*}{\omega}log\left(\frac{VS}{\omega}\right) - \left(\frac{V_{cr}S}{\omega}\right)
\end{aligned}
\tag{32}
$$

where,

C_t = Total concentration of sediment
ω = Fall velocity of particles
d_m = Median diameter of particles
v = Kinematic viscosity
u_* = Shear velocity
V = Average velocity of channel
S = Energy gradient

3.8.3   Ackers and White

In 1973, Ackers and White published a theory for sediment transport prediction of non-cohesive sediments. It was used to estimate the total load of uniform materials or morphological changes in the channel. There was an uncertainty in the application of this equation for fine and coarse sediments. An update to this was made with re-derivation of parameters

on extended data set (Wallingford, 1990). Proffitt and Sutherland (1983) and Day (1980) modified the original Wallingford (1990) multiplying it with hiding and exposure correction factors. The transport potential is given by Equation 33.

$$q_{tk}^* = \rho_w g h U X_{tk}^*$$
(33)

where,

q_{tk}^* = sediment transport potential
ρ_w = Water density
g = gravity acceleration
h = water depth
U = depth-averaged current velocity
X_{tk}^* = sediment concentration potential by weight

Sediment concentration potential is then determined using Equation 34.

$$\frac{X_{tk}^* h \rho_w}{d_k \rho_{sk}} \left(\frac{u_*}{U}\right)^n = \wedge \left(\frac{F_{grk}}{A_c} - 1\right)^m$$
(34)

where,

F_{grk} = sediment mobility factor
u_* = bed shear velocity
ρ_{sk} = sediment density
$\wedge$ = empirical coefficient
A_c = empirical coefficient
n = empirical exponent
m = empirical exponent

Proffitt and Sutherland (1983) gives the sediment mobility factor expressed by Equation 35 .

$$F_{grk} = \eta_k \frac{u_*^n}{\sqrt{R_k g d_k}} \left[\frac{U}{\sqrt{32} log_{10}(10h/d_k)}\right]^{1-n}$$
(35)

where,

ρ_{sk} = density of sediment
ρ_w = density of water
η_k = hiding and exposure correction factor
τ_b = bed shear stress
d_k = sediment diameter

$$n = \begin{cases} 1 & \text{for } d_{*k} \leq 1 \\ 1 - 0.56log_{10}(d_{*k}) & \text{for } 1 < d_{*k} \leq 60 \\ 0 & \text{for } *k > 60 \end{cases} \tag{36}$$

$$A_c = \begin{cases} 0.23d_*^{-1/2} + 0.14 & \text{for } d_{*k} \leq 60 \\ 0.17 & \text{otherwise} \end{cases} \tag{37}$$

$$m = \begin{cases} 6.83d_*^{-1} + 1.67 & \text{for } d_{*k} \leq 60 \\ 1.78 & \text{otherwise} \end{cases} \tag{38}$$

$$\wedge = \begin{cases} 2.791log_{10}(d_{*k}) - 0.98[log_{10}d_{*k}]^2 - 3.46 & \text{for } d_{*k} \leq 60 \\ 0.0025 & \text{otherwise} \end{cases} \tag{39}$$

According to Wu (2007), Ackers - White formula overpredicts the transport significantly for fine sediments less than 0.2mm.

3.8.4   Wilcock and Crowe

Wilcock and Crowe (2003) created a surface based bed load transport equation for sand and gravel beds. The Wilcock and Crowe (2003)'s transport potential is given by Equation 40.

$$q_{bk}^* = \frac{u_*^3 W_k^*}{R_k g} \tag{40}$$

where,

q_{bk}^* $\quad\quad\quad\quad$ = fractional bed-load sediment transport potential
$R_k = \rho_{sk}/\rho w - 1$ = submerged specific gravity of grain class
ρ_w $\quad\quad\quad\quad$ = Water density
ρ_{sk} $\quad\quad\quad\quad$ = sediment density
u_* $\quad\quad\quad\quad$ = bed shear velocity
g $\quad\quad\quad\quad$ = gravitational constant

The transport function is given by Equation 41.

$$W_k^* = \begin{cases} 0.002\phi^{7.5} & \text{for } \phi < 1.35 \\ 14\left(1 - \frac{0.894}{\phi^{0.5}}\right)^{4.5} & \text{for } \phi > 1.35 \end{cases} \tag{41}$$

where,

ϕ = sediment mobility

3.8.5   Van Rijn

According to (Van Rijn et al., 2007), the degree of exposure of grains in relation to other grains in neighborhood, is of great importance for the initiation of transport . The bed load transport is given by Equation 42.

$$q_b = 0.5\rho_s f_{silt,i} d_i [D_{*,i}]^{-0.3} [\tau'_{b,cw}/\rho]^{0.5} [\tau_i] \tag{42}$$

where,

q_b = bed load sediment transport potential
ρ_s = sediment density
f_{silt} = silt factor
d_i = particle size of fraction i
$D_{*,i}$ = dimensionless particle size of fraction i
$\tau'_{b,cw}$ = instantaneous grain related bed shear stress
τ_i = bed shear stress parameter

The formulas from Van Rijn are for the well sorted sediments. HEC-RAS 2D Technical Reference Manual presents the modified Van Rijn (Van Rijn et al., 2007; Van Rijn, 1984) formula to make it suitable for non uniform sediments using the hiding and exposure correction factor. The sediment transport is given by Equation 43.

$$q_{bk}^* = 0.015Uh \left(\frac{U - U_{crk}}{\sqrt{R_k g d_k}} \right)^{1.5} \left(\frac{d_k}{h} \right)^{1.2} \tag{43}$$

$$q_{sk}^* = 0.012Uh \left(\frac{U - U_{crk}}{\sqrt{R_k g d_k}} \right)^{2.4} \left(\frac{d_k}{h} \right) d_{*k}^{-0.6} \tag{44}$$

where,

q_{bk}^* = bed load sediment transport potential
q_{sk}^* = Suspended load sediment transport potential
U = effective depth averaged current velocity
U_{crk} = critical depth averaged velocity for incipient motion
R_k = submerged specific gravity of a particle
d_k = grain class diameter
h = water depth

3.9   Best Practices for a 2D Sediment Model

A good model setup results in a better output which is also true for 2D sediment modelling in HEC-RAS. Alejandro Sanchez (2020) provides some of the best practices that can lead to correct solution. One of the parameters that should not be ignored in model setup is the hydraulic warm-up period. It is important to wet the mesh before starting the computation as erosion in the beginning of simulation can result in bias results. A warmup period that wets the entire model in the first half should be selected. Another best practice is to develop a model with structured and aligned mesh without many small cell faces. Breaklines or refinement regions can be used for this purpose. While selecting the hydraulic equations, one should go for the Shallow Water Equation (SWE). DWE shall not be used with the sediment modelling. Lastly, a proper time step shall be chosen for 2D sediment modelling. Too large time step can cause instabilities in the model. Advanced time step control can be used to introduce dynamic time steps that changes according to computation requirement.

3.10   Lateral Structure Sediment Diversion

Latest version of HEC-RAS has the ability to model lateral weirs, gates, culverts, diversion rating curves and an outlet time series. One can model any combination of weirs, gates and culverts. In HEC-RAS, the lateral structures can be connected to another 2D Flow Area, storage areas or a river reach (Brunner, 2022a).

HEC-RAS 5.0 added sediment diversions to lateral structures. Default setting assumes the flow weighted split of sediment compared to the flow i.e. same percentage of flow and sediment through the lateral structures. The use of sediment diversion through lateral structures in unsteady sediment transport made it more useful. It might also be possible to model 2D sediment transport model in HEC-RAS in the future versions. When the lateral structure is linked with storage area in sediment model, the mass of sediment through structure is removed from the simulation (Gibson et al., 2017).

4   Working Model of Thesis

This section presents the general working model of this thesis as shown in Figure 4.1.
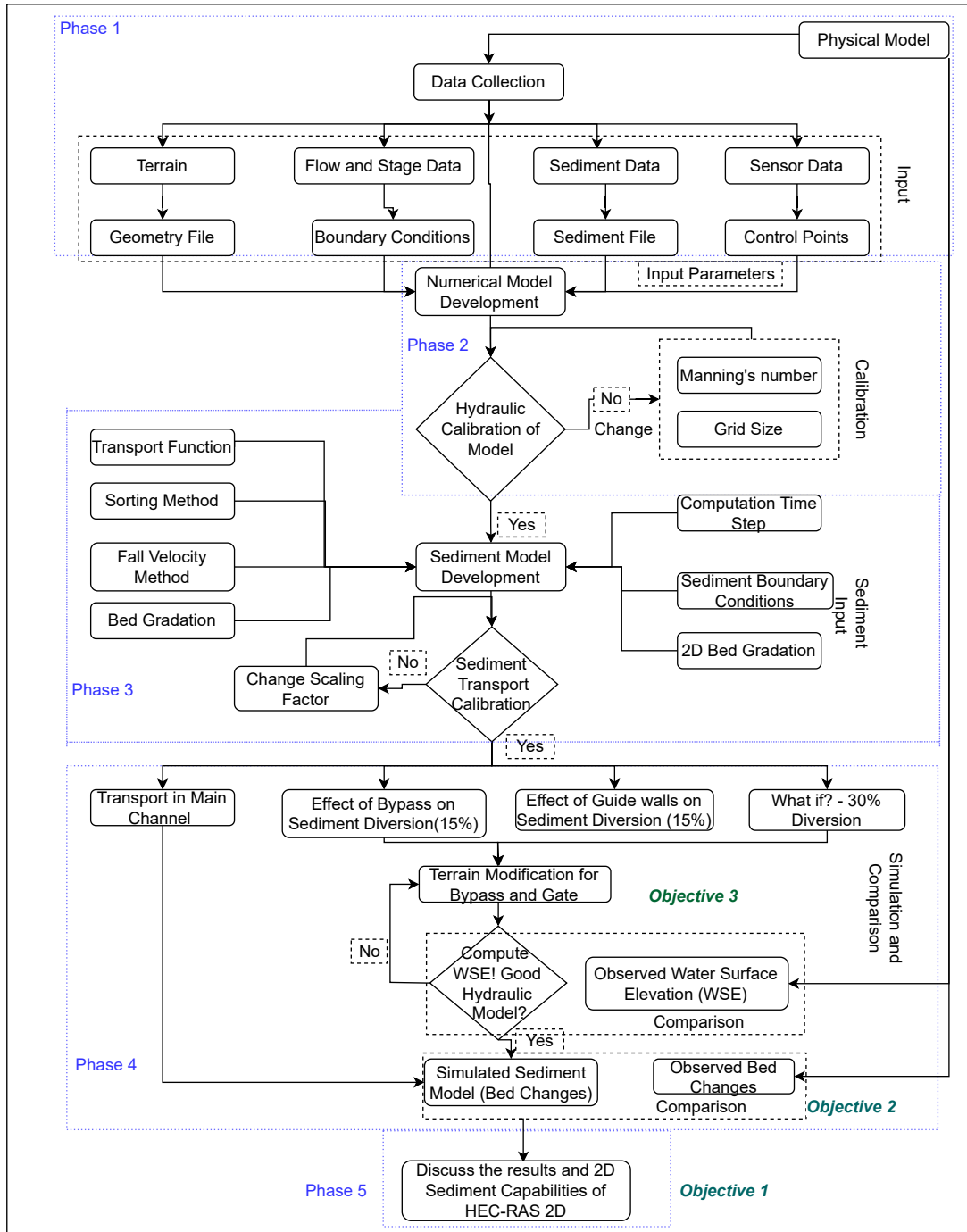
Figure 4.1: Working model of the thesis

Primary and secondary objectives of the study can be achieved in five different phases. The phases are represented by blue boxes in Figure 4.1 and are briefly discussed below.

4.1   Phase 1: Data Collection

The first phase of this study includes collection of data which was done from a physical model. The physical sediment transport model at Norsk Hydroteknisk Laboratorium, NTNU was used as a prototype for all the numerical analyses done in this study. This physical model was set up in the lab for a PhD study by Diwash Lal Maskey. Several tests at different discharges and conditions were done in the model which were later used as input data in this study.

The model banks were constructed using wood and concrete which are non erodible. The channel bed was composed of sand with diameter ranging from 0.1mm to 0.75mm which is erodible. The bed material gradation for this sand is shown in Figure A.2. A general methodology for the test in physical model includes preparing a smooth sand channel bed, run the test with certain discharge, observe the bed change with dunes and ripples formation and determine the amount of bed material eroded in downstream and through the sediment bypass tunnel. The data obtained from this was used as input sediment data as well as to calibrate and compare the results from the numerical model. The observation was made for different inflow discharges in channel and varied discharges through the sediment bypass tunnel. For the purpose of this study, the inflow discharge of 35 l/s was used with total discharge through bypass of 15% (5 l/s) and 30% (10 l/s) of the total inflow. These flow data were used as boundary conditions in the numerical model.

Scanning of this model before and after the test was done using Scanning Total Station. These scans are used to prepare Digital Elevation Model (DEM) and terrain files for the input in HEC-RAS 2D. Eight sensors were installed along the channel to record water surface elevation data and were used as control points for the water level in simulation. The data obtained from the sensor at the end of the channel has been used as a downstream boundary condition.

4.2   Phase 2: Setting up Hydraulic Model

Phase 2 of the study includes model development and hydraulic calibration of the model. Using the data obtained from physical model, a numerical model was set up in HEC-RAS 2D. Different values of grid sizes and manning's number were used to calibrate the model. This phase is important because it is a pre-requisite for the sediment modelling. This phase has been described in detail in Chapter 5.

4.3   Phase 3: Sediment Model Development

Phase 3 of the study focuses on the development of a sediment model. Selection of transport function, sorting method, fall velocity method has been done. A suitable computation time step was chosen. A sediment model was calibrated against an observed data from physical

model. If the comparison does not show an acceptable match between simulated and observed values, either several parameters in the transport function or the scaling factors can be changed to calibrate the sediment model. This phase has been explained in detail in Chapter 7.

4.4 Phase 4: Simulation and Comparison

After the model is calibrated, all the simulation and analyses was done in phase 4. Sediment transport simulation has been done in the test channel to observe the closeness of simulated result with this calibrated model. This model was used for calibration because it is the simplest model among all of the simulations without any external structures. Terrain modification seems like a good feature to modify the terrain according to the needs of a user. It is possible to use it to add the bypass channel as well as to introduce the guide walls. This modified model was compared with the observed physical model and after the result agrees with the observed ones, sediment modelling was performed. The comparison of observed and simulated bed changes has been done in this phase of the study. This phase has been described in detail in Chapter 7.

4.5 Phase 5: Discussion

This is the final phase of the study where the results are discussed. The deviations between observed and simulated model were analysed properly. Proper reasoning has been explored for the outcome of comparisons and the reasons for attaining the objectives are mentioned. This phase also focuses on the reasons why certain objectives could not be met due to the limitation in study, materials or the software itself. This has been discussed briefly in Chapter 8.

4.6 Tools Used

Various tools have been used in this study for proper analysis, reporting, visualization and finishing of various components and phases. Some of them has been briefly described in this section.

CloudCompare and ArcGIS have been used to read, interpolate, visualize, convert and map the point clouds scanned using the scanning total station. These softwares have been used to create the terrain file for input in the model. ArcGIS has been used to present the results obtained from the model. Python has been used for the data visualization obtained from physical as well as the simulated model. Calculations have been done using python and microsoft excel. HEC-RAS 2D has been used for all the simulations. The report is prepared in Overleaf.

5   Numerical Model Development

The numerical model is based on the physical model at Norsk Hydroteknisk Laboratorium, NTNU. Various results from the lab model are used for model development. Brief description of input data and steps are presented below.

5.1   Terrain Model

For accurate hydraulics and sediment model, a detailed terrain model is required. Scanning of the physical model was done to create the terrain file for the numerical model. The interpolation of scanned data was done using an application in ArcGIS called ArcMap and CloudCompare. Some point clouds were missing high elevation points in boundary of the channel. To solve this problem, boundary points were recorded in the lab and inserted separately before creating the raster. Different methods of interpolation were tested before an acceptable result was achieved. Finally, binning interpolation method with the NEAREST cell assignment type and LINEAR void fill method was used for interpolation. HEC-RAS uses gridded model for the terrain so a good quality terrain model was created with the grid size of 1cm x 1cm. Figure 5.1 shows a sample terrain that is used in HEC-RAS 2D. Some other terrain files that were used for model setup and comparison are presented in Appendix Figure A.1.
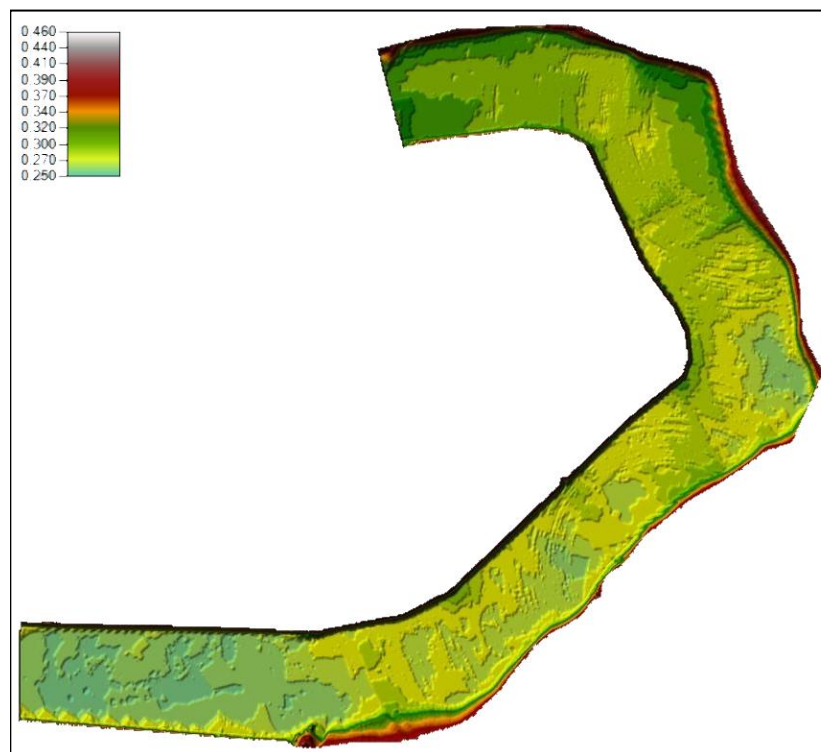
Figure 5.1: Terrain Model

5.2   Development of Structured Grid

Proper grid development is one of the important tasks in numerical modelling. The model consists of a structured grid throughout the length of the test channel with some exceptions at the boundary. The break line on the center of the channel was used to align the grid to flow direction whereas the break lines on the edges were used to separate the channel bed level from the channel banks. The model was also tested with grids that are not aligned with the flow and both hydraulics and sediment models were run using it. There was no problem with the stability of the model and it worked without any errors. But when the grids were aligned with the flow direction, the results obtained were much better. When the cells are aligned with the flow direction, most problems related to numerical diffusion are reduced. (Brunner et al., 2020)
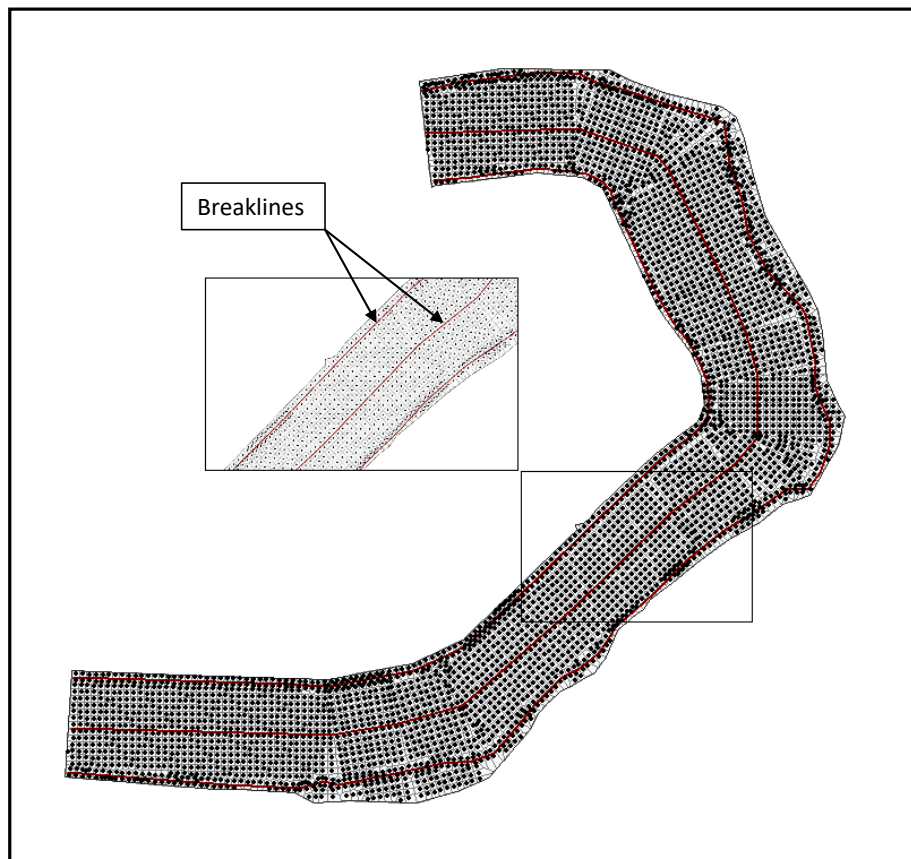
Figure 5.2: Grid Development

Figure 5.2 shows an example of a structured grid model with grids aligned with flow direction and break lines.

5.3 Boundary Conditions

Flow hydrograph was used for upstream boundary condition with the constant flow of 35 l/s to introduce water to the flow area. Stage hydrograph was used for the downstream boundary condition with variable water surface elevation. These are the observed series from physical model. The observed data were used directly as the input to the numerical model.

5.4 Equation Set

First, diffusion wave equation was used for a quick preliminary run and to check if the model was stable. Once the model was stable, the output was recorded. Then the shallow water equation was used to compute the result. Water surface elevations using these two methods were compared at different points. Significant differences were observed between the results from two equation sets and closer values were observed using SWE. Therefore, SWE was considered to be more accurate and used for calibration of the model.

5.5 Manning's roughness coefficient

The manning's roughness coefficient (n) was set to default value for setting up the model. Different values of manning's number was used to see if the output changes with the change in values of n. Once the model was found to be stable and is responding to changes in values of n, calibration was done to get the optimized value as described in 6.

5.6 Time Step

The time step in HEC-RAS simulation is the computation time interval. The time step was chosen based on the grid size and velocity of flow. After the grid size optimization, the cell size of 0.1m was selected. An average velocity of 0.5 m/s was found from initial test runs of the model. Assuming the courant number to be 1 or less, the computation time interval was calculated to be about 0.2 seconds. The minimum courant number was set to be 0.45. Maximum number of doubling and halving the base time step was taken as 4. Variable output time intervals were used for hydraulics and sediment model based on the required details.

6 Hydraulic Calibration and Validation

Hydraulic calibration and validation are required before sediment transport analysis can be done. A stable calibrated hydraulic model is a pre-requisite for a good sediment modelling (Alejandro Sanchez, 2020). For calibration, water level elevations were measured at different points along the channel at a fixed time step. These observed values were used to calibrate the simulated model. Hydraulic calibration was done in two steps by optimizing the grid size and by changing manning's number as a calibration parameter. The calibration can be described using the flowchart shown in Figure 6.1.

Two different terrains were used for the purpose of calibration. The terrains used for calibration are given the terms initial and final terrain. Initial terrain meaning the plain bed scanned before running the sediment transport test in lab. Whereas final terrain meaning the scanned bed after running the test. These terms will be used further in this report. In each of these cases, ten minutes of observed flow and water surface elevation data were taken for calibration.
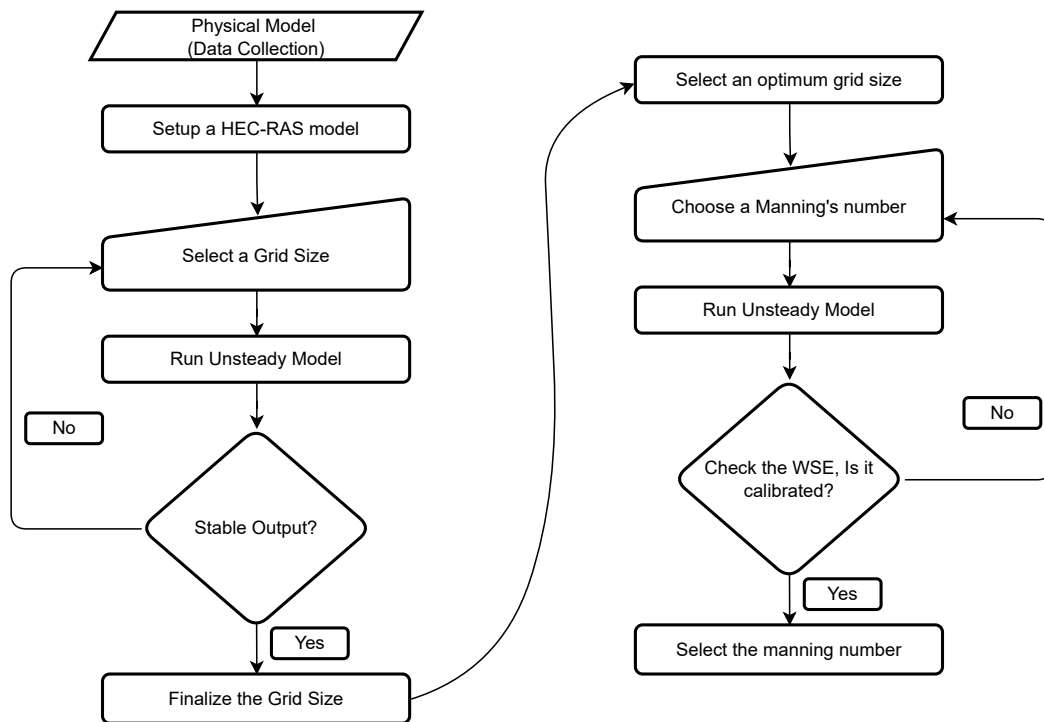
Figure 6.1: Flowchart showing grid size and manning's number Optimization

6.1 Water Surface Elevation

6.1.1 Location of Sensors

The locations for all the water level sensors are shown in Figure 6.2. WSM1 (Channel 1) represents the sensor at the upstream end whereas WSM 8 (Channel 24) represents the sensor at the downstream end of the channel. Comparison of water levels in all the simulations in this study has been done using data recorded at these sensor locations. Sensors named WSM1 to WSM 8 shall be used as sensor numbers 1 to 8 throughout this thesis. Any references to the sensor numbers shall be referenced to this section.
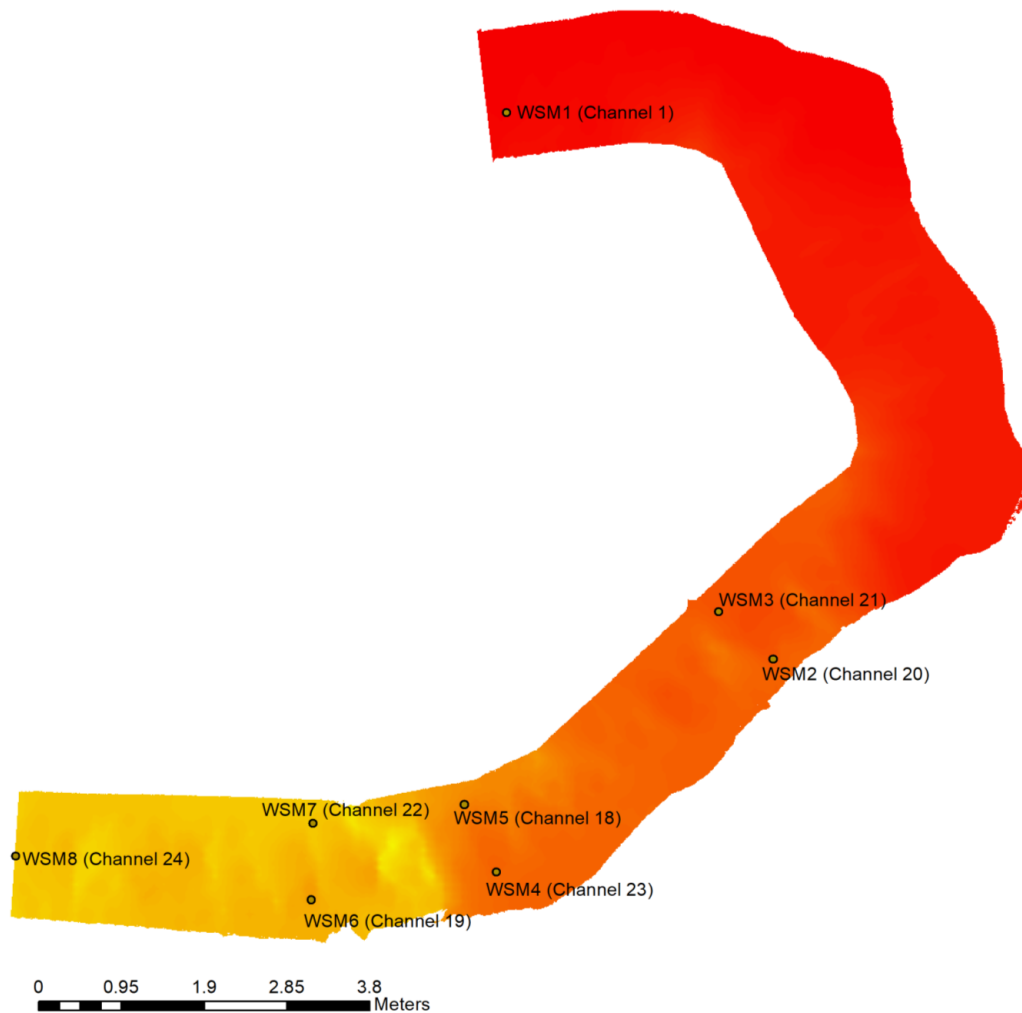
Figure 6.2: Water Level Sensors Location

6.1.2   Selection of Data for Calibration

To select the time stamps for calibration, water level elevations for entire run time for each sensors were plotted. Figure 6.3 is a sample data series for measured WSE. Similar data has been used throughout the cases in this study. It shows that the water levels are stable around 720 seconds. So, water levels from 720 seconds was used to calibrate the initial terrain model. And water level elevation of around 5000 seconds was used to calibrate the final terrain model. It is because at the time stamp of 720 seconds, there is little to no sediment movement which represents the initial terrain. Whereas, at the time stamp of 5000 seconds, there is maximum sediment transport as represented by the final terrain.
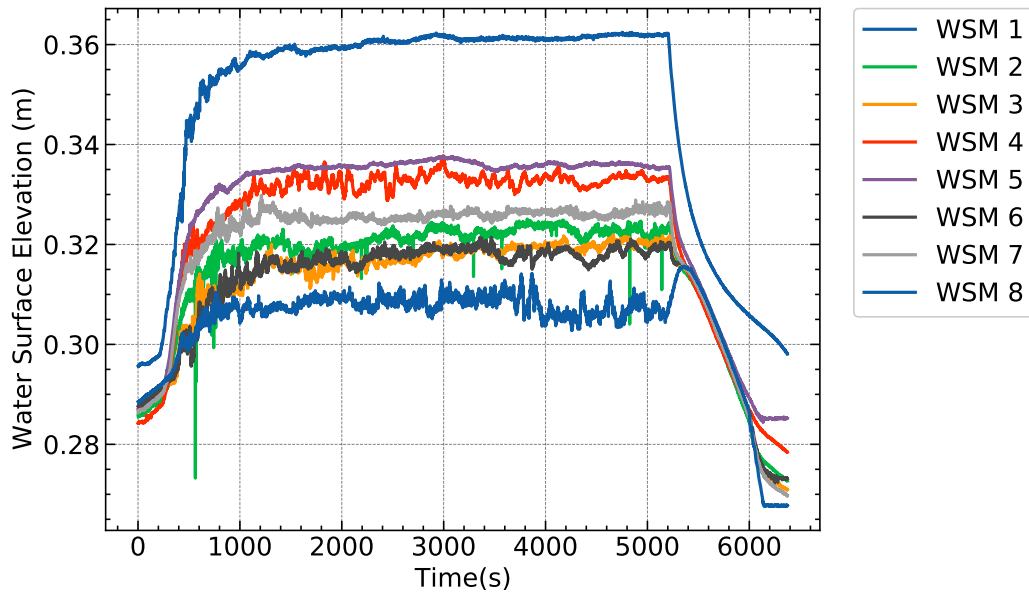
Figure 6.3: A typical plot for observed water sensor data

The rising limb on the left shows filling up of water in the channel. The falling limb on the right shows draining out of water after the completion of test. The plot is stable during the test run from 720 seconds to 5000 seconds. WSM 1 to WSM 8 represents the sensors from 1 to 8 as shown in Figure 6.3.

6.2 Grid Size Independence Test

To decide on the size of grid for computation, the grid size independence test was carried out. For this, the simulation was done with a constant manning's number of 0.01 with the grid sizes ranging from 0.05 m to 0.2 m. Figure 6.4 shows the plot of different values obtained by changing the grids. These values are presented in Appendix Table A.1.
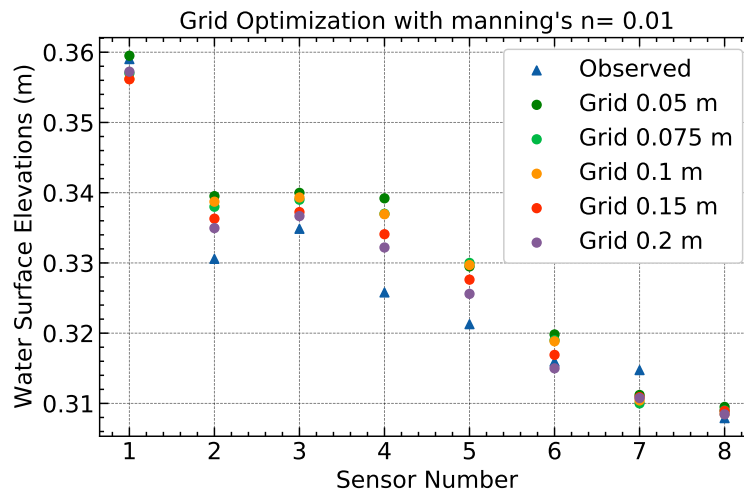
Figure 6.4: Grid size optimization with manning's n = 0.01

The computation showed a good result when the grid size of 0.2m was used. But this grid size was considered quite big for the model. So, various simulations were done reducing the grid size by constant ratio and the difference in results obtained with the reduction in grid size was calculated. Figure 6.5 shows that when grid size was reduced from 0.1m to 0.075m, the difference obtained is close to zero for most of the sensor data. The values used for this plot is presented in Appendix Table A.2.
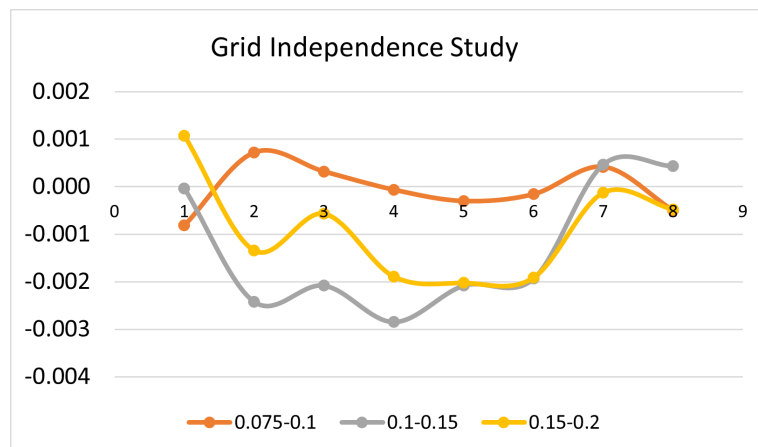
Figure 6.5: Grid Size Independence Study

Figure 6.5 shows that when the grid size was reduced from 0.1m to 0.075m, the difference in results obtained was minimal restricting the difference values near to zero. In order to check this, the number of cell faces associated with different grid sizes was found. Table 6.1 shows the number of computation cell faces with each cell sizes used. Water surface elevations from each of these settings were determined and compared with the observed values. The total absolute differences between the observed and simulated elevations were determined and plotted as shown in Figure 6.5.

Table 6.1: Number of cell faces associated to different grid sizes

Grid sizes	0.050	0.075	0.1	0.15
No of Cell Faces	33891	15120	8962	4054
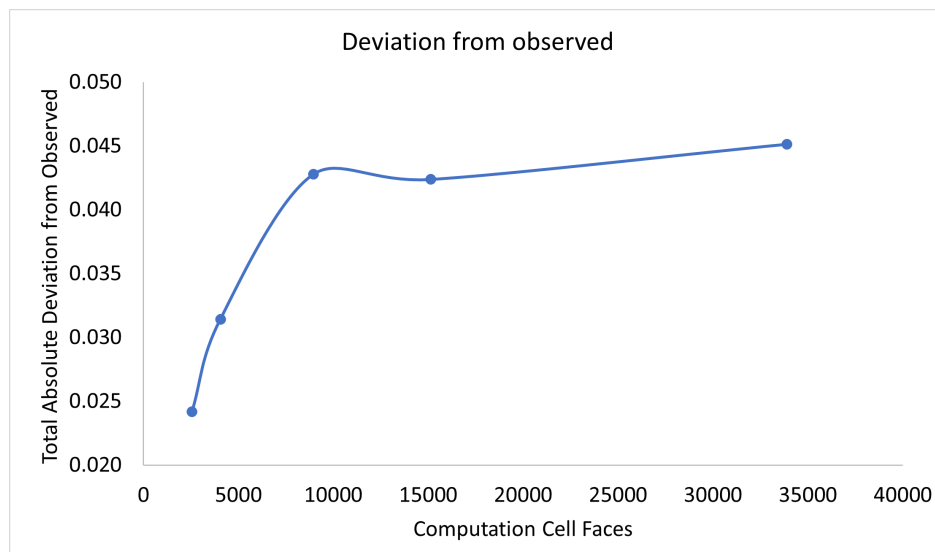
Figure 6.6: Deviation from observed values based on number of cell faces

Figure 6.6 shows that when the number of computation cell faces were increased from 4054 to 8962, the total difference in the result increased considerably. When the cell faces were increased from 8962 to 15120, the difference in result was not found to be too large. So, in order to reduce the total computation time, 8962 cell faces were taken for further analysis. This number of cell faces corresponds to the cell size of 0.1 m. From this test, it is clear that the results obtained from the simulation is free from grid effects. Though the results obtained from larger grid cells were good, significant effects of cell size was observed and hence was discarded. Grid size of 0.1m was taken for further analysis.

6.3 Calibration Using Manning's n

After obtaining the optimum grid size for computation, model was further calibrated using manning roughness coefficient n. Water surface elevations at different time steps were provided as the downstream boundary conditions to calibrate the model. Manning's number was taken as the calibration parameter. Manning's number used in the calibration of initial plain bed ranges from 0.005 to 0.01. Coefficient of determination (R^2) was calculated to find the accuracy of simulated result. Same value of n was used for the entire terrain.
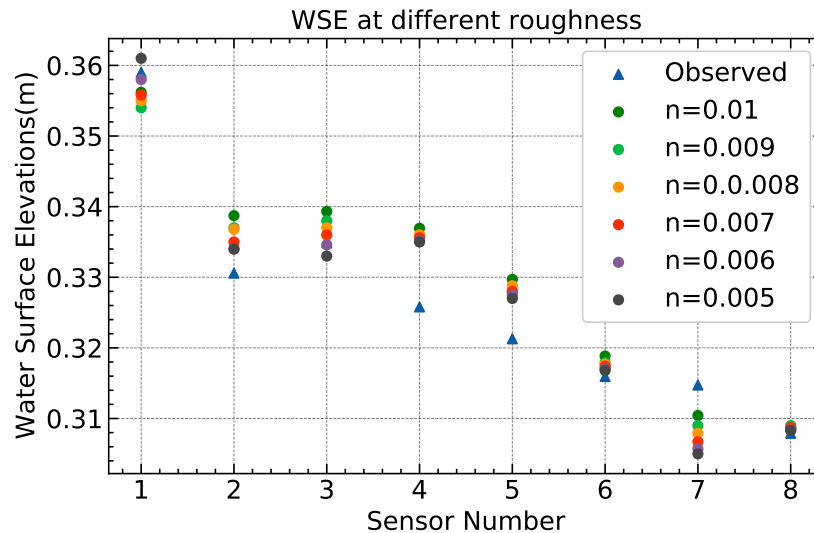
Figure 6.7: WSE at different roughness for initial run

Figure 6.7 shows that manning's number of 0.006 gave the result closest to the observed water surface elevation. It gave the highest coefficient of determination (R^2) of 0.87. Increasing and decreasing the manning's number resulted in lower value of R^2 value as can be seen in Figure 6.9 a. Statistical index (R^2) was used to determine the closeness of simulated values with the observed values. The values used for this plot has been presented in Appendix Table A.4.

Same steps were repeated for the calibration of final terrain model. A final terrain model is the one which is obtained by scanning the physical model after the sediment test is complete. It means that this terrain model contains ripples and dunes, erosion and sedimentation sections. Hence, the manning's n value can be different for this terrain. To calibrate this model, optimized grid size of 0.1m was used and n values were varied from 0.008 to 0.02. The obtained water surface elevations were compared with the observed values which is presented in the Figure 6.8. The values used for this plot has been presented in Appendix Table A.5.
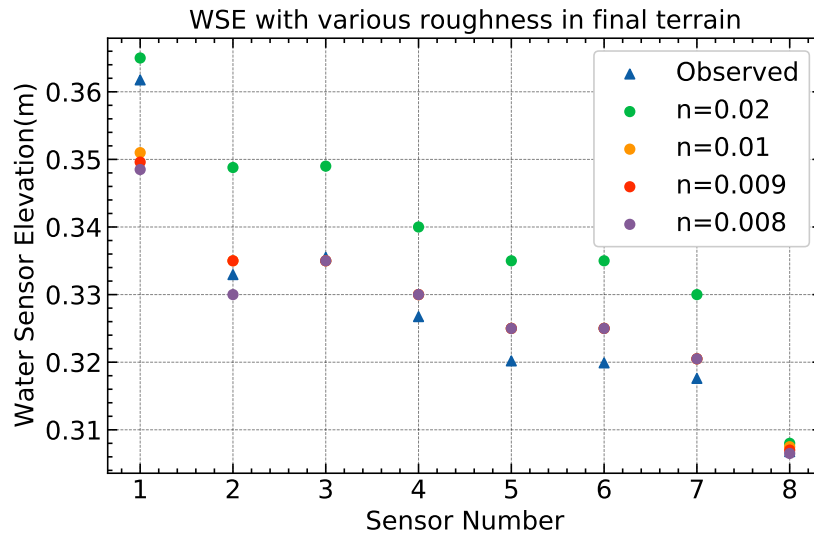
Figure 6.8: WSE at different roughness for final terrain

It was found that the simulated results were closer to the observed values at the manning's roughness of 0.01 with coefficient of determination (R^2) of 0.9 as shown in Figure 6.9 (b). Hence, this value was used for further simulations.
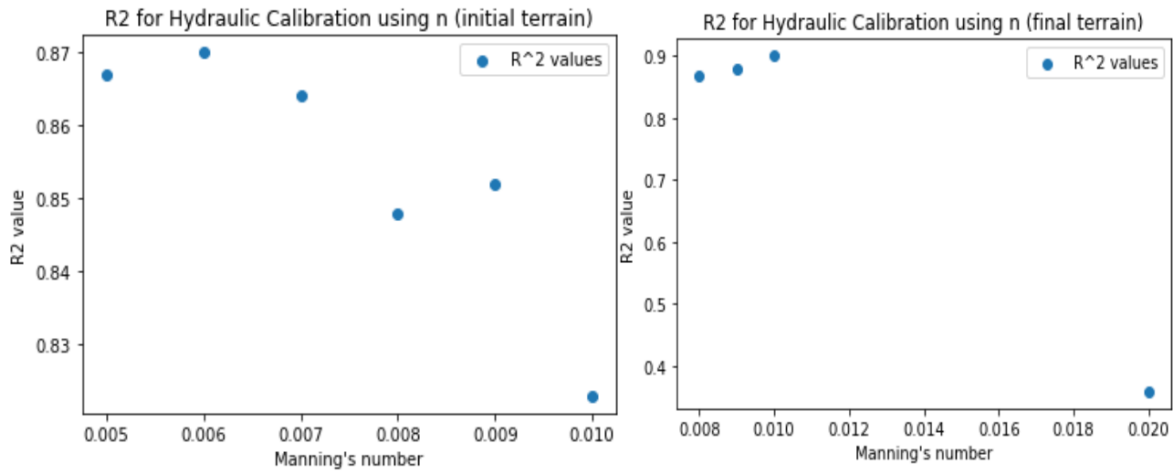
Figure 6.9: R^2 plot for (a). initial terrain model (b). final terrain model

7   2D Sediment Transport Modelling

After calibrating the hydraulic model, sediment transport modelling was done. The model was well calibrated and validated before running the bed transport model.The physical model test was carried out for 35 l/s ($0.035m^3$/s) and the same was used for sediment modelling. Downstream stage hydrograph was used as boundary condition with respective stage height for each test cases. The model grid and manning roughness values were adopted from calibrated hydraulic model. The flow of 5 l/s ($0.005m^3$/s) was used for the bypass channel. Same input data and parameters used in hydraulic simulation were used in sediment modelling. It includes the input geometry, grid sizes, break lines, hydraulic boundary conditions, hydraulic equations, time steps, courant conditions, manning's roughness coefficient etc. Only the settings and input specific to the sediment modelling was changed.

Various transport functions were tested for simulation of sediment transport model. With careful understanding of hydraulic conditions, assumption and grain sizes, few transport functions were used and the results were compared. Finally, Meyer Peter Muller transport function was chosen for all the sediment transport simulation. Active layer was used as the sorting method. Van Rijn method was used as the sediment fall velocity method. Clear water boundary condition was defined for the upstream boundary of terrain as no sediment was introduced externally. In the active layer options, the active layer thickness of xd90 was taken with multiplier of 10 as the bed material was sand.

Percentage finer was used to plot the gradation profile of the bed material. The percentage finer was defined by the upper bound of each grain class. As seen in Figure A.2, all the materials passed through 1 mm sieve size and retained in 0.075 mm. The terrain has been divided into two different regions. The side walls were defined as "non- erodible surface" whereas the channel bed was defined as "bed gradation" with the particle size distribution shown in Figure A.2.

Simulation of sediment transport through the terrain was done for different cases. The simulation can be divided into three different phases/cases:

- Transport of Sediment in Main Channel

- Effect of Sediment Bypass Tunnel on Sediment Diversion

- Effect of Guide walls on Sediment Diversion

These tests were performed in the physical model. Numerical simulation was done to analyse the difference in results from physical observation. All of the cases are described in detail below:

7.1 Transport of Sediment in Main Channel

For this case, the sediment transport in only the main flow channel was considered without the use of bypass channel. This test was performed to see the accuracy of HEC-RAS in sediment modelling as well as for the purpose of evaluation. Careful simulation of this case could help to assign the calibration parameters and observe how representative the results were. Manning's number of 0.1 was used as calibrated in hydraulic model. Various transport functions were used and compared to determine the best function and parameters for further computations. The simulation was done for 3 hours as in the physical model.

7.1.1 Comparison of Bed Change Pattern

Various transport functions were used in the sediment model to achieve best results with bed change and sediment output in downstream. Different functions resulted in different output along the cross sections. All these trial tests were done to find out the best transport function to be used for all other simulations. Figure 7.1 shows the location of profile lines used for comparison of bed changes in cross sections numbered from 1 to 6. The lines were drawn with respect to the position of water level sensors. Arrows represent the orientation of cross section lines from left to right in the direction of flow. Figure 7.2 shows the changes in bed elevation at different locations indicated in Figure 7.1 as observed in the physical model.
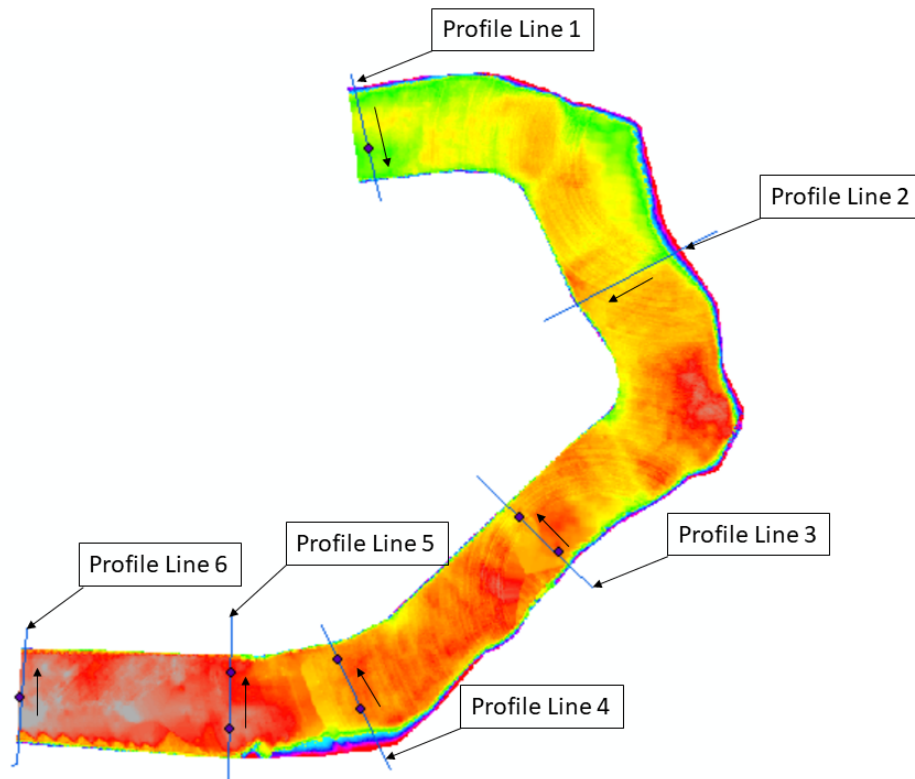
Figure 7.1: Location of Profile Lines
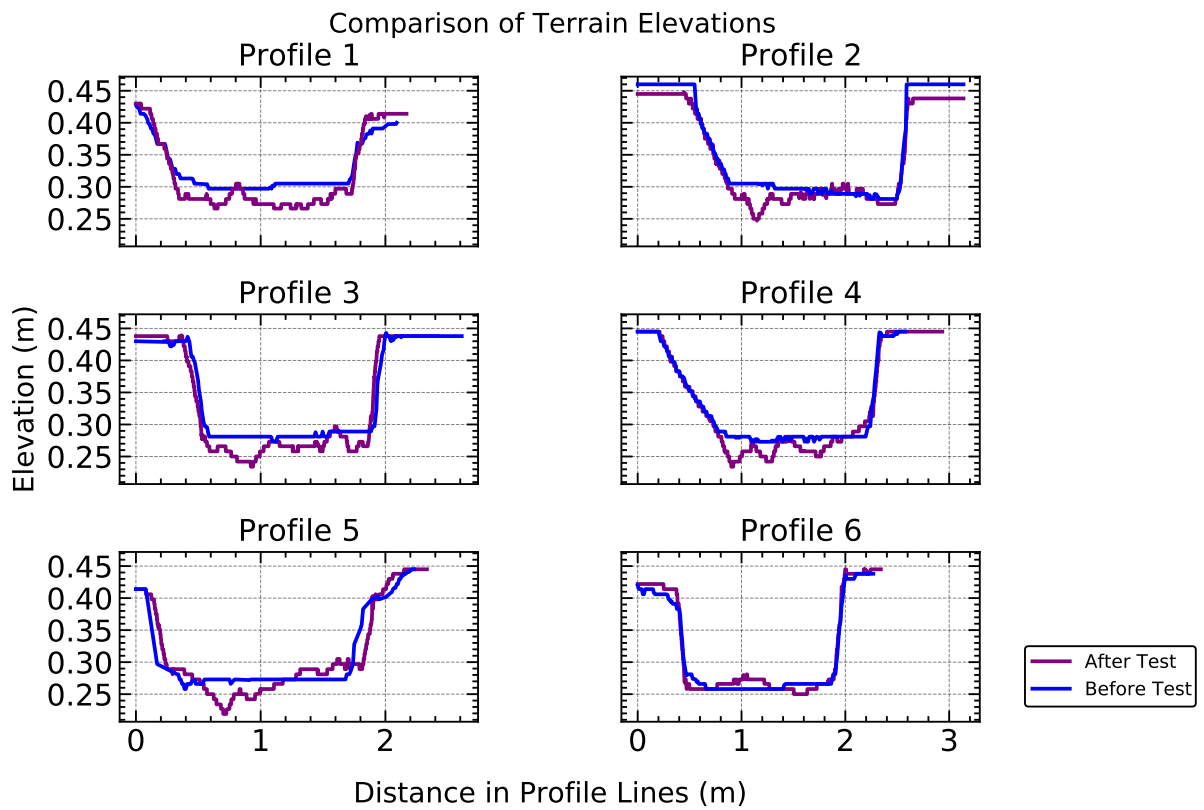
Figure 7.2: Comparison of terrain elevations before and after test

Figure 7.2 shows that there is erosion on the outer bend and deposition on the inner bend. High erosion can be seen in the upstream section of the channel represented by profile 1. The maximum depth of erosion along the selected sections is observed to be around 4 cm in profile 5.

Numerical simulations of this case were done using various transport functions and the results are briefly described below.

Meyer Peter Muller (MPM)

MPM was used because it is the bed load transport function and is primarily based on experimental data. The particle size ranges from 0.4 to 29 which is for well graded sediment. The width of test flume ranges from 0.5 ft to 6.6 ft (Brunner, 2022b), which is closer to the physical case model in this study . Use of Meyer Peter Muller transport function gives a very close approximation of the observed bed changes in physical model as can be seen in Figure 7.3. It seems to overestimate the erosion near profile 1. The minimum elevation level in simulation was found to be in profile 1 which is close to 0.2m with the total erosion thickness of about 10cm. But only 4cm was observed in this section in physical model. However, for other reference profile lines, it seems to approximate the observed values.
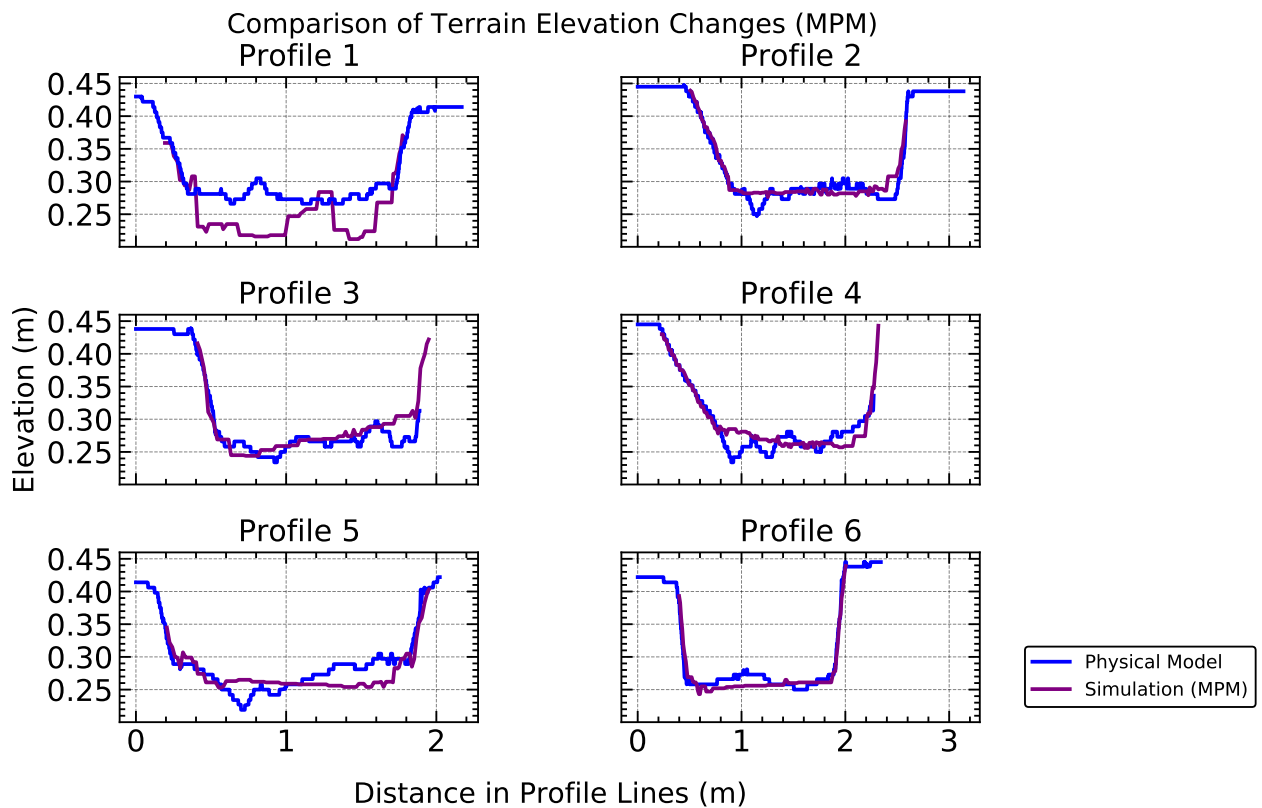
Figure 7.3: Comparison of observed and simulated bed elevations using MPM

Yang

Yang's method was used because the research for yang's formula was performed in flume experiments and also with field data under wide range of conditions in alluvial channel. The particle size ranges from 0.062 to 7 mm which is between 0.1mm to 0.75mm in the physical model. The energy slope used in Yang's experiment is from 0.000043 to 0.029 (Brunner, 2022b). Use of Yang transport function gives a good approximation of the observed bed changes in physical model as can be seen in Figure 7.4. There is still some overestimation of changes in the profile 1. Bed change in Profile 1 is a bit less than that in MPM which makes it closer to the observed value. Changes in other location seems similar to that of MPM. The minimum elevation level was found to be in profile 3 which is close to 0.22m with the erosion thickness of 6cm which is close to the observed value. Changes in region around profile 2, profile 3 and profile 4 are not closely simulated.
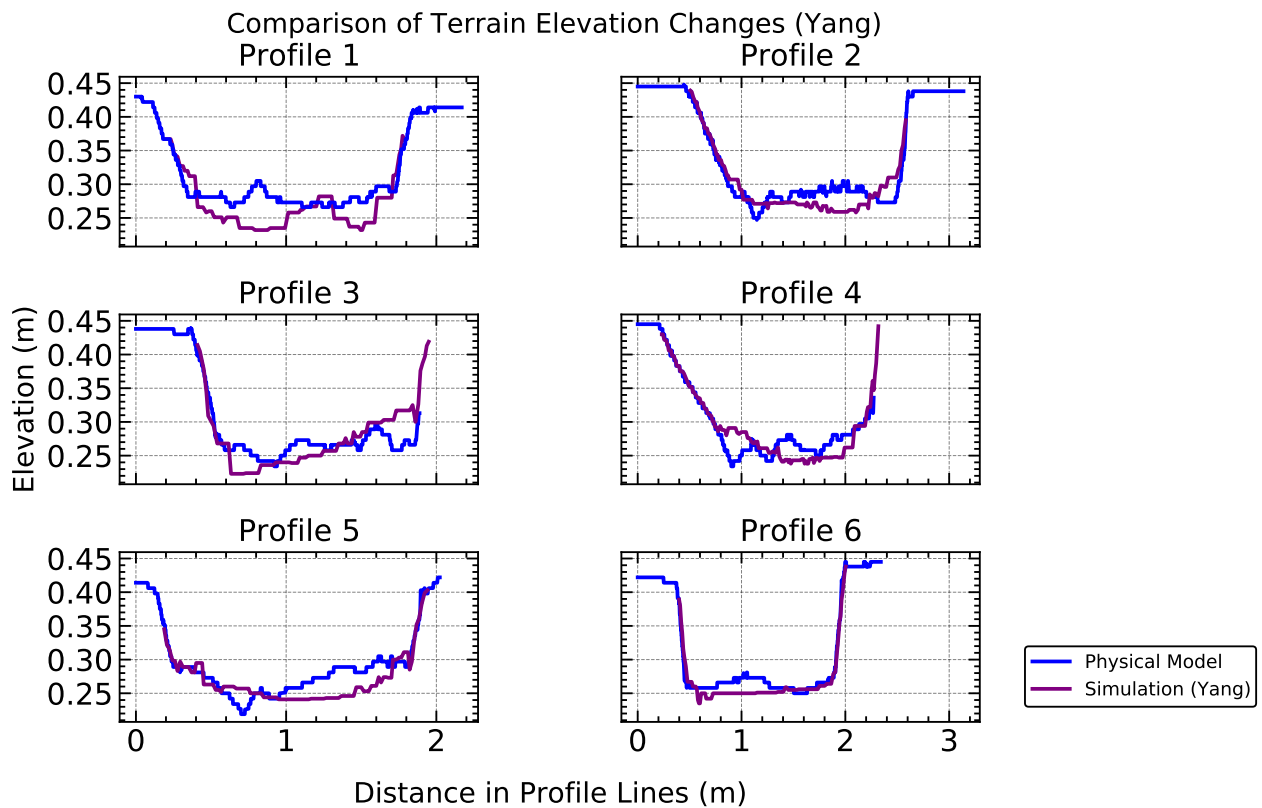
Figure 7.4: Comparison of observed and simulated bed elevations using Yang

41

Ackers White (AW)

This transport function was considered because it is suitable in the case of flume experiments and was originally derived based on 1000 flume experiments. A variety of bed forms were used including plane, rippled, dune forms etc (Brunner, 2022b). The sediment diameters used in this transport function ranges from 0.04 mm to 7 mm which includes the range of prototype used. Use of Ackers and White(AW) transport function provides a very good approximation of the observed bed changes in physical model as can be seen in Figure 7.5. But it does not represent the pattern of erosion and deposition in the selected profile lines. The changes look quite similar to that observed in Yang. The minimum elevation level was found to be in profile 3 which is close to 0.22m with the erosion thickness of 6cm which is close to the observed value. Changes in the other regions are not closely simulated. However, the deviations are not too large.
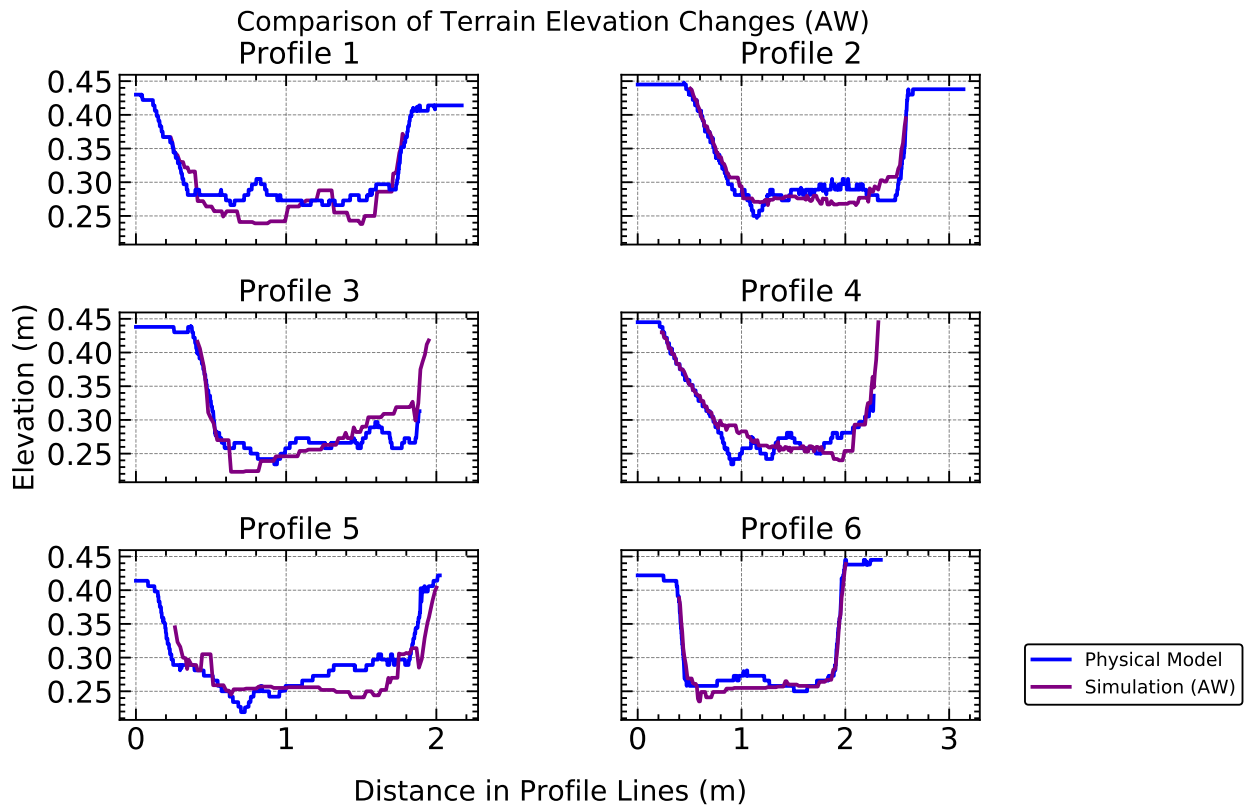
Figure 7.5: Comparison of observed and simulated bed elevations using AW

Van Rijn

Use of Van Rijn transport function provides a reasonable approximation of the observed bed changes in physical model as can be seen in Figure 7.6. But the erosion and deposition are not well represented at different points. Lowest elevation was observed in profile 3 which is 0.22m with the erosion thickness of 6cm which is close to the observed value again. The deviations do not seem to be too large.
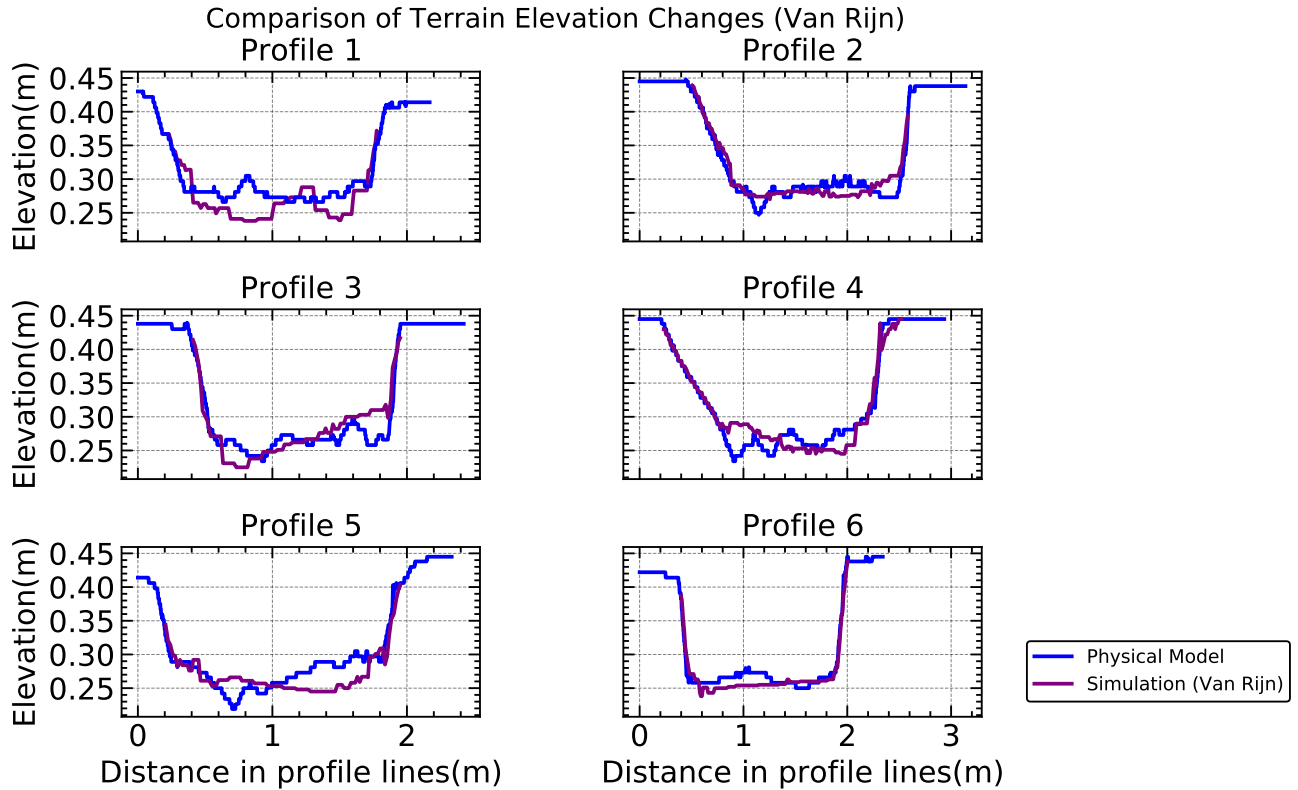
Figure 7.6: Comparison of observed and simulated bed elevations using Van Rijn

Selection of Transport Function

The simulations using four different transport functions were compared to each other and also with the observed change as shown in the Figure 7.7. Graphical comparison shows MPM to represent the observed terrain changes well except for profile 1. MPM is usually used for coarser sand bed. However, according to Table 3.1, it is also applicable in the case where channel depth is 0.03 to 3.9m, energy gradient of 0.0004 to 0.02, width of channel of 0.5 to 6.6 ft which represents the properties of model used in this simulation. This function also represents the pattern of erosion and deposition better than the other transport functions when entire simulated channel is observed as in 7.17.
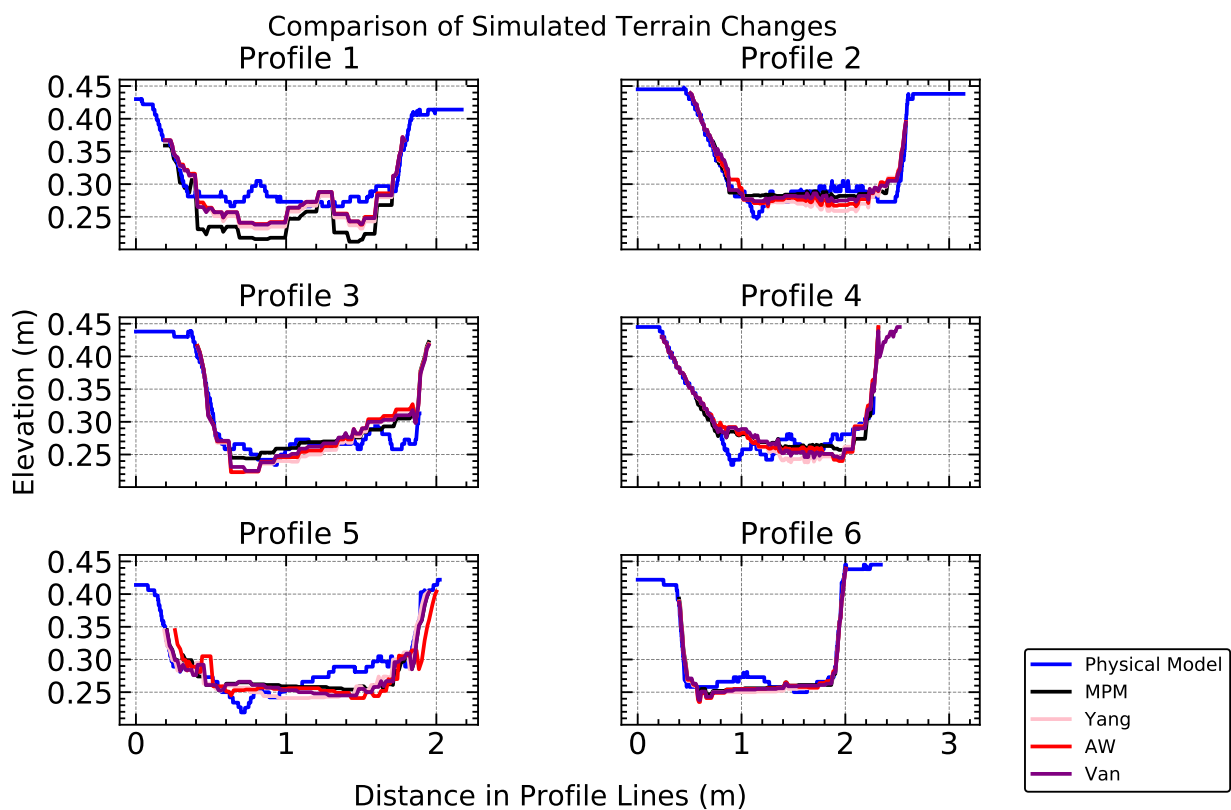
Figure 7.7: Relative comparison of simulated bed elevations using different transport functions

Eventhough the representation of bed elevation seems promising in Figure 7.7, visual interpretation can sometimes be misleading due to the scales of x and y axes. So, statistical analysis was done for all the points along profile lines using four different transport functions shown in Figure 7.7. For this purpose, interpolation was done to determine the same values of x for all y values for both observed and simulated models. Large number of points associated with observed and simulated bed elevations were compared to find the best transport function.
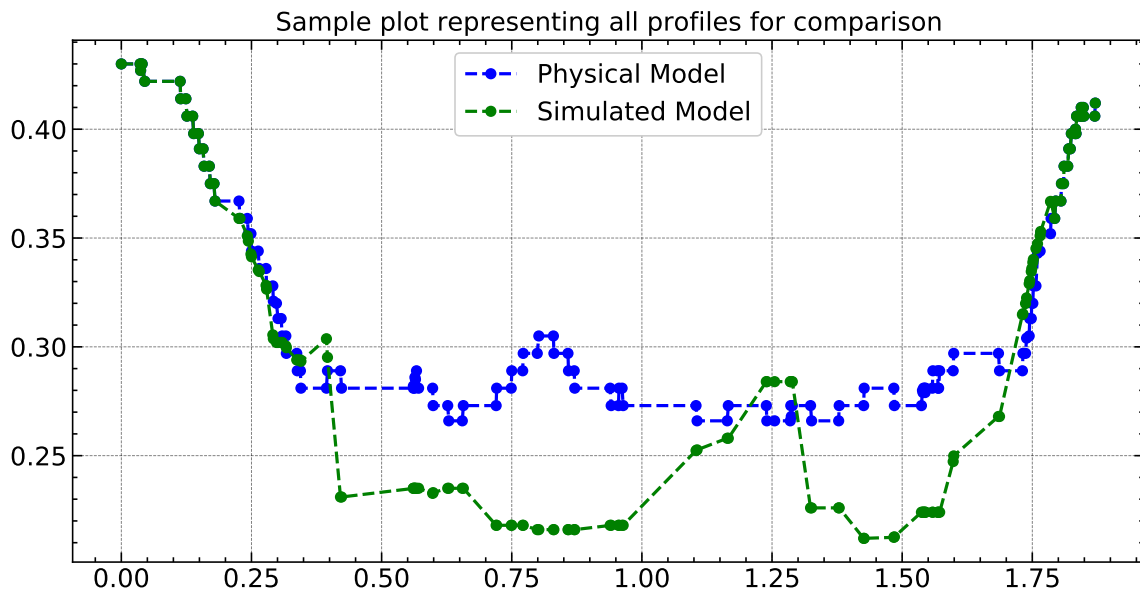
Figure 7.8: Sample plot representing comparison points interpolated for all profile lines

Figure 7.8 presents a sample plot representing all the profile lines from 1 to 6. It shows the points for comparison between bed elevations of terrain obtained from observed and simulated models. The blue plot represents the bed terrain from observed model while green plot represents the bed elevations from simulated model.

Correlation coefficient was calculated between the compared models. The mean absolute error was determined to compare the results from different functions. The function with least value of mean absolute error and highest correlation coefficient can be selected as the best transport function for the model. It is easy to visualize and compare if these values are plotted along with the simulated bed elevations from profile lines obtained using different transport functions.
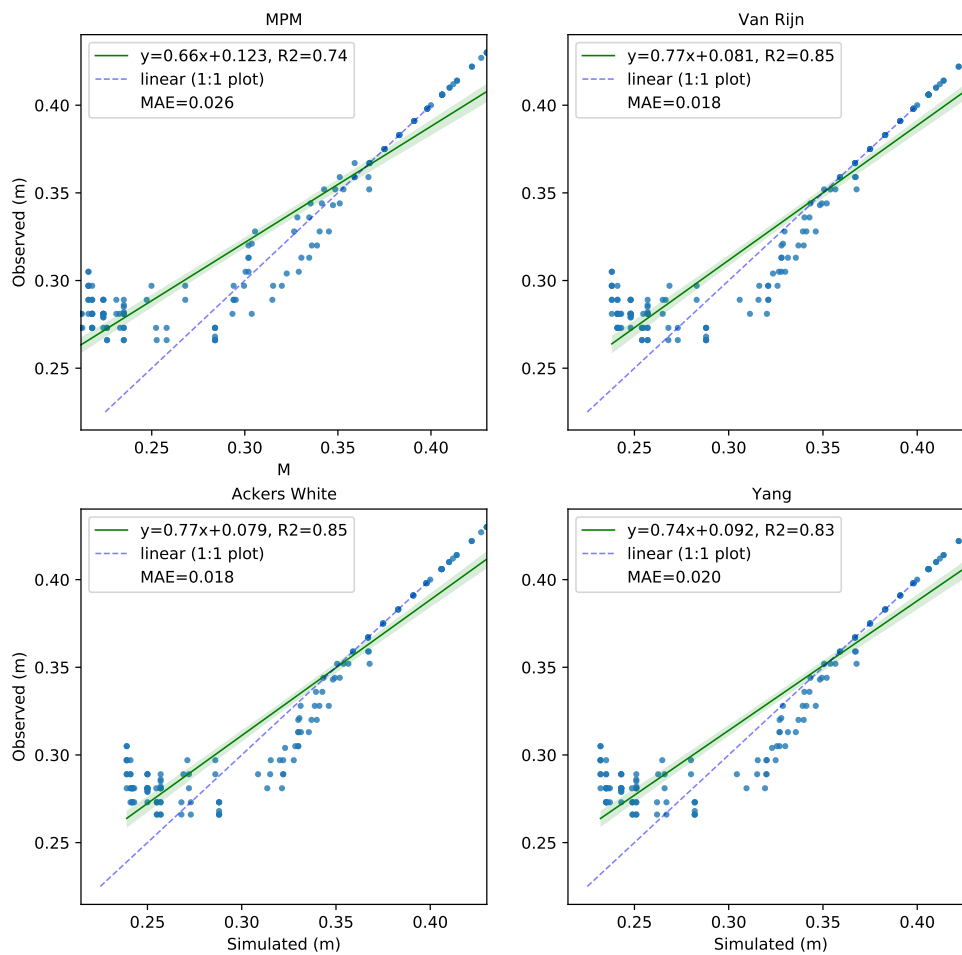
Figure 7.9: Scatter plot of observed vs simulated bed elevations for profile 1 including Mean Absolute Error (MAE) and Correlation Coefficient (R^2)

Figure 7.9 shows the correlation plots for profile 1 generated using different transport functions as shown. From the figure, it can be seen that Van Rijn and Ackers white transport functions show highest correlation coefficient with the value of 0.85 and MPM shows the value of 0.74 which is not bad but the lowest among all. The mean absolute error using MPM function was found to be 0.026 being the highest and 0.018 using Van Rijn being the lowest. Looking at plots and the comparison for profile 1, Van Rijn was found to be the best function for the model.
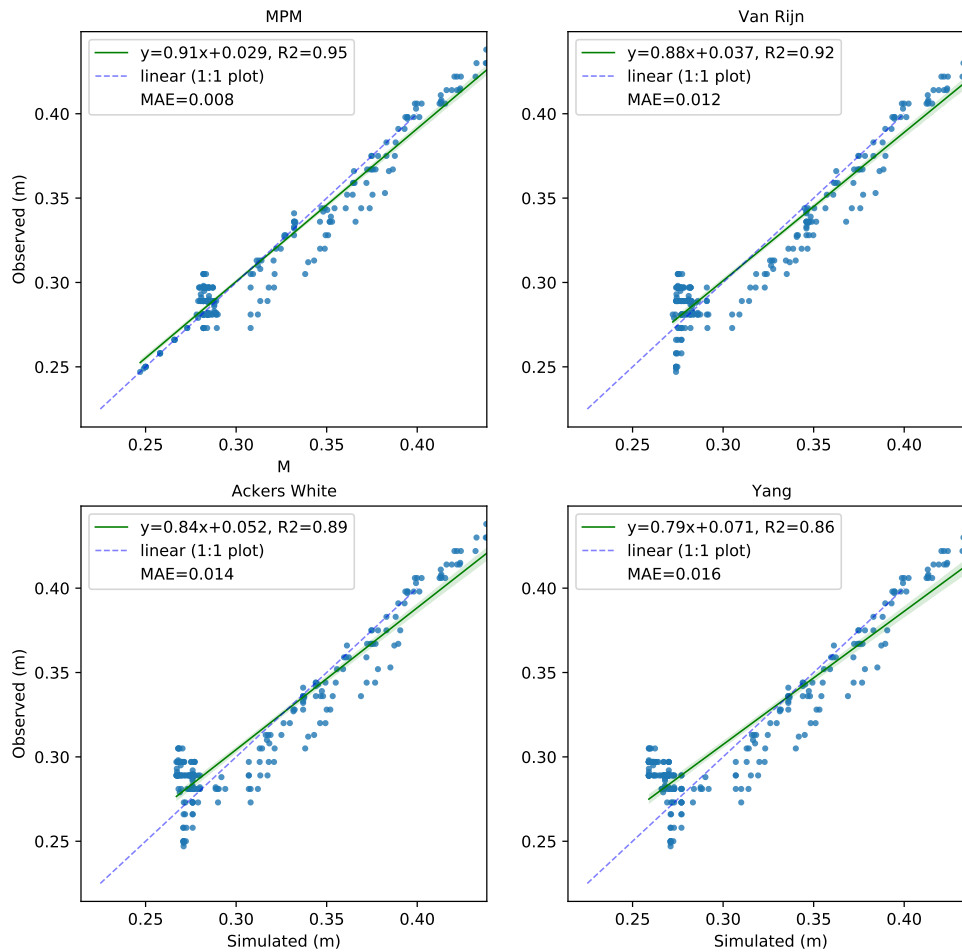
Figure 7.10: Scatter plot of observed vs simulated bed elevations for profile 2 including Mean Absolute Error (MAE) and Correlation Coefficient (R^2)

Figure 7.10 shows the correlation plots for profile 2 generated using different transport functions as shown. From the figure, it can be seen that MPM shows the highest correlation coefficient of 0.95 and lowest mean absolute error of 0.008. Van Rijn and Ackers white transport functions show correlation coefficients of 0.92 and 0.89 which is also very good. Yang gives the coefficient of 0.86. Observing the results for profile 2, MPM is found to be the best function for the model.
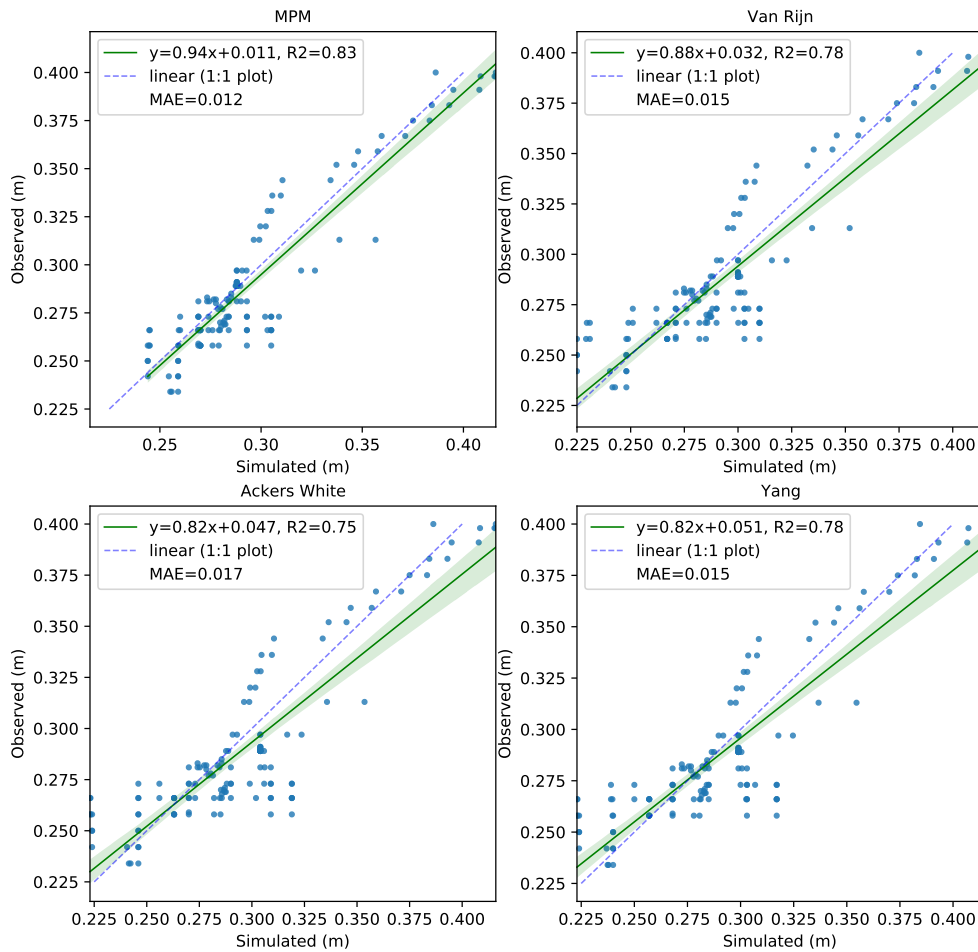
Figure 7.11: Scatter plot of observed vs simulated bed elevations for profile 3 including Mean Absolute Error (MAE) and Correlation Coefficient (R^2)

Figure 7.11 shows the correlation plots for profile 3 generated using four different transport functions as shown. From the figure, it can be seen that MPM shows the highest correlation coefficient of 0.83 and lowest mean absolute error of 0.012. Van Rijn and Yang shows same correlation coefficient of 0.78 with MAE of 0.015. Whereas, Ackers White shows the correlation coefficient of 0.75 with MAE of 0.017.

Correlation fit: Observed vs Simulated bed elevation for Profile 4
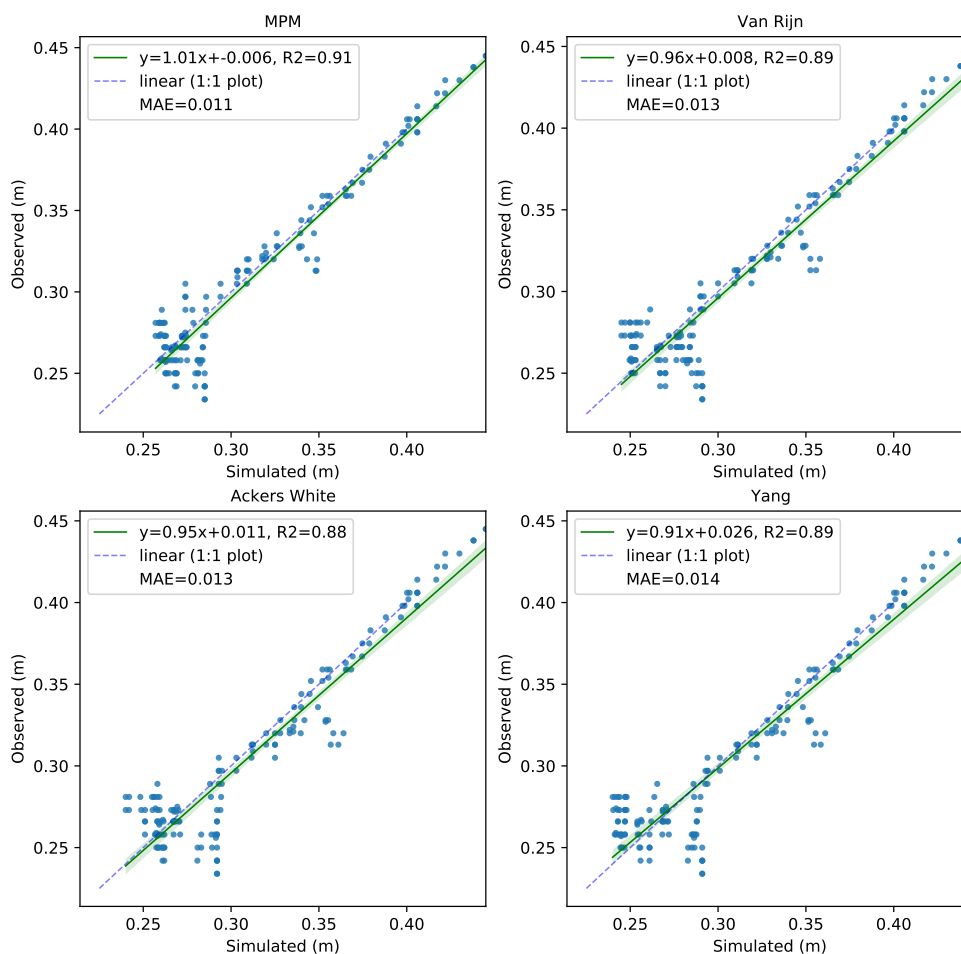
Figure 7.12: Scatter plot of observed vs simulated bed elevations for profile 4 including Mean Absolute Error (MAE) and Correlation Coefficient (R^2)

Figure 7.12 shows the correlation plots for profile 4 and it presents MPM with highest value of correlation coefficient of 0.91 with MAE of 0.011 followed by Van Rijn and Yang with the same correlation coefficient of 0.89 whereas the MAE using Van Rijn is 0.013 which is lower compared to Yang with MAE of 0.014. Correlation coefficient using Ackers White was found to be 0.88.

Correlation fit: Observed vs Simulated bed elevation for Profile 5
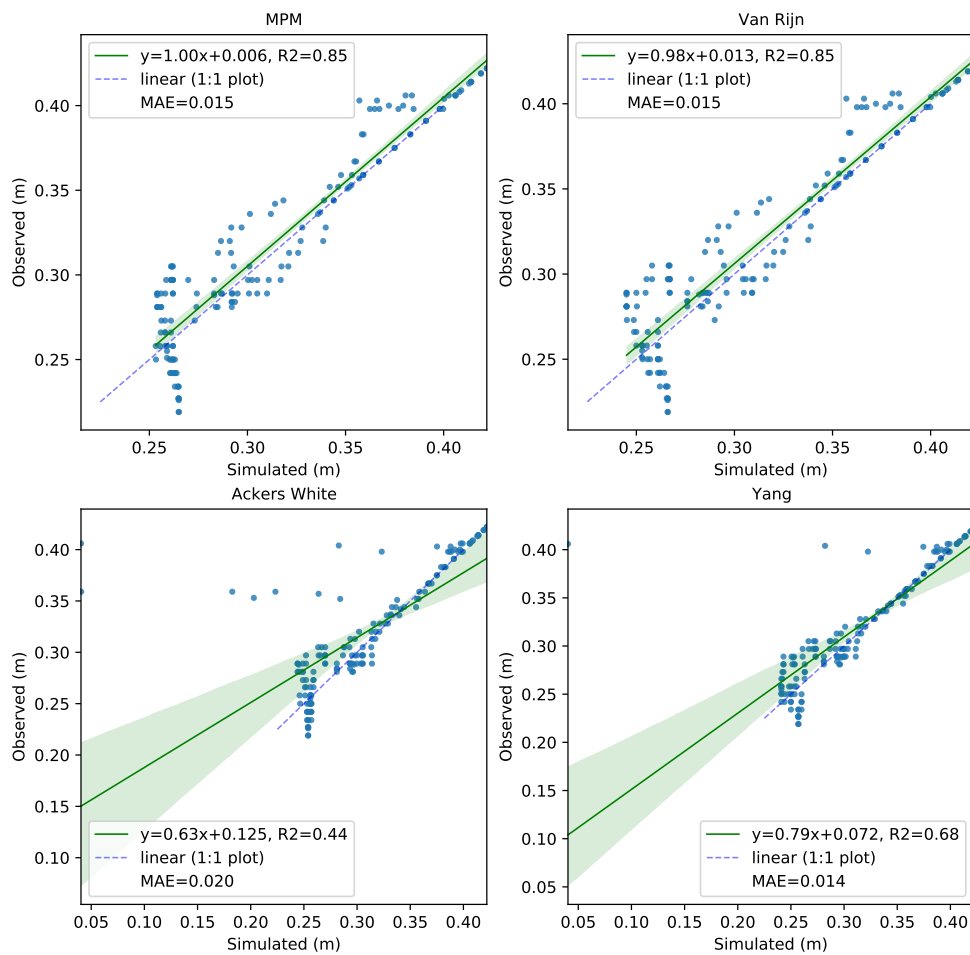
Figure 7.13: Scatter plot of observed vs simulated bed elevations for profile 5 including Mean Absolute Error (MAE) and Correlation Coefficient (R^2)

Figure 7.13 shows the correlation plots for profile 5 and it presents MPM and Van Rijn with highest value of correlation coefficient of 0.85 and lowest MAE of 0.015. Yang shows a good correlation with coefficient of 0.68 and MAE of 0.014. Ackers White gives a poor correlation coefficient of 0.44 and with MAE of 0.020.

Correlation fit: Observed vs Simulated bed elevation for Profile 6
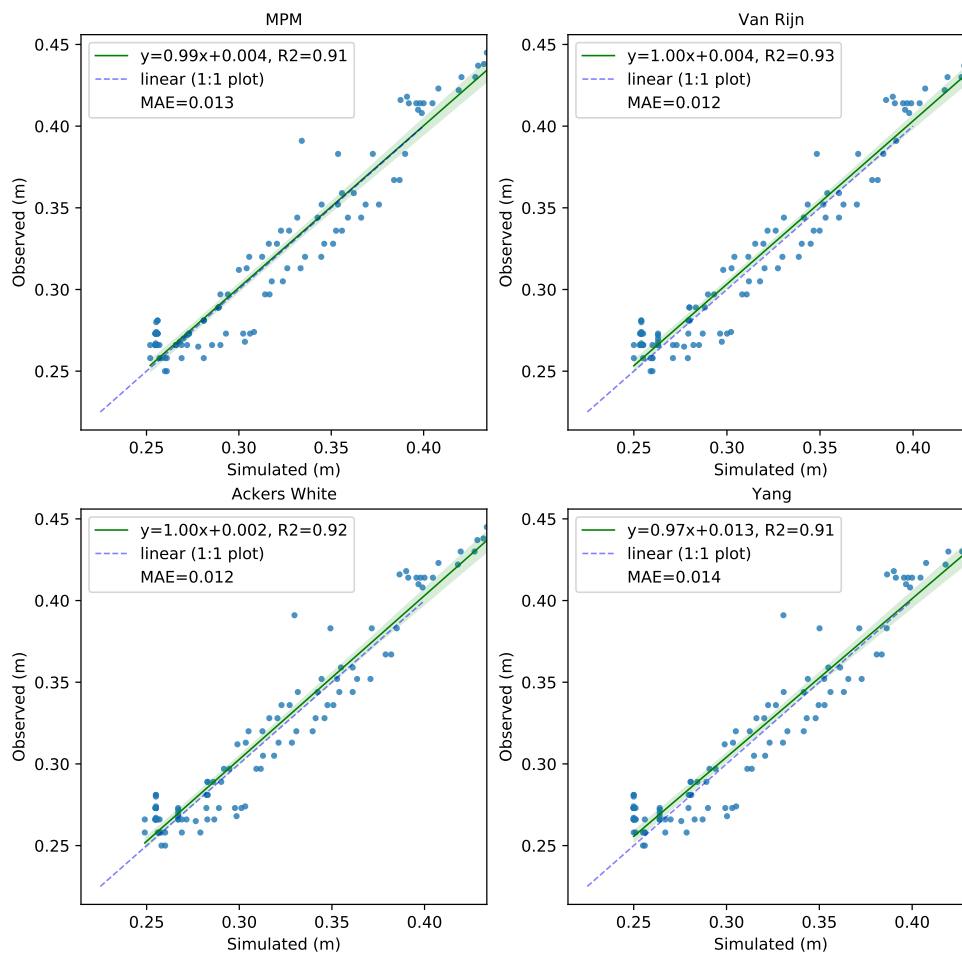
Figure 7.14: Scatter plot of observed vs simulated bed elevations for profile 6 including Mean Absolute Error (MAE) and Correlation Coefficient (R^2)

Scatter plot for profile 6 in Figure 7.14 shows good agreement between observed and simulated terrain points with correlation coefficients above 0.90 for all the transport functions and MAE below 0.014.

The presented statistical analyses for all the profile lines show that MPM function results in very good correlation between the observed and simulated model with low mean absolute error except for profile 1 representing the start of channel. So, the Meyer Peter Muller transport function can be considered as the best for this model. However, the results from Van Rijn is almost close to that of Meyer Peter Muller function in all the comparisons. So

it cannot be ignored completely. In order to find the best function between MPM and Van Rijn, bed change maps for these functions were plotted for another visual comparison.
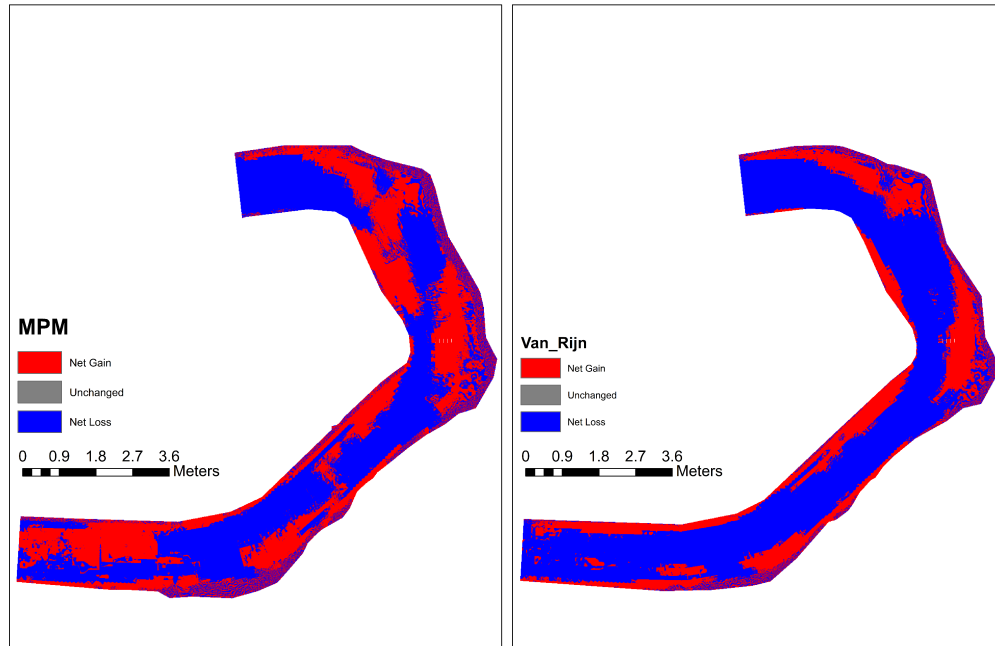
Figure 7.15: Comparison of Bed Changes obtained from (a). MPM vs (b). Van Rijn

Figure 7.15 (a) and (b) shows the comparison between bed change maps generated using MPM and Van Rijn respectively. MPM results in both erosion as well as deposition whereas Van Rijn results in more erosion as represented by blue area around center and downstream. These maps can be compared with the observed map of bed changes as shown in Figure 7.17 (a). Comparing these two figures and also with the observed map, it can be clearly seen that the MPM function represents the model change well compared to Van Rijn and other functions. Specially, the area around the first bend and around the downstream are well represented by MPM function. Therefore, MPM was selected for further computation and simulations. Note: The comparison shown in Figure 7.15 shall be read along with Figure 7.17 (a) for proper understanding.

Though the pattern of erosion and sedimentation looks promising in MPM function, the amount of sediment eroded from the channel to downstream was more compared to observed mass of sediment collected in physical model. Hence, if the MPM function was to be used, it had to be calibrated before further simulations were carried out.

7.1.2   Calibration of Transport Function

Sediment transported to the downstream area were collected, dried and weighted for every tests in physical model. The dry weight of sediment collected in the downstream for this test was found to be around 150 kg. In the simulated model, sediment concentration data at the downstream boundary was extracted and converted to weight using simple calculation in python. The simulated weight at the downstream of channel was found to be around 360 kg. So the transport function has to be calibrated to match the observed and calibrated results.

There are two methods to calibrate the transport functions. One is to change the individual parameters and coefficients in the transport equation. Equation 30 is used in HEC-RAS to compute the transport using MPM. Default setting uses the coefficient of 8, critical shield's stress of 0.047 and the power raised to 1.5. These can be changed depending on the condition of the model to get output close to the observed one. Wong and Parker (2006) proposed a correction to Equation 31, which can also be used in HEC-RAS automatically. However, it is recommended to use the scaling factors to calibrate the model. It is found under Options in sediment data editor. Increase in Transport Function Scaling Factor increases the transport whereas increase in Critical Mobility Scaling Factor reduces the transport (Alejandro Sanchez, 2020). With several trials and errors, Transport function scaling factor was set to 0.5 and critical mobility scaling factor was set to 5 as shown in Table 7.1. The use of this calibration factor reduced the sediment output mass to 165.195 kg which is close to the value obtained in physical model.

Table 7.1: Calibration of MPM Function

Scaling Factors		
Calibrating Factor	Value	Function
Transport Function Scaling Factor	0.5	Increasing this factor increases transport
Critical Mobility Scaling Factor	5	Increasing this factor reduced transport

7.1.3   Results from Calibrated Model

Calibrated model resulted in slightly lower erosion from the channel. Change in scaling factors resulted the model to be similar to the physical model. Figure 7.16 shows the comparison between observed, simulated and calibrated results. The problem with high erosion volume along Profile 1 seems to have reduced with the use of scaling factors. Similarly, the erosion - deposition pattern seems to have improved in Profile 2, Profile 3 and Profile 5. While the pattern in other profile lines seem unchanged.
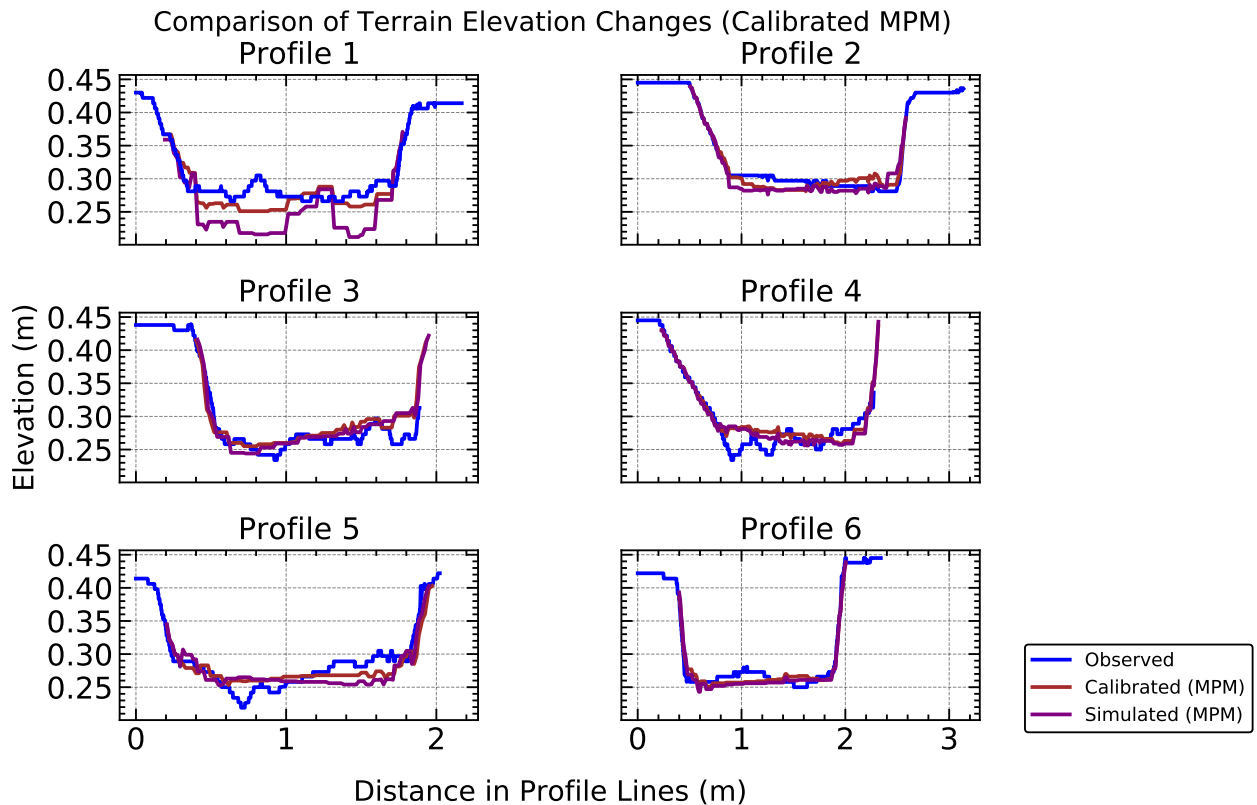
Figure 7.16: Changes in bed elevation with a Calibrated MPM function

Figure 7.16 shows the changes along six profiles. However, the bed changes exist over the entire flow area. To visualize the changes across the entire channel, a bed change plot has to be plotted as shown in Figure 7.17.
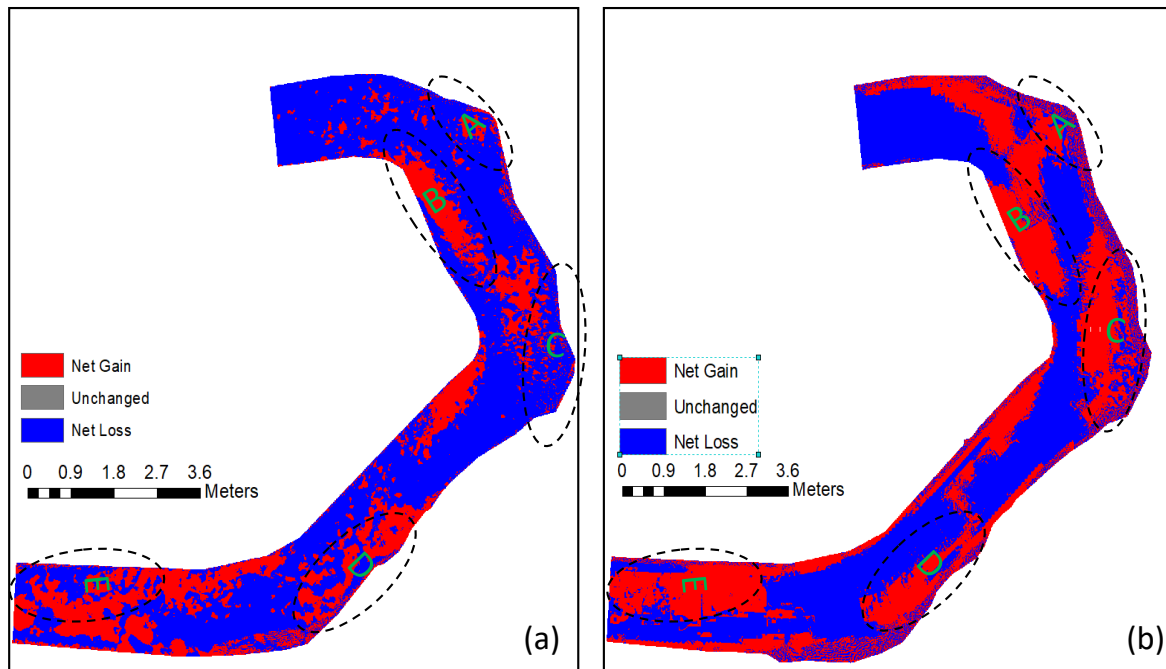
Figure 7.17: Comparison of Bed Changes : (a). Observed vs (b). Simulated

Figure 7.17 shows the comparison of bed changes between observed (a) and simulated (b) model. Red area represents the net deposition in channel while blue area represents the net erosion. It can be seen that the general pattern of simulated bed change matches with the bed changes in physical model. Deposition takes place in the inner bend and erosion in outer bend. Observing the area distribution, it seems to have over predicted the changes in upstream area while in the downstream area specially after the bend, the pattern is similar. However, the depth of erosion and deposition is not that high and the volume of sediment eroded is similar to that of the observed one. The entire area has been divided into five zones from A to E for comparison. The simulated model shows overestimation of deposition in zone A. There is more erosion in zone A in the observed model and few patterns of deposition. Zone B seems similar in both the observed and simulated models. It is the inner bend where deposition seems dominant. Zone C has similar pattern but the deposition is more in the case of simulated model. Zone D and E also seems to represent the results from physical model.

From these comparisons, it is quite clear that HEC-RAS 2D is able to simulate the water surface elevation, bed surface elevation as well as pattern of bed changes.

7.2 Effect of Sediment Bypass Channel on Sediment Diversion

A sediment bypass channel was added in the model to check its effect on sediment diversion. It was introduced at the same point as in the physical model. The opening of bypass intake is 15cm x 15cm with invert at 10cm. It consists of a gate to regulate the flow through the bypass channel. An inclination of about 45 degrees exists right after the intake. A similar structure has been introduced in the numerical model.

7.2.1 Defining Bypass Channel

As the scanning of bypass section was difficult, the terrain model of it was not available. So, it had to be defined in HEC-RAS to imitate the physical structure. This was done using a feature called Terrain Modification in RAS Mapper. 1D and 2D capabilities of HEC-RAS was used to solve this problem. Cross sections were defined with required elevation points to create an interpolated surface layer which was later added to the existing terrain. This layer replaces the overlapped terrain values and defines a new region with desired values and terrain shape.
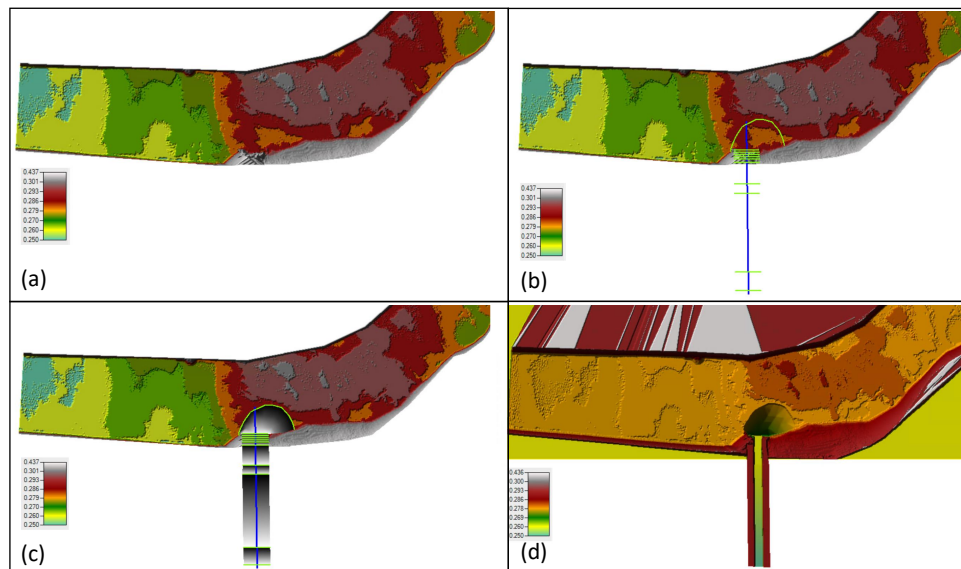
Figure 7.18: Terrain Modification to define bypass channel (a). Existing Terrain (b). Defining Cross Sections (c).Interpolation of cross sections (d). Merged Terrain

Figure 7.18 (a) shows the existing terrain where the bypass section is to be added. Figure 7.18 (b) shows the definition of a river channel with several cross-sections. Each of these cross sections have defined points to shape the sections for bypass channel. The invert levels for each cross sections differs to provide the necessary slope for the flow. The invert level at intake is 0.1m. The width of channel was defined as 15cm. After defining the cross sections, it is interpolated to get a raster as shown in Figure 7.18 (c) . This layer is then exported as a

raster. When this exported layer is imported as a terrain along with the existing terrain file, the merged terrain in Figure 7.18 (d) is obtained.

7.2.2 Modelling of Bypass Gate

A gate was introduced in the sediment bypass channel to regulate the flow. SA/2D Area Conn feature in HEC-RAS was used to accomplish this. The line was drawn from left to right in the direction of flow to ensure that the software recognizes upstream and downstream of the gate. The flow area mesh was modified such that the cell faces align with this line. Weir equation was used as a method of overflow computation. Sluice discharge coefficient of 0.5 was taken with orifice coefficient of 0.8. Weir coefficient of 1 was used in the model. Figure 7.19 (a) and (b) show the plan and section view of the gate defined in numerical model.
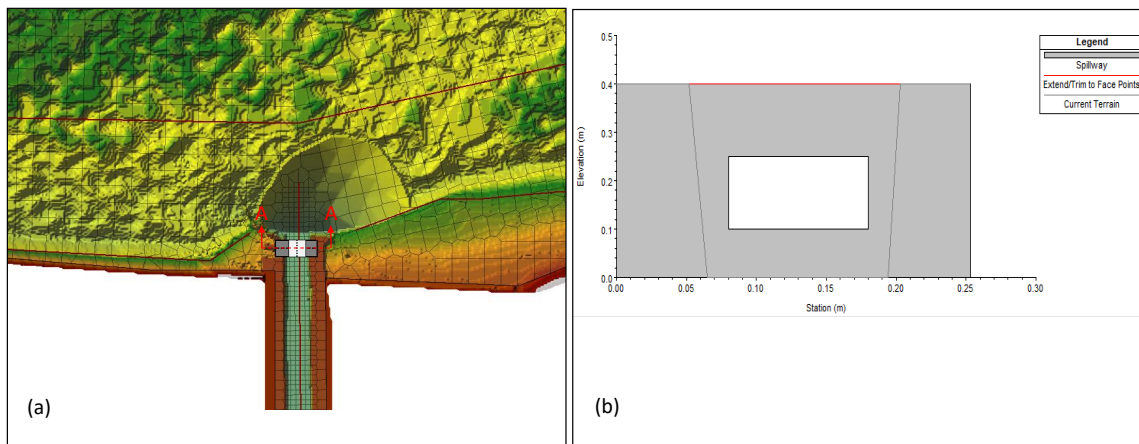
Figure 7.19: Modelling of Bypass Gate: (a). Hydraulic Structure - Gate (Plan view) (b). Hydraulic Structure - Gate (Section A-A)

The opening of the gate was fixed to be the same as in physical model. The white area in Figure 7.19 (b) represents the opening with gate and grey area represents a weir or a barrier. The gate defined here is similar to a sluice gate, opening at the bottom. So, the flow of water is sub-surface. With the introduction of hydraulic structure, a SA/2D area boundary condition needs to be defined for it. In this case, T.S Gate opening was used as the boundary condition where one can define the height of gate opening. Flow Hydrograph with the constant flow of 5 l/s was used as external boundary condition at the end of bypass channel as was done in the physical model.

7.2.3   Hydraulic Simulation

Hydraulic simulation of the model was done to check if the model is hydraulically correct before running the sediment model. Upstream boundary condition with constant flow of 35 l/s was used with the stage hydrograph at the downstream. Constant flow hydrograph of 5 l/s was used in the bypass channel. The gate opening set for hydraulic model was 0.06m. Figure 7.20 shows the water surface elevation profiles through the gate.

(a)   (b)
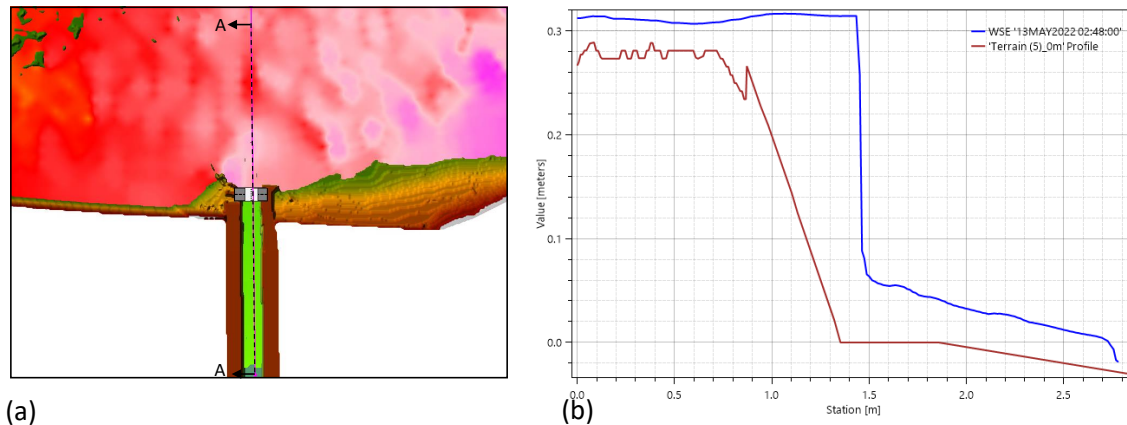
Figure 7.20: (a). Simulation through Bypass Gate (Plan view) (b). Water Surface Elevation (Section A-A)

From Figure 7.20 (b) it can be seen that the water flows through the gate opening forcing it below the elevation of 0.1m. It increases the velocity of flow and increases sediment transport. Velocity of water through the gate is around 1 m/s which is close to what was obtained in the physical model. Water surface elevations at different points were recorded for the entire time and was used to verify if the model was hydraulically correct.

Figure 7.21 and Figure 7.22 shows the comparison of water surface elevation simulated through the gate and observed in the prototype. Figure 7.21 shows that there exists a gap between observed and simulated water levels at and around sensor 4 (WSM4) near the lower bend as shown in Figure 6.2. Small gaps can be seen in WSM 1, WSM 2 and WSM 6 which is only few mm and not so significant. Figure 7.22 shows most of the points are close to the linear plot meaning less differences between observed and simulated models. It also shows the correlation coefficient of about 78% which means that the simulated result is good.
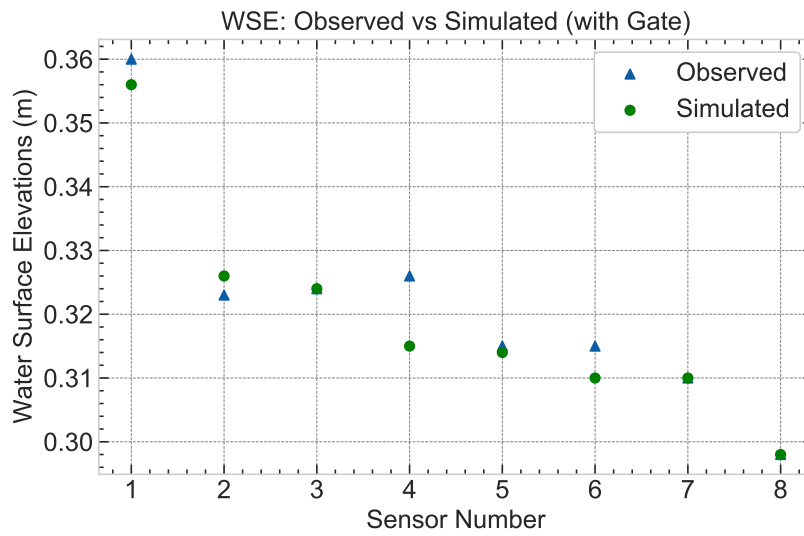
Figure 7.21: Water Surface Elevation: Observed vs Simulated (with gate)
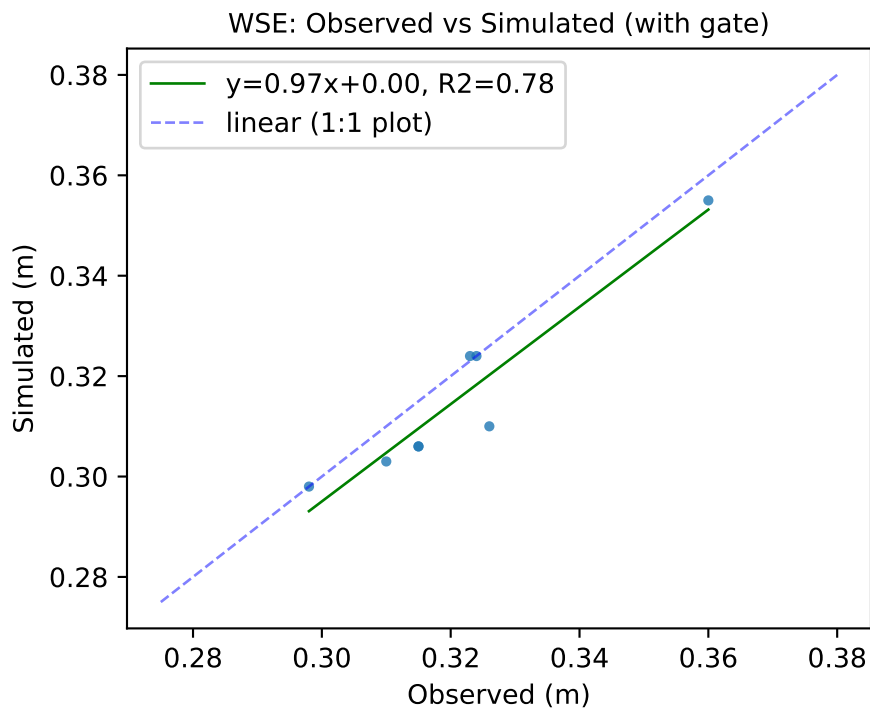
Figure 7.22: Goodness of fit between Observed and Simulated WSE (with gate)

7.2.4   Problem Encountered with Hydraulic Structure

As mentioned in 7.2.2 , a hydraulic structure (weir and gate) was introduced to simulate the condition similar to prototype. A hydraulic model was run with the same condition used in previous case. It clearly simulates the condition similar to the one in physical model with gates. Eventhough it can handle the hydraulic simulation well, the new version of HEC-RAS 6.2 does not seem to support models with the combination of structures and sediments as of now. The error message generated is shown in Figure 7.23.
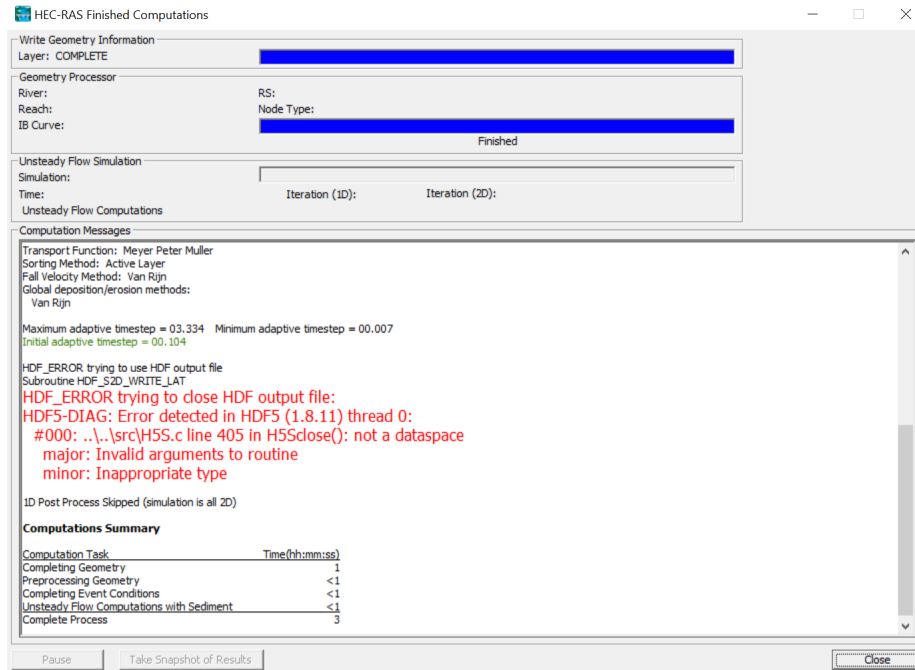
Figure 7.23: Error message generated with Hydraulic Structure

Various attempts were made to run the simulation with structures. The combination of weir and gate was first tested. Then the combination of weir and culvert was chosen to simulate the similar condition. The idea of introducing a bridge right above the intake area in bypass channel with thick deck failed as well. So, it was decided not to use any structures with the bypass channel and look for an alternative method.

7.2.5 Alternative for Hydraulic Gate

As the software was not able to handle the gated structure along with sediment transport, a workaround method was adopted. The intake gate and weir was removed and simulation was done in an open channel. The absence of weir and gate causes increased depth and decreased velocity which may not replicate the simulation with gate. So, the intake cross sectional area was reduced such that the velocity at the entrance is similar to that in the model with gate. One problem with this method was that the water level in the bypass section could not be replicated as in the gated model. Modification to the gate is shown in the Figure 7.24. The cross section at intake was reduced from 15cm (represented by grey dotted line) to 5cm (represented by blue line). With same discharge, if the cross sectional area of flow is controlled, it is possible to obtain the velocity which is similar to that of the gated inlet.
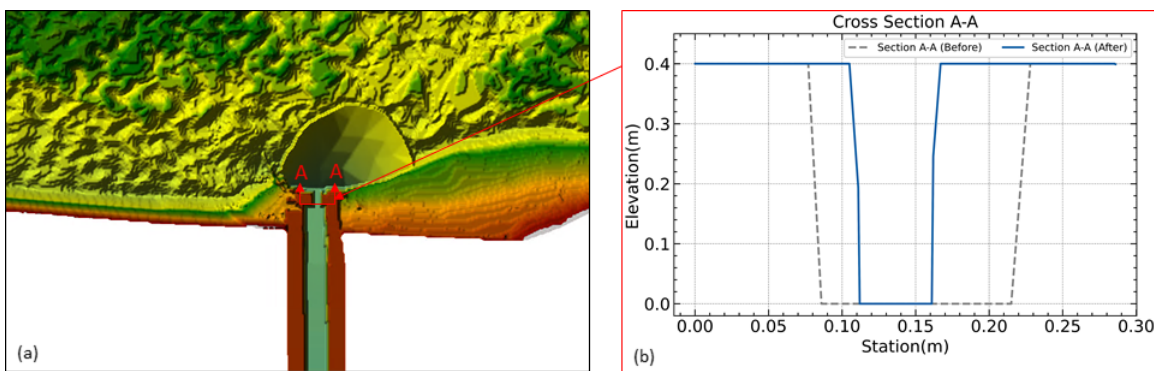
Figure 7.24: Modification in Inlet of Bypass Tunnel (a). Plan view (b). Cross Section A-A showing cross sections before and after modification

Figure 7.25 shows the velocity layer near and in the sediment bypass section. Figure 7.25 (a) shows the velocity layer when the gate is used in hydraulic simulation. The velocity right in front of the gate seems to be low because water gets accumulated there due to the presence of weir. The velocity starts to get high when flow passes through the gate with submerged opening. Figure 7.25 (b) shows the velocity layer when the gate is removed and intake is modified. There is no accumulation of water in front of the gate so the velocity pattern changes compared to Figure 7.25 (a). The velocity in these two cases are not exactly the same but somewhat similar so as to use the modified section as an alternative to a gated model.

Figure 7.25 (c) shows the velocity profile at section B-B as indicated in Figure 7.25 (a) and (b). The blue (dotted line) represents the velocity profile for the bypass section with gate while green line represents the velocity profile for modified bypass channel. The brown line represents the underlying terrain. From this figure, it can be seen that the velocities and the pattern in these two cases seem similar. The gate is located at around 0.8m (Figure 7.25 (c)) and the velocity pattern at that point looks promising. The velocity profiles before the gate looks similar in both the cases. So it was decided to use this modified section for further simulations.
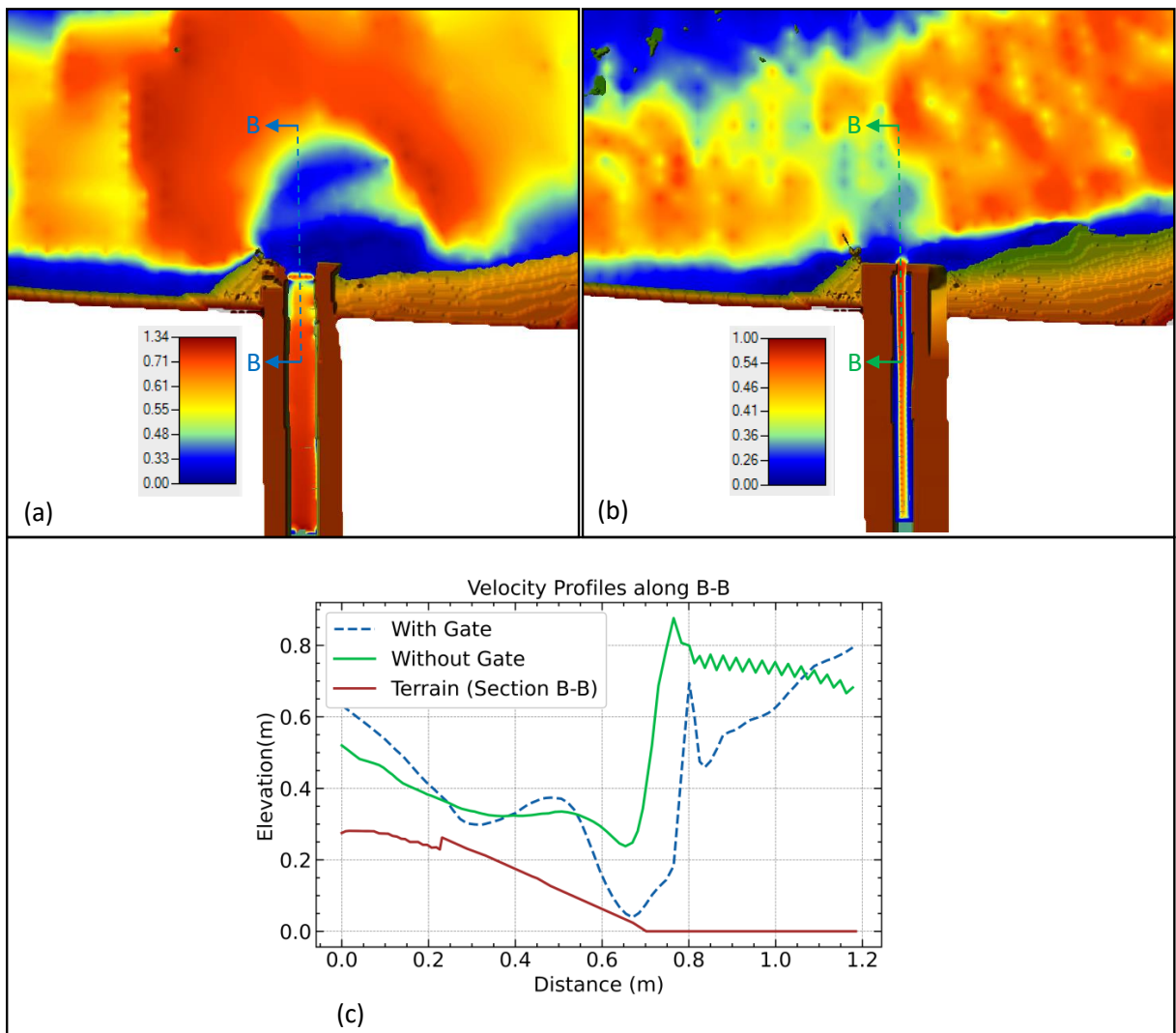
Figure 7.25: Velocity layers in Bypass Tunnel in two cases in Hydraulic Simulation (a). With Gate (b). Without gate through the modified opening (c). Velocity profile at section B-B for both cases

Along with the velocity profile, water surface elevation of the model was also checked. The assumption for modification was that the water surface elevation should not change a lot in the entire channel. However, some changes were expected. Figure 7.26 shows the water surface elevation in the entire channel.
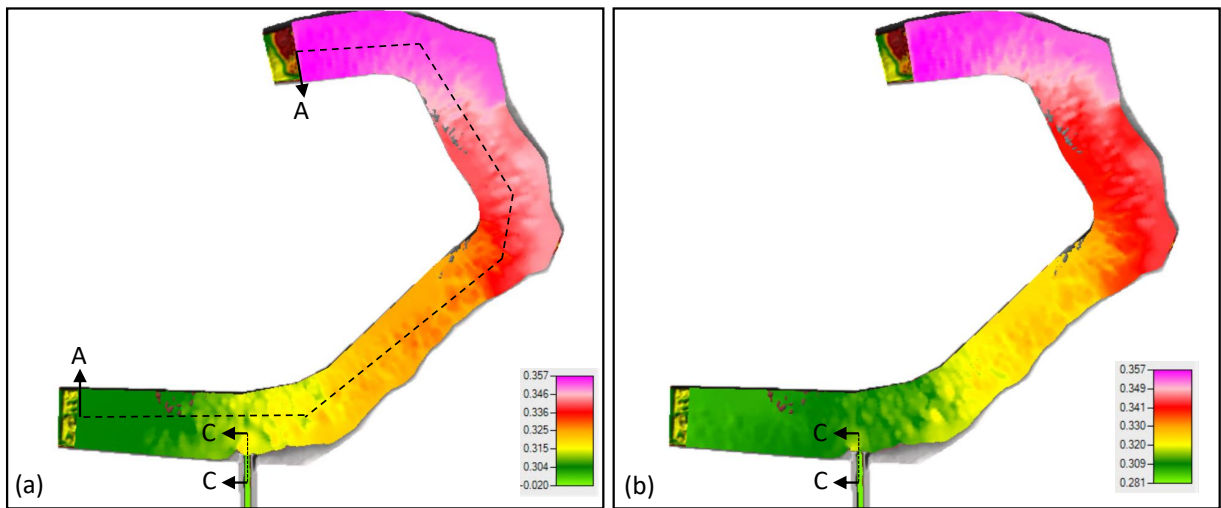
Figure 7.26: Water Surface Elevation in two cases in Hydraulic Simulation (a). With Gate (b). Without gate in bypass section

It can be observed that the water surface elevation is quite similar in the model with gate and without the gate. Higher water surface elevation is observed in the upstream region with values up to 0.357m. The surface elevation of water in the downstream part also looks quite similar in the two cases. However, some changes can be observed near the area with bypass channel. To see the difference between observed and simulated water elevation over the entire channel, a longitudinal profile was drawn at the center of the channel. Water surface elevation along the channel is shown in Figure 7.27.
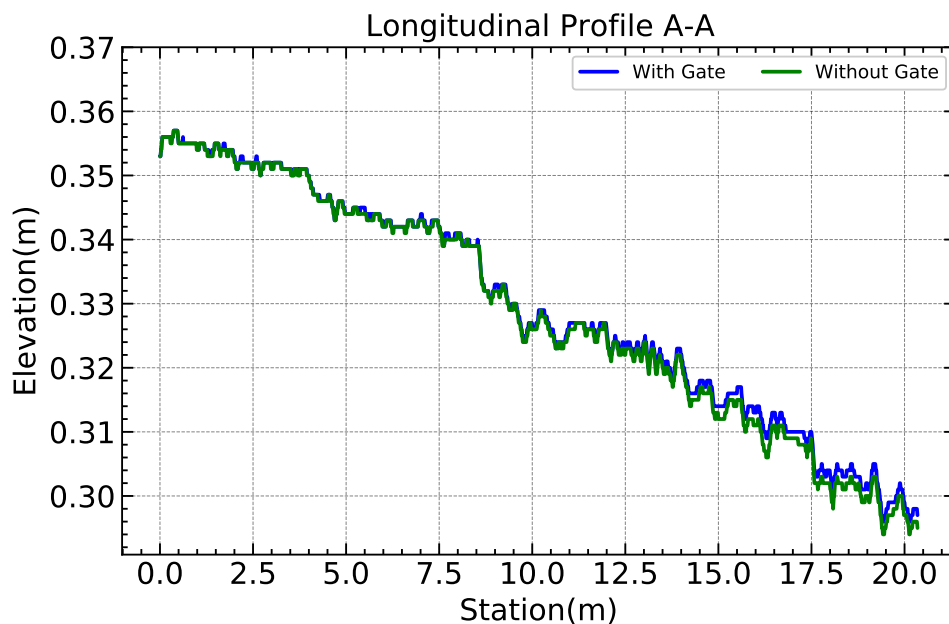
Figure 7.27: Water Surface Elevation along the longitudinal profile A-A

63

Figure 7.27 shows that the level of water in observed and simulated model is similar upto about 11m from upstream. Then, some deviations can be observed near the point of inlet of bypass channel. The blue line represents water level elevation with gated structure which seems to be higher than the green line representing the water surface elevation of model without gated structure. It is because of the reason that when a gate is installed with the weir, water is accumulated and water level rises up. It is not seen in the case of open channel flow because there is no structure to hold water up.
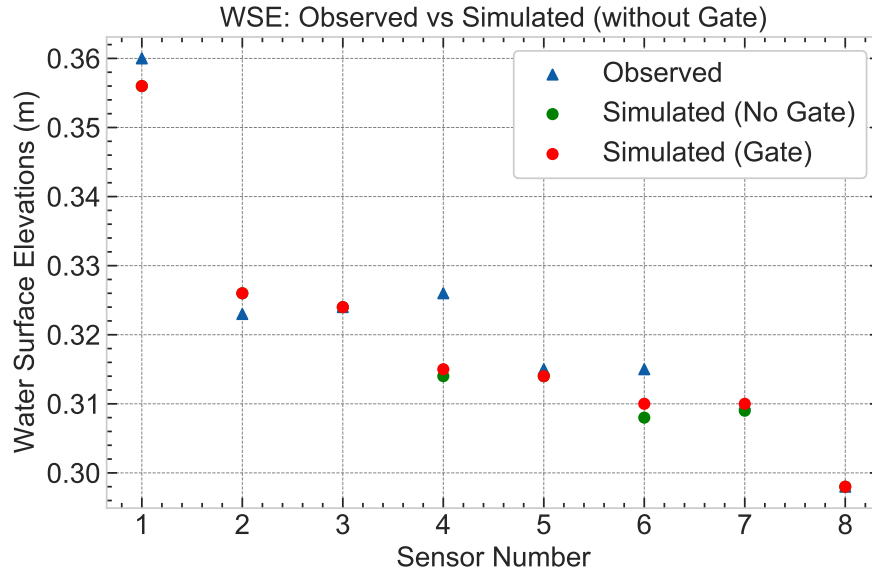
Figure 7.28: Water Surface Elevation in the sediment bypass channel at section C-C

Figure 7.28 also shows that the water levels at different sensor locations simulated with and without gate are close to each other except near sensors 4 and 6 which is near the bypass inlet. Figure 7.29 shows the goodness of fit of WSE simulated without gate with the observed values. The observed values are plotted in x axis whereas the simulated values are plotted in y axis. The plot was prepared in python with the R^2 function which gave the value of 0.9.
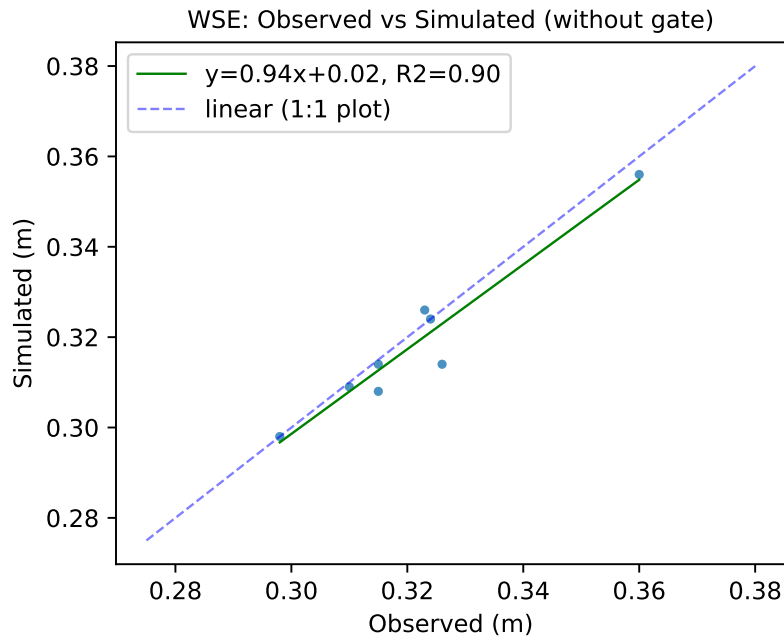
Figure 7.29: Water Surface Elevation in the sediment bypass channel at section C-C
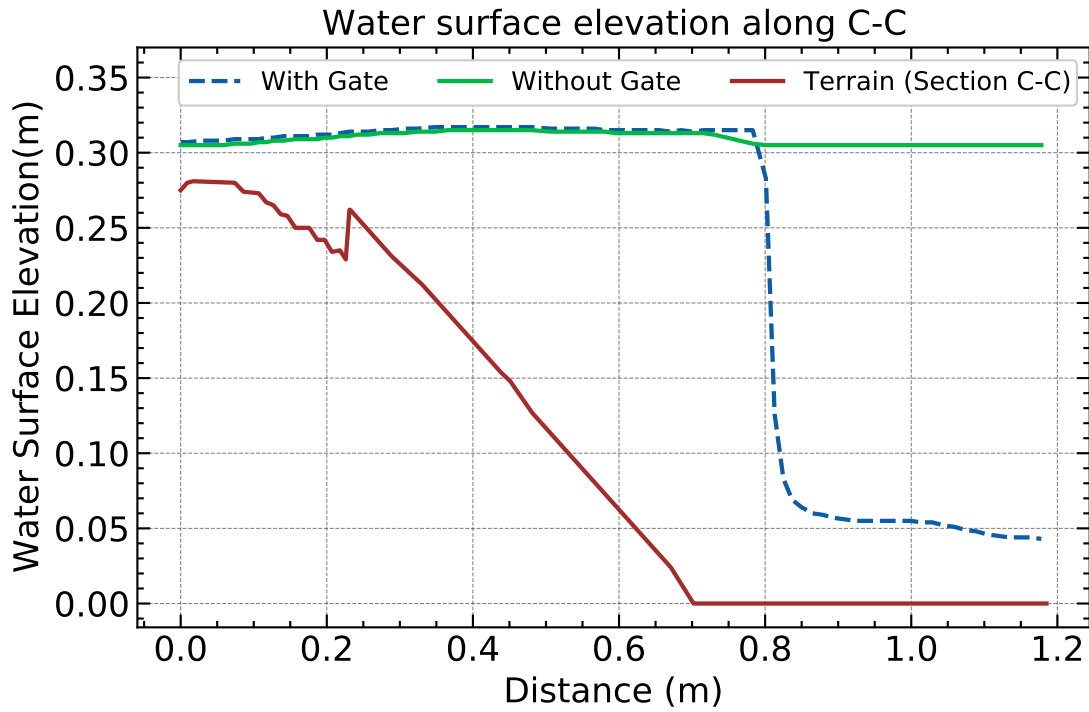
Figure 7.30: Water Surface Elevation in the sediment bypass channel at section C-C

Figure 7.30 shows the water surface elevation along the section C-C as shown in 7.26. The water level for gated structure (blue dashed line) is forced down to the level of around 0.05 at the distance of about 0.8m due to the presence of submerged gate opening. However, it is difficult to simulate it in the open channel flow as no any structure is present to force down the water level. Even after the modification of the bypass inlet and cross section, water level is not the same in the bypass section. It has the same discharge of 5 l/s with similar velocity but with smaller cross section which keeps the level of water higher compared to gated structure. This modification was adopted for further simulations.

7.2.6   Sediment Simulation

Comparison of the bed elevations after sediment transport test has been done in Figure 7.31. Figure 7.31 (a) shows bed elevation map observed in the physical model. Figure 7.31 (b) shows bed elevation map in simulated numerical model. The observed model does not consist of bypass channel because it was difficult to scan it in physical model. The color grading representing different elevations is shown in the comparison. However, there is a little difference between the maps in (a) and (b). Due to the presence of sediment bypass channel and its bed elevation, the lower elevation limit in simulated model is lower than in observed model which changes the colors to some extent. The numbers in figure represent the numbers assigned to all the profile lines to compare the elevation in cross section.
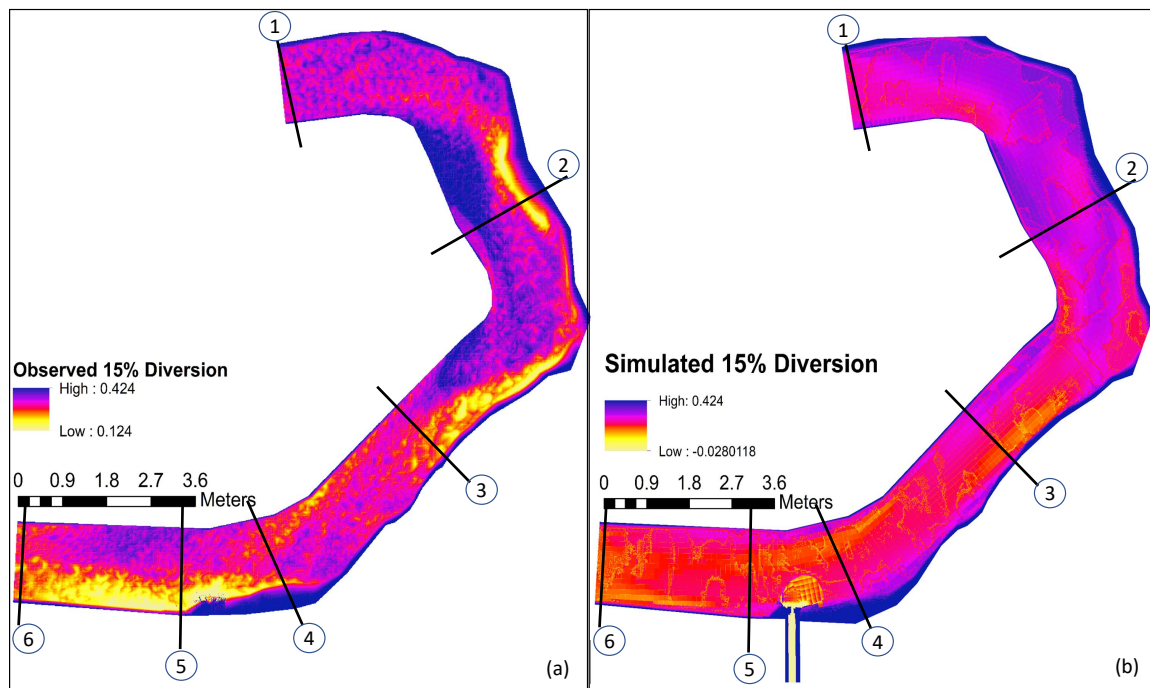
Figure 7.31: Comparison of Bed Elevation Levels: (a). Observed vs (b). Simulated (15 % Diversion through Bypass)

The bed elevation points for each profile lines were exported from HEC-RAS and were plotted to see the actual bed elevations that is difficult to visualize in Figure 7.31. Figure 7.32 shows the comparison of bed elevations between observed and simulated model along the profile lines. It shows that the pattern and level of erosion and deposition in profile 1 in simulated model is very close to that of the observed model. The model could not simulate the pattern and levels of cut and fill around profile 2. In profile 3 and 6, it tends to follow the erosion and deposition pattern. Profile 4 and 5 shows that the simulated model was not able to replicate the cut on left bank which might have caused due to the presence of sediment bypass channel.
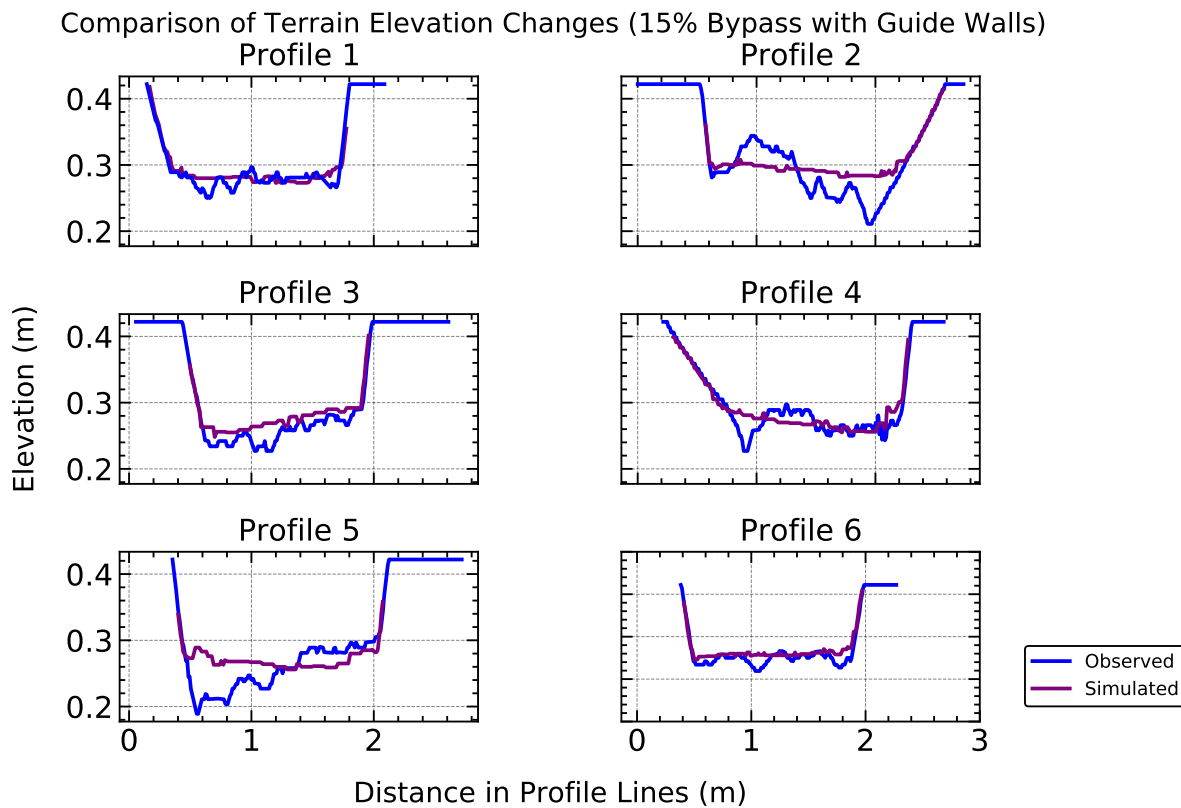
Figure 7.32: Bed change: Observed vs Simulated (15 % Bypass) at different profile lines

The actual change in bed due to the induced flow can be observed in Figure 7.33. The section of bypass channel was cut out because it does not exist in the scanned data from physical model. It was found out that the bypass channel is not able to transport enough sediment load through it in this model. As the water level in bypass section is as shown in Figure 7.30, it may not be able to transport enough sediment. The comparison between observed and simulated bed changes in plan view is shown in Figure 7.33.
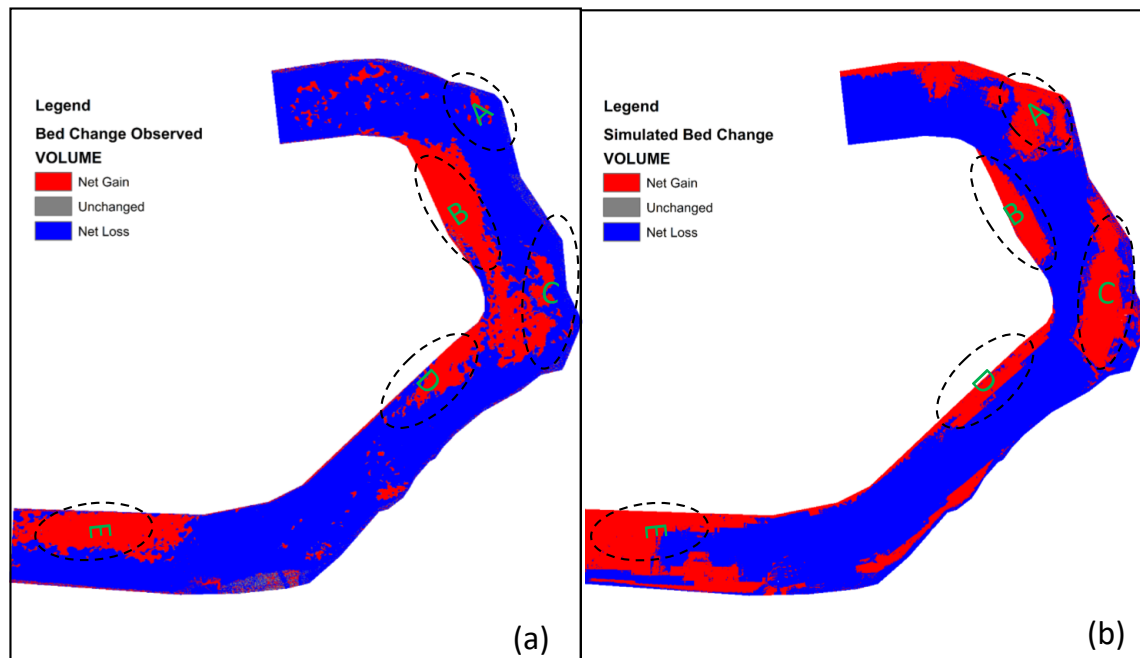
Figure 7.33: Comparison of Bed Changes in (a). Observed and (b). Simulated Model with 15% flow through the Bypass

From Figure 7.33, it can be seen that the simulated model tends to follow the pattern from observed model. However, there are more discrepancies in this case compared to Case A as discussed in 7.1. The entire region is divided into five different zones for comparison. The first difference can be seen on the first outer bend represented by zone A. There is erosion in the observed terrain whereas in the simulated terrain, we can see deposition. Similarly, in the first inner bend shown by zone B, deposition volume seems lower in simulated model than in the observed one. The reason for these could be the velocity of flow in this region. The velocity is higher at a certain part and it results in erosion. The velocity in central region is higher than in the outer bend due to the effect of boundary condition. Zone C tends to be similar but in the observed result, bed change is pushed more towards the inner bend. Zone D looks similar with only little difference. In the downstream area, there is no deposition in left area near sediment bypass channel in observed model. The reason for this could be the presence of the bypass channel and its efficient transport of sediment. But, in the simulated model, there is deposition maybe because the bypass channel is not functioning well and sediment deposits instead of passing through the channel.

7.3   Effect of Guide Walls on Sediment Diversion

The guide walls were added in the model to check its effect on sediment diversion and the flow. Guide walls are meant to increase the efficiency of sediment bypass section. The transport of sediments in the channel and through the bypass is studied in this section. Three guide walls were introduced at the same location as in the physical model. The top width of guide walls used was 0.1m while the bottom width was 0.3m with appropriate slopes. The top surface elevation was set to be 0.45m.

7.3.1   Defining Guide Walls

Proper scanning of guide walls was difficult because of the capture resolution of scanner. It was not properly captured in the terrain scan. So it had to be added in HEC-RAS using vector modification tool.

Figure 7.34 shows the process of defining the guide walls in existing terrain. As a reference, the scanned terrain from physical model was used which consists of the hints of guide walls as shown in (a). Vector terrain modification with the modification as high ground was used to draw the guide walls in the terrain as shown in (b). Dimensions can be assigned to this terrain using Ground Line editor dialog in RAS-Mapper. The assigned dimensions are shown in (c). It modifies the terrain completely along the profiles drawn and assigns new values to it. The final view of guide walls can be seen in (d) with highest elevation set at 0.45m. This was all done in a modification layer which can be copied to a different terrain. The guide wall layer was then copied from this reference terrain to the plain terrain where simulation was to be performed.
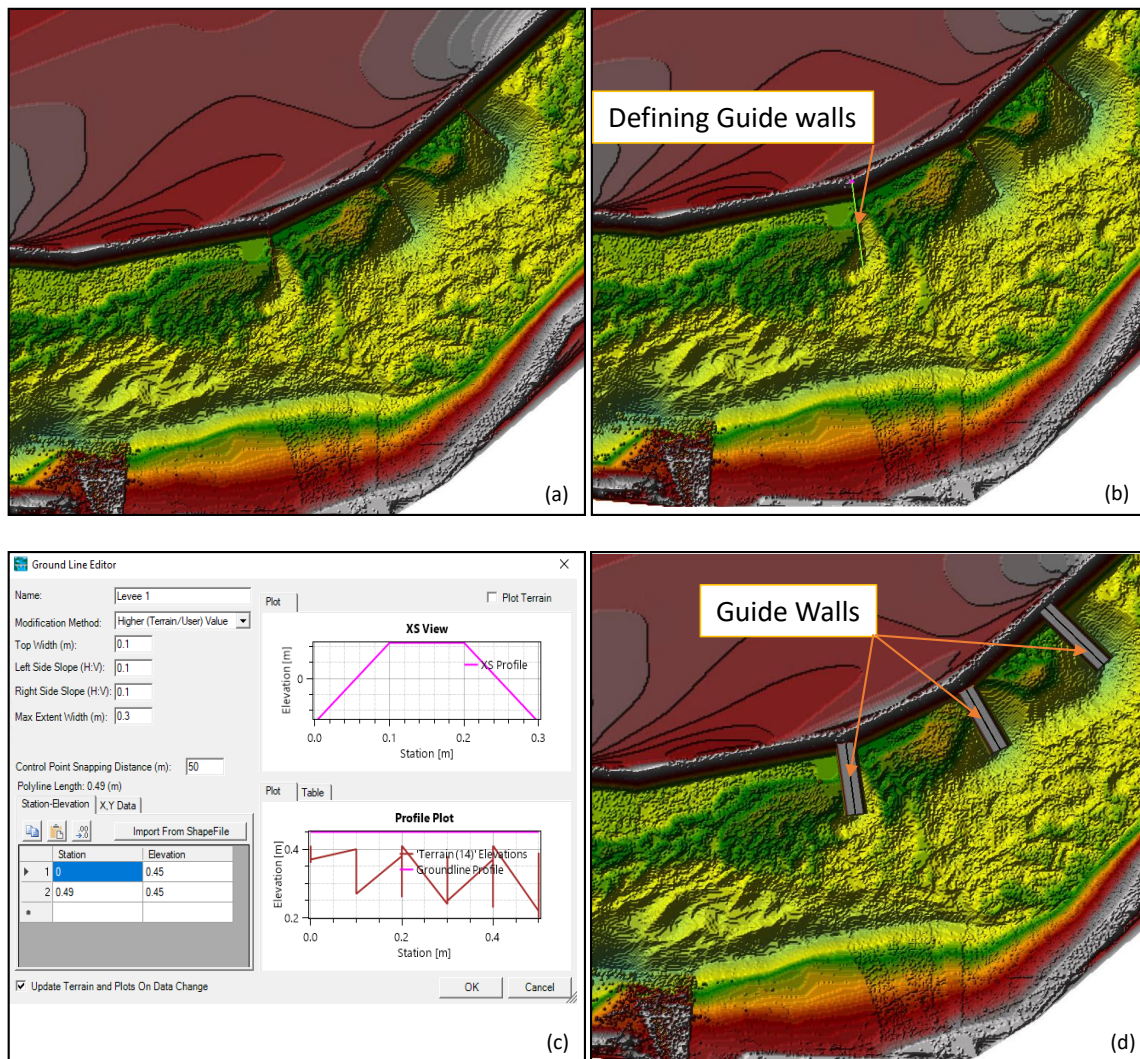
Figure 7.34: Terrain modification to define guide walls (a). Terrain data with guide wall in physical model (b). Defining high ground terrain modification lines as guide walls (c). Assigning dimensions to guide walls (d). Final view of lines converted to guide walls

7.3.2   Hydraulic Simulation

Hydraulic simulation of the model was done to check if the model is hydraulically correct before running the sediment model. Upstream boundary condition with a constant flow of 35 l/s was used with stage hydrograph at the downstream. Constant flow hydrograph of 5 l/s was used in the bypass channel. The model was simulated with same settings and input parameters as in 7.2. Figure 7.35 shows the water surface layer map with guide walls. The presence of guide walls pushes water away from them. It creates an effect similar to an artificial bend. The velocity of flow seems very low behind and between the guide walls.
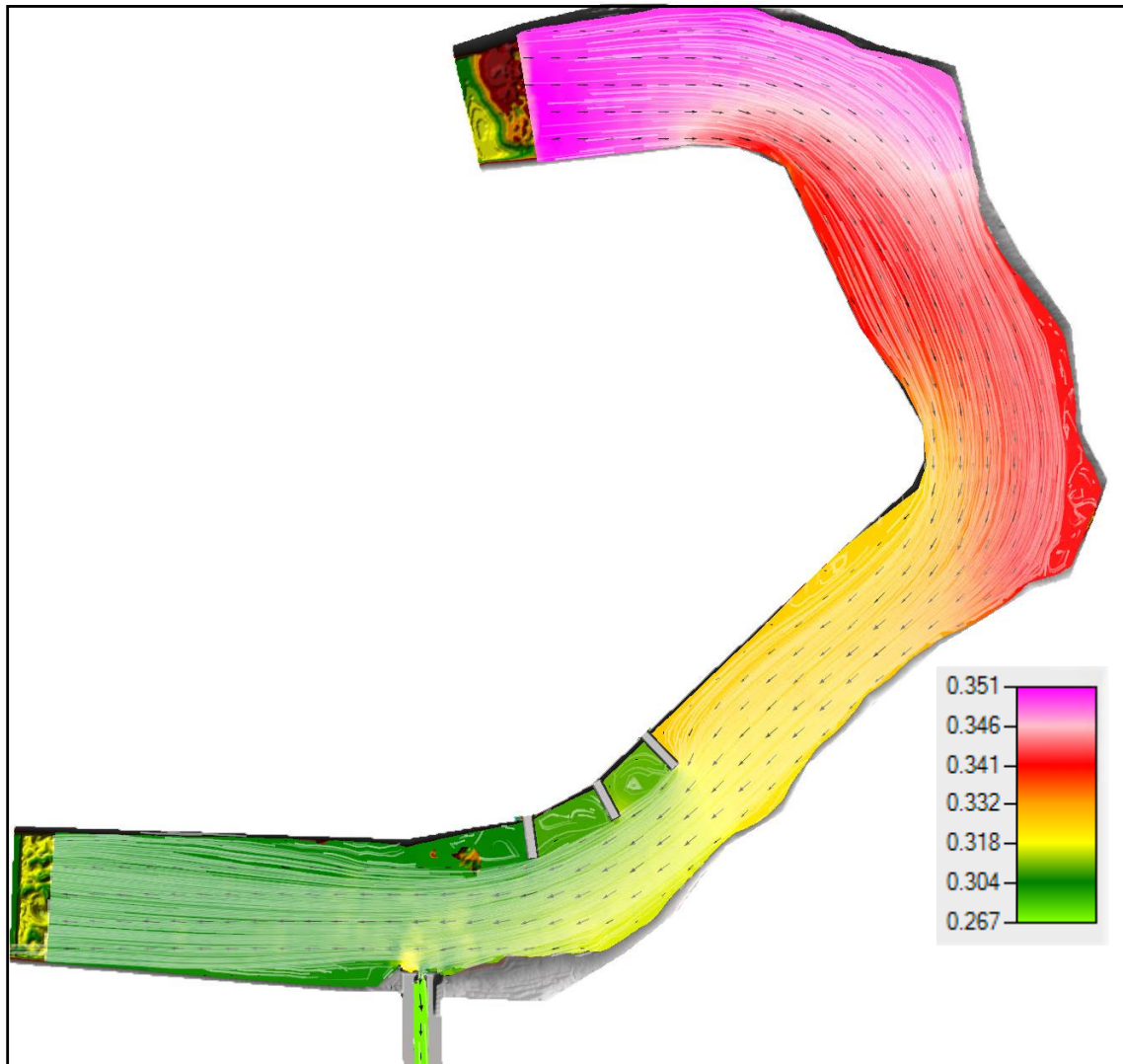
Figure 7.35: Water Surface Elevation and flow pattern with Guidewalls (15% Bypass)

The water level at various points were then compared with observed values. The comparison of observed and simulated water surface elevation values is shown in Figure 7.36. The values used for this plot has been presented in Appendix Table A.7.
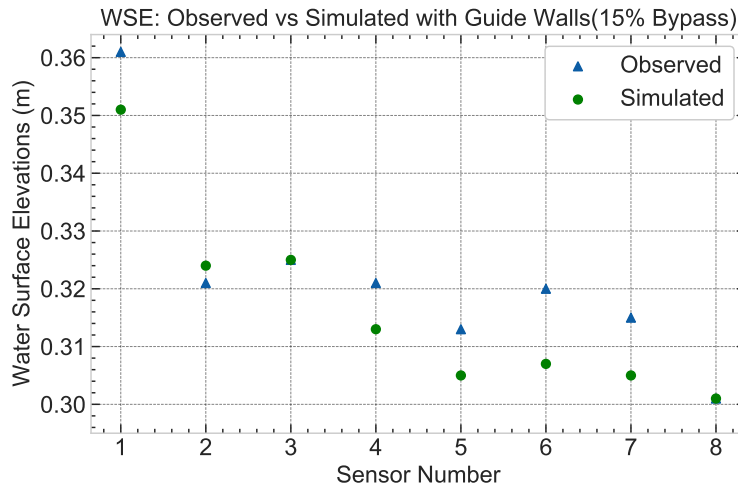
Figure 7.36: Water Surface Elevation: Observed vs Simulated with Guidewalls (15% Bypass)

It can be observed that the simulated water surface elevation deviates around sensor numbers 4, 5, 6 and 7 which is near to the gate. The influence of absense of gate and the presence of guide walls can be observed here. However, the difference in elevation is not too large and the closeness of these values with observed can be seen in Figure 7.37.
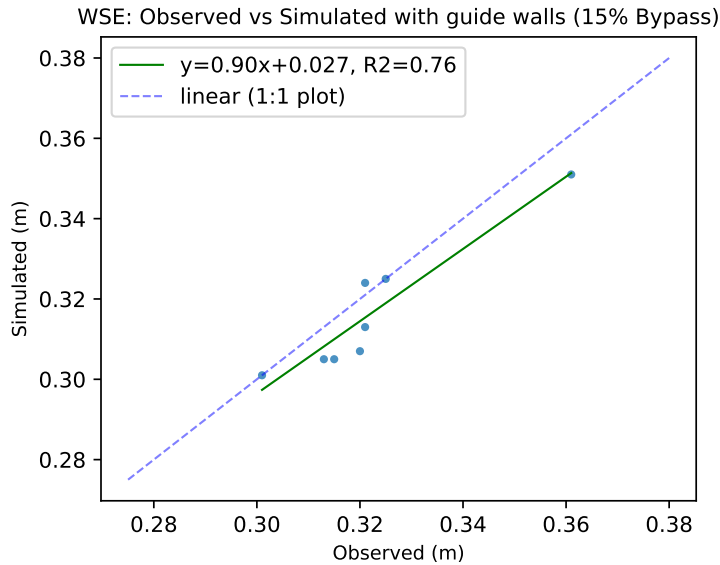
Figure 7.37: Goodness of fit between Observed and Simulated WSE with guidewalls

Figure 7.37 shows the scatter plot with goodness of fit between observed and simulated water surface elevation with the R^2 value of 0.76 which is quite good. Many points seem far from observed values but the differences are not that high.

72

7.3.3   Sediment Simulation

Guide walls were added using vector terrain modification tools in RAS-Mapper. However, 2D bed gradation in HEC-RAS is set to the user defined bed gradation by default. It means that the defined guide walls would get eroded along with the bed materials. One should be careful about it before running a sediment model. It is therefore, important to define the guide walls as non erodible structures. Sediment bed material layer can be created from the map layers in RAS-Mapper. Definition of bed gradation materials can be done under 2D bed gradation in sediment data dialog.

Comparison of the bed elevation maps obtained after running the test has been done in Figure 7.38. Figure 7.38 (a) shows bed elevation map observed in the physical model. Figure 7.38 (b) shows the bed elevation map in simulated numerical model. The difference in color gradient is observed due to the presence of low bed levels in sediment bypass channel in simulated model. Observed model does not contain the elevation for bypass channel as it was difficult to scan the terrain in prototype due to its narrow section. The numbers in figure represents the numbers assigned to all the profile lines which were later used to plot the cross sectional views. From the elevation maps, some similarities can be seen between the observed and simulated results.
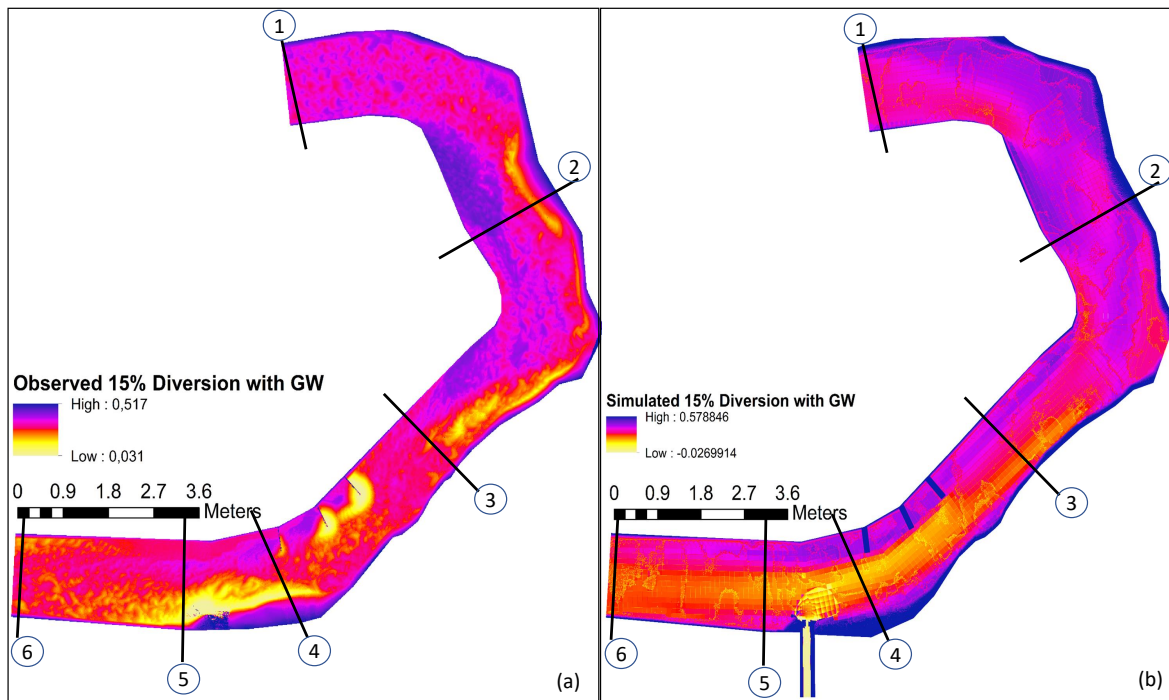
Figure 7.38: Comparison of Bed Elevation Levels: (a). Observed vs (b). Simulated (15 % Diversion through Bypass with Guide walls)

73

The bed elevation points for each profile lines were exported from HEC-RAS and were plotted to see the actual bed elevations that is difficult to visualize in Figure 7.38. Figure 7.39 shows the comparison of bed elevations between observed and simulated model along the profile lines. It shows that the simulated model represents area around profile 1 well. The model does not seem to be in agreement with the observed result around profiles 2 and 5. The erosion seems to be higher in these areas. Profiles 3, 4 and 6 are represented well by the simulated model.
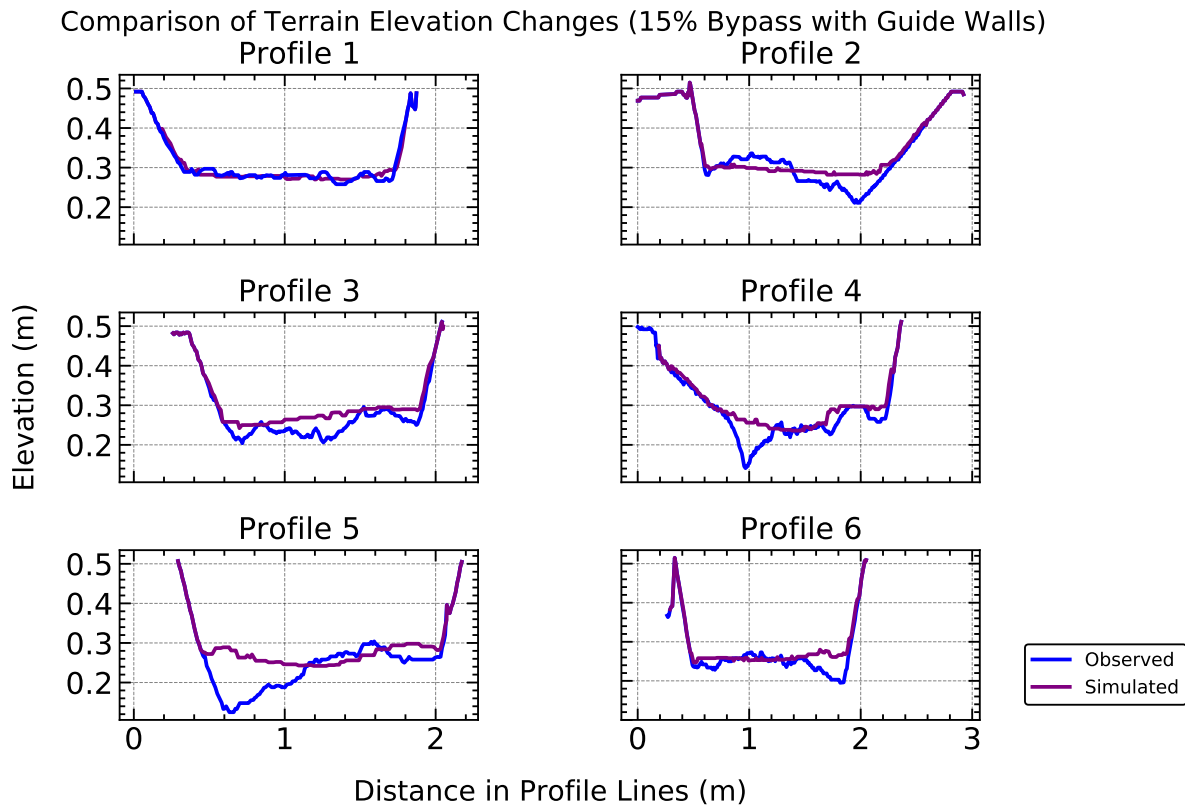
Figure 7.39: Bed change: Observed vs Simulated (15 % Bypass with Guidewalls) at different profile lines as indicated in Figure 7.1
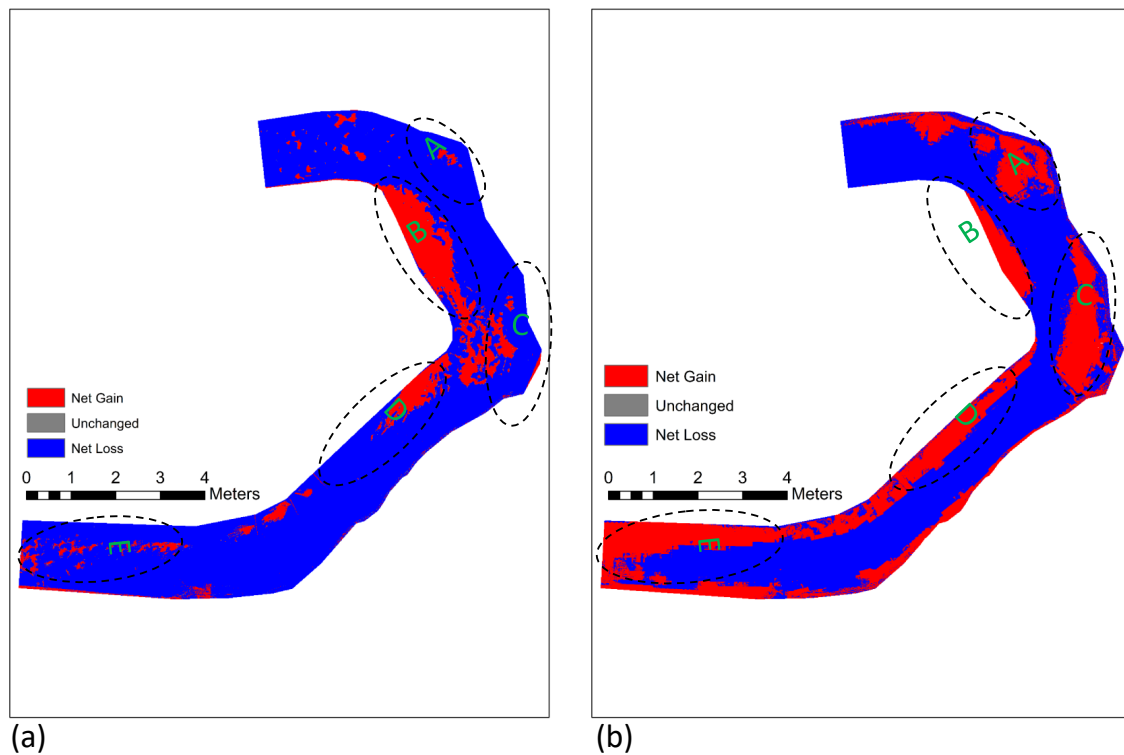
Figure 7.40: Bed changes: (a). Observed vs (b). Simulated with Guidewalls (15% Bypass)

Figure 7.40 shows the comparison of bed changes between observed and simulated model. The simulated result seems to have over-estimated the deposition. The area is divided into five zones from A to E for comparison. Observed changes show that there is no deposition at zone A as can be seen in simulated bed changes. This seems to be a problem that can be seen in all the simulations. Boundary condition might be the reason for this deposition because the pattern of flow is somewhat close to the inner bend. At zone B, the simulated model seems to be following the pattern of deposition as can be seen in the observed map. However, it seems to have been underestimated in this zone. Similarly in the zone C, there is little to no deposition in observed case whereas the simulated model shows considerable deposition. Zone D is the effect of presence of guide walls. In the observed model, there is scouring near the guide walls and minor deposition between the walls whereas in the simulated model, there is deposition due to the diversion of flow and reduction in velocity as can be seen in Figure 7.35. Zone E has no deposition in the observed model whereas there is high deposition in the simulated model. It could be because the sediment mass is not transported properly through the bypass channel and hence got deposited near the intake and in the downstream. Figure 7.40 shows that the dynamics introduced by the guide walls is not well represented by the simulated model.

7.3.4   Comparison of Sediment Concentration through Bypass Channel

The comparison of sediment concentration through bypass channel was done between the simulated models with guide walls (explained in 7.3) and without guide walls(explained in 7.2) installed. The sediment passing through the bypass in presence of guide walls was expected to be more because along with the flow, sediment was also expected to be diverted to the outer bend allowing more to pass through the bypass channel. Comparison between the two cases is shown in Figure 7.41.
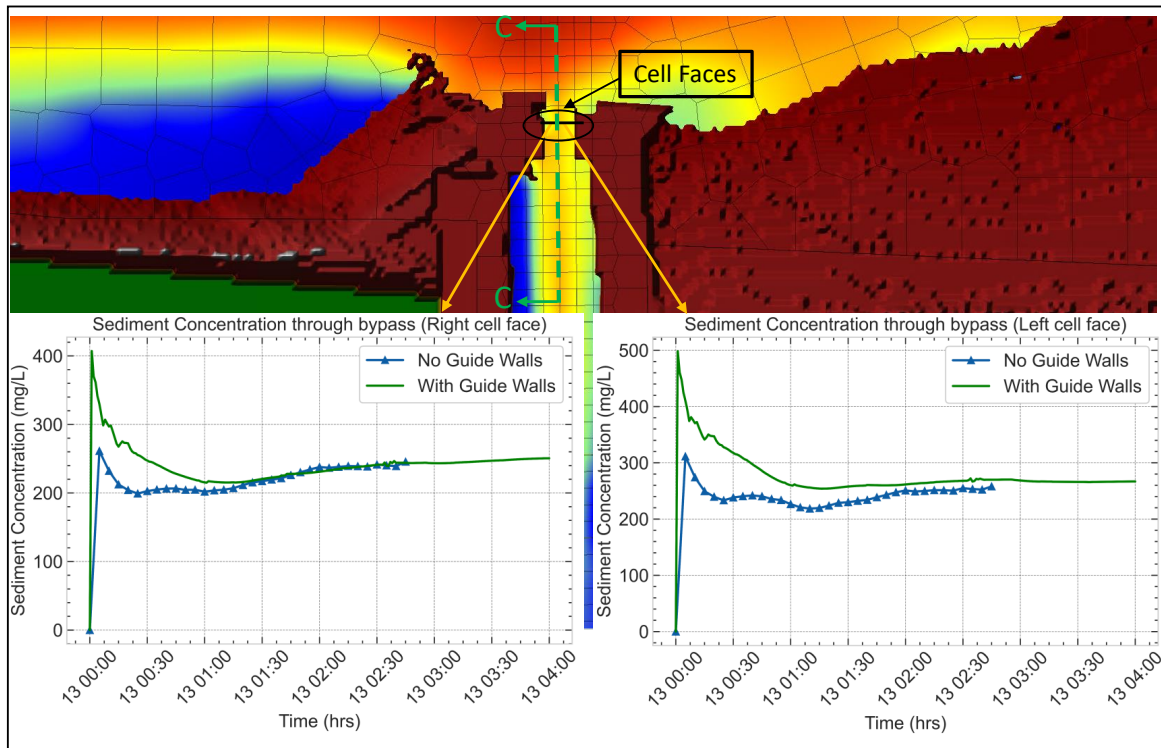
Figure 7.41: Comparison of sediment concentration through bypass channel with and without guidewalls installed.

Note: 7.41 shows the total concentration of sediment passing through bypass channel. The bypass channel has two cells and hence two cell faces across it. It is possible to get the data for sediment concentration at a cell face in RAS-Mapper. With active total concentration layer, right clicking on the left and right cell faces (sides based on flow direction) gives an option to plot the total sediment concentration at the cell face.

Figure 7.41 shows that it is possible to increase the flow of sediment through bypass channel by installing guide walls. At the start of simulation, the concentration seems very high when the guidewalls are present. The reason for this could be that the flow is forced towards the bypass along with sediment hence, carrying more sediment to the bypass channel.

However, the level of flow in bypass seems to be similar as in 7.30, the case without guide walls. The comparison can be seen in Figure 7.42. It indicates that there is no change in pattern of flow and guide wall is solely responsible for the increase in sediment concentration and hence sediment mass. Hence, guide walls cause the changes in pattern of bed change as well as sediment concentration in the HEC-RAS 2D model.
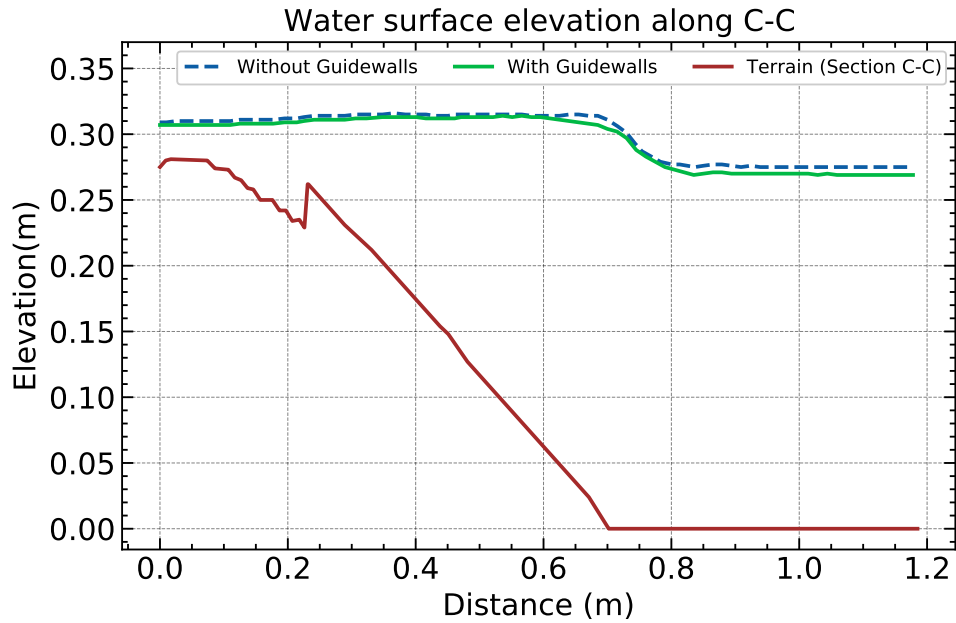
Figure 7.42: Changes in water level at bypass channel with and without guide walls

7.4 Effect of Increased Discharge through Bypass (Verification Test)

Studying the outcomes from various simulations, it is seen that the sediment bypass channel is only diverting certain percentage of sediment than it actually should. So an extra simulation was done to check whether increasing the flow through bypass will actually increase the concentration of sediment. Guide walls were not introduced in this simulation because there is no observed data available to compare. So a simulation with 30% water diverted through the bypass channel was done without any guidewalls in it.

In order to make the comparison fair, inflow to the main channel was maintained at 35L/s as in all the other cases in this study. However, the flow through bypass was increased to 30% of total flow i.e. 10 l/s using flow hydrograph boundary condition. More water is being diverted from the bypass channel so some changes in the water surface elevation at downstream was expected. So, the stage hydrograph at the downstream boundary was set to around 0.295m for the entire simulation time. Same terrain model as well as geometry file was used for the simulation as in 7.2.

7.4.1 Hydraulic Simulation

Hydraulic Simulation was done for 15 minutes of simulation time. The time was so chosen that the flow in entire channel is stable. The water surface elevation at the end of simulation was then compared with the observed values. Figure 7.43 shows the comparison of observed and simulated water levels at different control points. Appendix Table A.8 shows the data used for this plot.
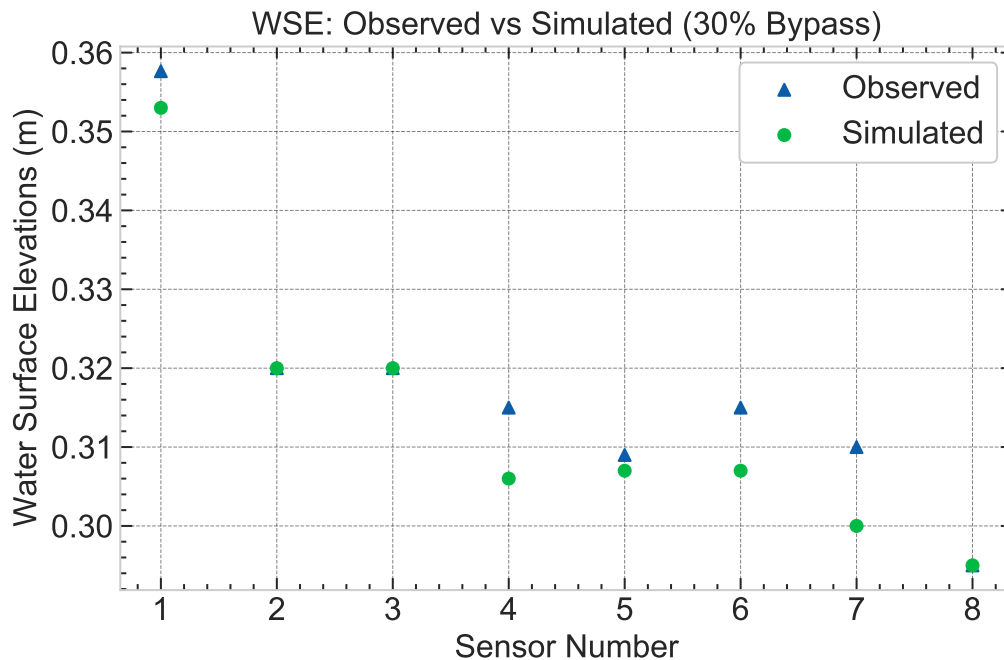
Figure 7.43: Water Surface Elevation: Observed vs Simulated (30% Bypass)

It was found that the water levels observed and simulated are close enough to continue with sediment transport modelling. Some differences were observed at sensors 4, 6 and 7. However, the deviation was not too large. Some points seems to fit perfectly which is an indication of a good model.
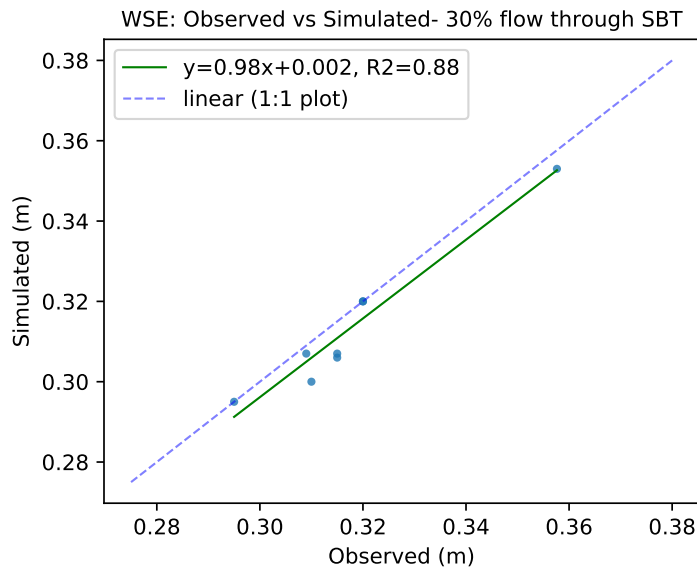
Figure 7.44: Goodness of fit between Observed and Simulated WSE (30% Bypass)

Figure 7.44 shows the scatter plot and goodness of fit between observed and simulated water surface elevations. The correlation coefficient was found to be 0.88 which is a good fit. Some points are far from the 45 degrees line which are the same points as can be seen in Figure 7.43's sensor numbers 4, 6 and 7.

It would be interesting to see the changes in water surface elevation also in the bypass channel. It is important because the water level determines flow of sediment through the channel. If the water depth is high as can be seen in Figure 7.42, sediment passing through bypass opening might deposit there without further movement. If the depth of water is high and velocity is high too, the sediment passing through the opening can actually be transported further away and hence increase the total sediment transport.
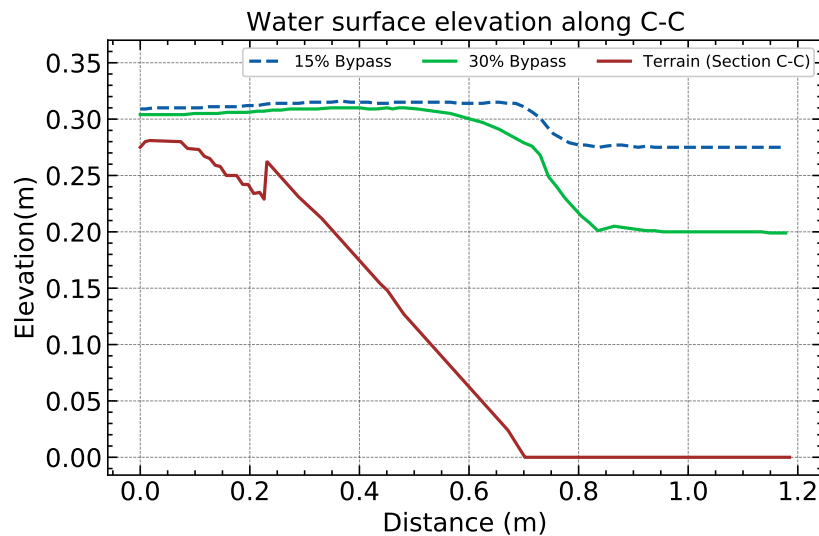
Figure 7.45: Changes in water level at bypass channel with varied inflow (15% and 30%)

Figure 7.45 shows the comparison of water surface elevation in the bypass channel section C-C as shown in Figure 7.41. It was interesting to see the reduced water level elevation when the flow through bypass was increased from 15% (5 l/s) to 30%(10 l/s). The velocity through this section is higher as well. However, the water level in front of the intake seems to be same as in the case of 15% diversion. With these conditions, higher sediment diversion can be expected.

7.4.2   Sediment Transport Simulation

If transport of sediment is proportional to the discharge of water through the channel as mentioned in 3.10, higher sediment transport shall be observed in this case. Also, the level of water through bypass is lower as shown in Figure 7.45 which results in higher velocity and efficient transport of sediment through the bypass section.

Comparison of the bed elevations between observed and simulated model after sediment transport test has been done in Figure 7.46. Figure 7.46 (a) shows bed elevation map observed in the physical model. Figure 7.46 (b) shows bed elevation map in simulated numerical model. The color grading representing different elevations is shown in the comparison. Because of the presence of sediment bypass section and its lower elevation in the map, colors are slightly different in simulated model for the same elevation range. The numbers in figure represents the numbers assigned to all the profile lines to compare the elevation in cross section.
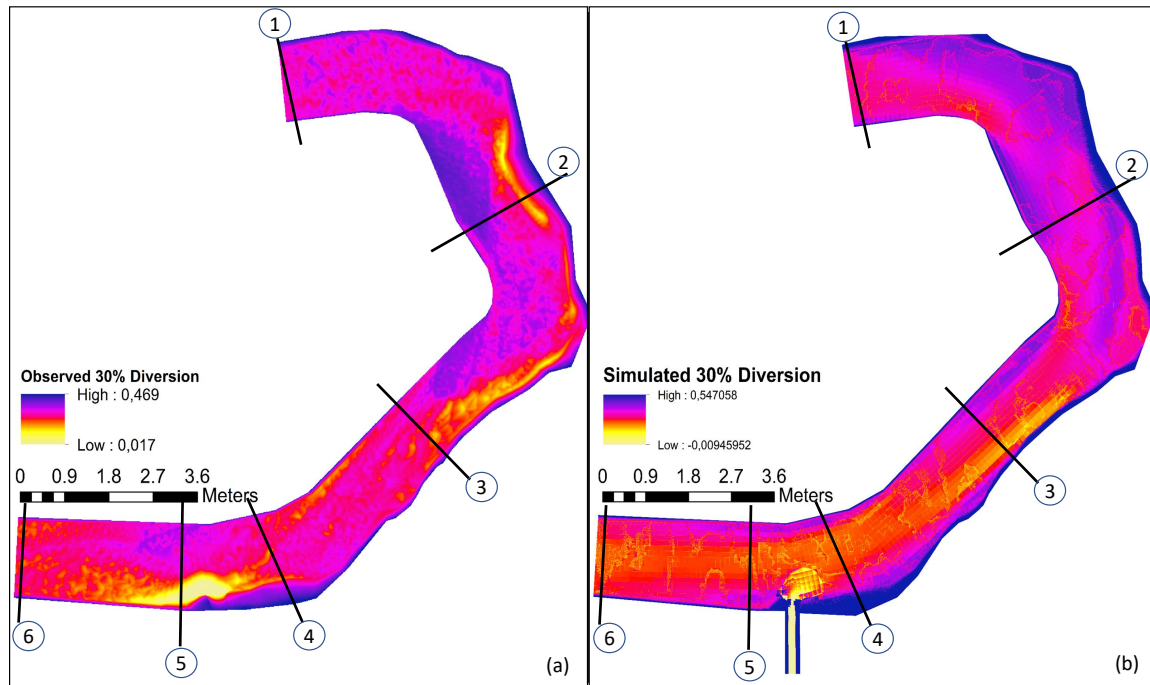
Figure 7.46: Comparison of Bed Elevation Levels: (a). Observed vs (b). Simulated (30 % Diversion through Bypass)

The bed elevation points for each profile lines were exported from HEC-RAS and were plotted to see the actual bed elevations that is difficult to visualize in Figure 7.46. Figure 7.47 shows the comparison of bed elevations between observed and simulated model along the profile lines. It shows that the cross sections 1, 3, 4 and 6 in simulated model are in good agreement with the observed model. Slight deviation can be observed in profile 2. The simulated model does not seem to represent the patterns of erosion and deposition in profile 2 very well. The major difference between the two models can be found in area around profile 5. High erosion can be seen in the observed model which the simulated model does not replicate. This deviation could be because of the presence of sediment bypass tunnel and eroded sediment passing through it.
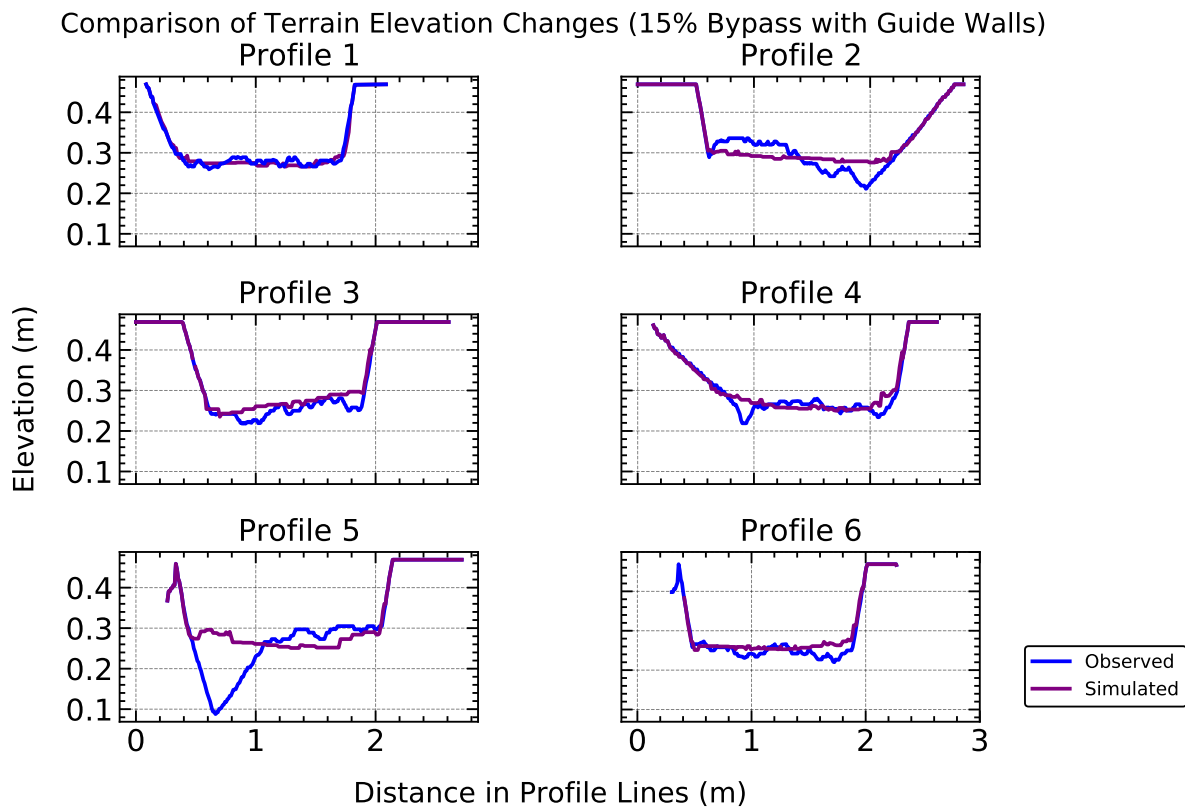
Figure 7.47: Bed change: Observed vs Simulated (30 % Bypass) at different profile lines as indicated in Figure 7.1

Figure 7.48 shows the comparison of bed changes in observed and simulated model. The simulated result seems to have over-estimated the deposition volume. The bed change layer has been divided into five zones from A to E for comparison. Observed result shows that there is no deposition in zone A whereas the simulated layer shows deposition in the same zone. The simulated model seems to have estimated the pattern of deposition in B whereas it is slightly underestimated. The pattern seems correct also in zone C, however, it can only be seen at the center portion and not on the extreme outer bend as seen in simulated. The deposition at zone D is more or less correct. The simulated model roughly estimates the deposition at zone E which is not perfect but it is able to catch the pattern. Apart from this, the erosion pattern in both the observed and simulated model seems comparable.

(a)   (b)
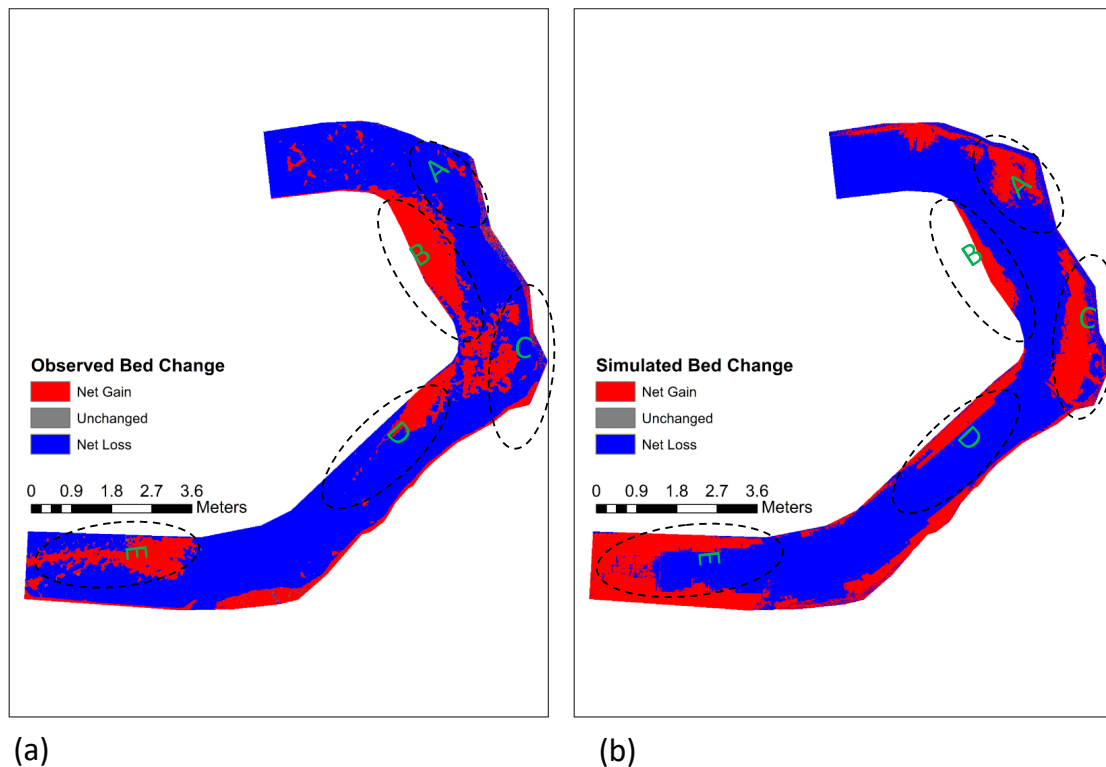
Figure 7.48: Bed changes: (a). Observed vs (b). Simulated (30% Bypass)

7.4.3   Comparison of Sediment Concentration through Bypass Channel

The comparison of sediment concentration through bypass channel was done between the simulated model with 15% diversion (explained in 7.2) and 30% diversion through bypass. Concentration comparison was done to see the increase in sediment concentration passing through the bypass with the increase in flow. Figure 7.49 shows the map of sediment concentration over the entire channel at final time step of 4 hours. At the final stage, the sediment concentration looks higher in the downstream section compared to upstream. It also shows the zoomed in image of the inlet of sediment bypass channel with direction of flow with left and right cell faces.
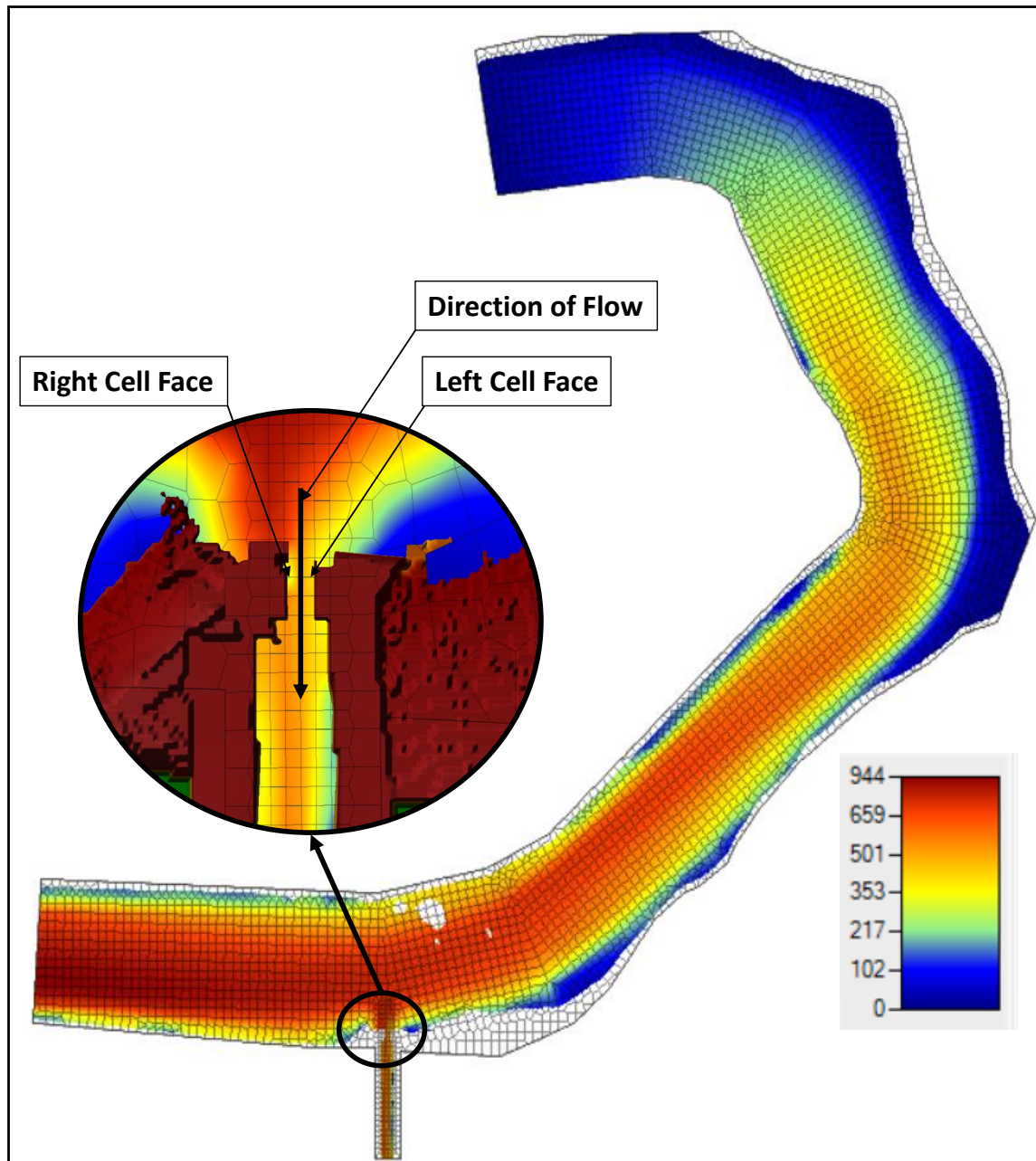
Figure 7.49: Sediment concentration map in the entire section (30% Diversion). The numbers in legend represent sediment concentration in mg/L in main channel at a time step.

Figure 7.49 was used as a reference to plot the sediment concentration at two cell faces for comparison between the sediment concentration when discharge through bypass was 15% and 30% of the total inflow.
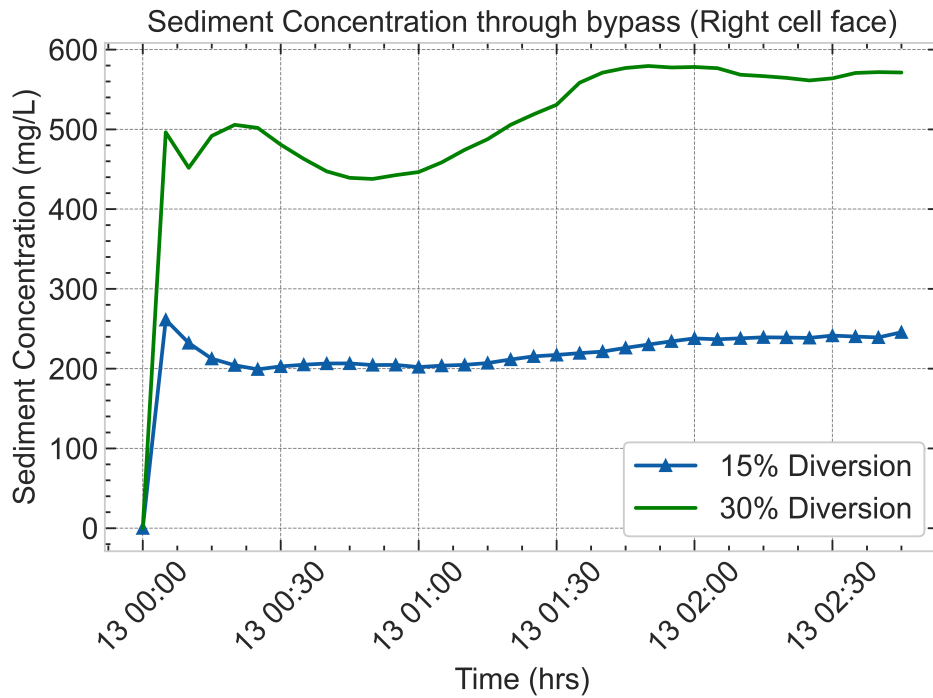
Figure 7.50: Comparison of sediment concentration through bypass for 15% and 30% diversion (Right Cell)
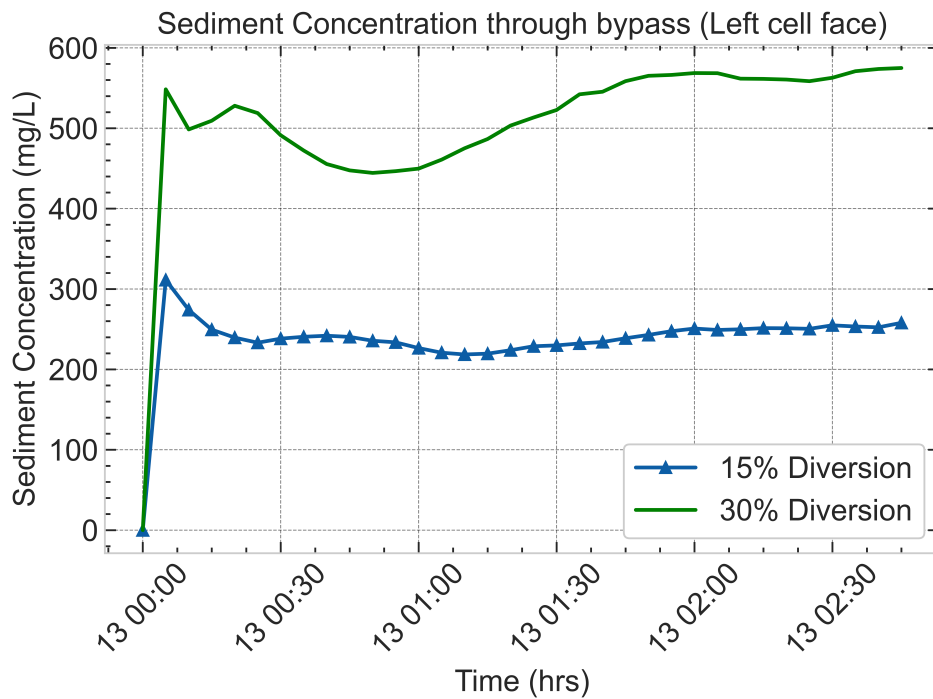
Figure 7.51: Comparison of sediment concentration through bypass for 15% and 30% diversion (Left Cell)

Figure 7.50 and Figure 7.51 shows the sediment concentration passing through right and left cells respectively. Comparison was done for 0 hours to 2:45 hours for both the cases. It can be seen that the concentration increases with the increase in flow through the channel. When flow increases from 15% to 30%, the concentration increases from around 200mg/L to around 500 to 600 mg/L. From this result, it seems evident that the sediment concentration is proportional to the flow through channel.

8   Discussion

The study shows some interesting results that has to be discussed for clarification. Discussion of the results obtained in this study has been done in this section. It has been divided into various sub sections for clarity.

8.1   Hydraulic Simulation in the Channel

Hydraulic simulation was done for the discharge of 35 l/s through the main channel. Water levels at eight different locations were measured continuously for the total test period. These values were used for the calibration of hydraulic flow in the model. The calibrated hydraulic model resulted in the R^2 value of 0.90 which is a good fit. The agreement between observed and simulated model was found to be good. Among all the manning's number used for calibration, the value of 0.01 gave the best result for simulation.

Both simulated and observed water levels at the downstream boundary was same because the model was able to simulate the level defined by boundary condition. According to Olsen (2007), it is a good practice in a numerical model to use cells aligned with the direction of flow to avoid any unwanted diffusion. It is true in the case of HEC-RAS 2D too. When the cells were aligned with direction of flow in every sections, the results changed drastically. The model was more stable and simulated values were closer to the observed ones. Surprisingly, the simulation was very good when a larger grid cell size was used which is not always the case. But as defined by Brunner (2022a), HEC-RAS uses sub-grid bathymetry as described in 3.2 which allowed this model to run properly with the larger grid cell size with good agreement between the observed and simulated values. This concept justifies the good results obtained with coarser mesh in this study. However, as mentioned by J.Tu and C.Liu (2007), using very coarse grid or very fine grid can both lead to a poor result. Eventhough, the results were good with larger grid cells, when the cell size was changed, changes in the simulated water level was observed which is not considered a reliable result. So a grid independence test has been carried out to find the optimal size. It has been presented in Figure 6.5.

The difference between observed and simulated water surface elevation is high at the beginning shown by sensor number 1. Water level is underestimated by the sensor at this point. The reason for this could be due to the boundary condition being near to the sensor. In the physical model, inflow point to the channel was way upstream compared to that in numerical model. This difference in the point of introduction of flow in physical and numerical models might have caused some deviations in the results. Also, this is the hydraulic calibration and the model was run without sediment transport. However, the physical model was run along with sediment. The transport of sediment during the observation could have changed the observed water level to some extent. Some differences could also have been observed due to the values taken for comparison. Water level sensors were used for observation which captures five values per second. And these average values may fail to represent the correct physical model in simulated one as a fixed average value of water surface elevation has been

used for calibration.

8.2   Hydraulic Simulation in the Bypass

First of all, based on the results obtained in this study from simulation in gated model, it can be said that HEC-RAS 2D is capable of simulating flows with hydraulic structures (weir and gate) properly. There is a very good agreement between observed and simulated water levels in the model. This model can be further improved with the use of optimized coefficients and parameters for gated structures. However, due to the limitation of software, it could not run models with integrated gate and sediment transport. So, the study was done without using gates in bypass i.e. as an open channel. Hence, some deviations were observed in the simulations.

One obvious difference that was observed between physical and numerical model without gate was accumulation of water right in front of the bypass intake. Figures 7.27 and 7.28 shows the drop in water level near intake specially at sensor numbers 4 and 6 which lie right in front of it. It may be due to the free water flow in simulation. Also, the inflow of water in bypass in the physical model is sub-surface. However, it is open channel in the simulation. This could have resulted in uncertainties in both hydraulic and sediment simulated model. Figure 7.30 shows the difference in level of water in bypass channel. It exists due to the location of intake in gated structure. This difference plays a vital role in sediment transport.

8.3   Selection of Transport Function

Selection of transport function was one of the most important and difficult tasks in this study. During the initial testing and verification stages, simulation results show MPM as a good transport function for the model used. Kuriqi et al. (2020) shows that MPM can be used as transport function in flume experiments for bed load transport under varied hydraulic conditions. But, the sediment grain size in their experiments was around 3.5mm which is much larger than the one used in this thesis. In a study made by Damte et al. (2021), Ackers and White transport function shows the most accurate estimate of total load transport with similar gradation of bed materials. Table 3.1 shows that Meyer - Peter Muller can be used for the sediments with particle diameter between 0.4 and 29mm. However, the particle diameter analysed in this thesis ranges from 0.01mm to 0.75mm which is lower as compared to MPM. Looking at the same table, it can be seen that the width of channel for which MPM was used is around 0.5 to 6.6 ft (around 0.1 to 2m). The width of our prototype ranges from 1 to 2 m. Some indicators show that MPM can be used while others show that it could be questionable.

To tackle this problem, more simulations were done using four suitable transport functions as shown in Section 7.1. The bed surface elevations obtained from simulations were compared against the ones obtained from physical model. The visual comparison done in Figure 7.7 presents MPM and Van Rijn as the possible transport functions. Sometimes, the visual comparison could be misleading because of the scales used and the perspective of the observer. So, statistical analysis was done comparing the bed surface elevations at different cross sec-

tions. This result showed MPM as the best function representing the prototype model. At the same time, Van Rijn results were also close to that of MPM and observed results. So, an additional comparison was made between the bed change maps obtained from only these two functions. The comparison of bed change maps show that MPM represents the observed changes better than Van Rijn. With this, final selection of the transport function was made and MPM was used for all other simulations.

8.4   Sediment Transport Simulation

The sediment transport modelling can be divided into various parts. Comparison and validation of sediment transport results have been done with bed elevation maps and cross sections, bed change maps and sediment transport concentration. One common pattern that can be seen in all the bed change results in Chapter 7 is the area represented by zone A. Independent of the flow through bypass and presence of guide walls, there is deposition in this zone. However, in all the bed change results obtained from physical model, there is erosion or very less and partial deposition in this section. This difference could mainly be because of the presence of upstream boundary condition near this bend. This could be the boundary effect caused because of boundary being near to the zone in numerical model. In the physical model, the actual point of inflow lies far away from profile 1. Another reason for this could be the velocity of flow in this area. Looking at the velocity pattern in simulations, it can be observed that the highest velocity exists at the same points in all time steps. Erosion in the simulated model seems to take place at the same areas as the highest velocity. Another pattern that can be observed in the sediment model is the change of flow pattern. In the physical model, change in flow pattern in a particular area is observed when there is erosion or deposition. If there is deposition in a certain region, this accumulation of sediment in the bed directs the flow to the outer bend causing change in the flow path of water as observed in physical model. However, in the numerical model, this pattern is not properly observed. Same trend in flow and its path is seen from the start to end of simulation time period which might have resulted in similar pattern in bed changes.

Some similarities can also be observed in all the results when simulations are done with bypass channel diverting water from the main channel. The major similarity can be seen in the level of water in bypass channel. This is mainly due to the use of open channel bypass section in simulations as opposed to the gated structures in physical model. Figure 7.30 shows how the level of water is in the bypass. Williams (1970) shows that the water depth can play a significant role in sediment transport. With the decrease in water depth, there is an increase in transport of sediment due to increase in velocity of flow. In contrary, increase in water level can greatly reduce the sediment transport. The water level cannot be reduced because gated structures do not work with sediment models in HEC-RAS 2D yet. This could be a reason for the observed bed change patterns in all the results in Chapter 7. In all the results with sediment bypass channel, deposition of sediment can be observed in the area near to bypass inlet. This effect can be seen in Figures 7.33, 7.40, 7.48. The reason for this could be inefficient sediment transport from the channel due to increase in height and

reduction in flow velocity. Another reason for some deposition at the inlet section could be the modification of terrain in that area. As can be seen in Figure 7.24 (a), there is slight modification at the inlet section of sediment bypass channel which allows transition of terrain from the high elevation to bed level of bypass. This was done to make the model more stable and to guide water through bypass. Because of this modification and high water depth at the inlet, most of the sediment seems to have deposited in this depression and has been reflected in the bed change layer.

In the simulated model with guide walls and 15% diversion, zone D in Figures 7.40 seems to have obvious deposition because the velocity of water is low around that zone. The flow is hindered by guide walls at zone D which lowers the velocity and increases deposition. However, in the case of physical model, there seems to have erosion. The simulated model in this case might not have been capable to replicate the dynamics of flow and did some simple flow calculation. It might be possible to do it changing some settings or maybe it is not capable of replicating it. This property has to be studied further in HEC-RAS 2D as well as in other available 2D softwares. Actually, HEC-RAS uses various settings and parameters. Some of the parameters were determined while some default parameters were also used. The default parameters might have been setup for a large model. This could have resulted in some deviations in simulated model.

While comparing the sediment concentration through bypass channel between cases explained in section 7.2 (without guide walls) and section 7.3 (with guide walls) in Figure 7.41, it can be seen that the transport of sediment increases in the simulation with guide walls. The presence of guide walls resulted in increased diversion of sediment through the bypass channel. This was the same pattern observed in the physical model. The diversion seems higher in the initial time steps which reduces gradually as the time passes. When the simulation starts, the flow might have been diverted towards the bypass inlet along with the sediment resulting in increased concentration through it. Figure 7.42 shows effectiveness of guide walls for sediment diversion because the water level in bypass section with and without guidewalls is the same. It shows that the water depth in bypass section has less effect on the increase in sediment concentration. The increase in the concentration is solely because of the flow dynamics introduced by the guide walls. Hence, it is possible to model the cases with guide walls in HEC-RAS as a 2D software.

Evaluating the comparison between the model with 15% diversion through bypass without guide walls and 30% diversion without guide walls shown in Figure 7.50 and Figure 7.51, significant difference in concentration can be observed. Increasing the flow from 15% (5 l/s) to 30% (10 l/s), the sediment concentration increased by almost two times. Increase in discharge is not the only factor that increased the sediment concentration through bypass. Figure 7.45 shows that when discharge through bypass is doubled, the water depth through the section goes down. Again, according to Williams (1970), sediment transport should increase with decrease in depth. And this results confirms with the general pattern observed.

8.5   Limitations of HEC-RAS 2D 6.2

Latest version (6.2) of HEC-RAS 2D has been used for all the simulations in this study. During the time of this study, this version of HEC-RAS is relatively new. Most of the planned features might not have been implemented yet. One of the problems faced during the thesis was simulation using gated structure. The hydraulics was simulated well using gates. The comparison results between observed and simulated water level elevation was good. But when simulation was done with a gate in bypass inlet, the software crashed. A lot of time was invested on how to introduce the bypass channel using terrain modification and on installation of gate and weir in the channel. Lots of trials were made to make the gate work with sediments. With some alternative checks like installation of weir in the main channel, it was found out that this version of the software does not support simulation with sediment and structures together. It was the main difficulty faced during this study. Many alternatives were tried before a suitable open channel inlet size was determined as shown in Chapter 7.

Another unsuccessful attempt made with the software was the use of internal boundary. It is possible to define an internal boundary in HEC-RAS 2D defined inside the 2D flow area. This method was tried in this study. The initial idea of using this feature was to define stage hydrograph as internal bounday at the start of the bypass section. Defining the stage to the same elevation as provided by the gate would ensure proper imitation of gate effect in the numerical model.
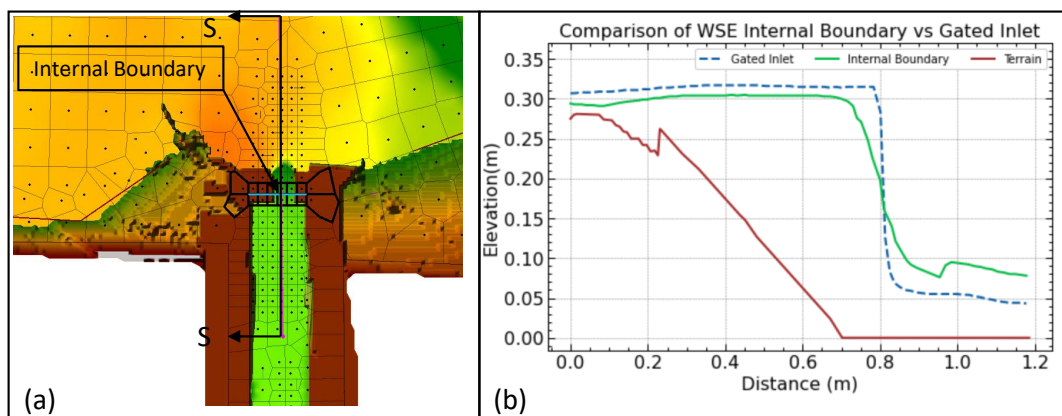
Figure 8.1: Comparison of WSE with Internal Boundary and Gated Structure in Bypass: (a). Plan view (b) Section view

Figure 8.1 (a) shows the plan view of WSE when internal boundary is used in the model. It is represented by the blue line in the figure. Figure 8.1 (b) shows that when internal boundary is used in the model, it is possible to force the water level to the elevation almost same as in the gated structure. This could have been the best approach for the study. Unfortunately, when the internal boundary was used with sediment transport, the model crashed. Like with the gated structure, HEC-RAS 2D was not able to run the sediment transport model with internal boundary.

91

8.6   Recommendation for Future Studies

Some uncertainties still exist in the study that has to be assessed properly. Due to the limitation in time of research, some of the possible tasks could not be performed. This section provides some recommendations for future work and studies.

- First of all, any uncertainties in the model has to be accessed properly for better accuracy and representation of the numerical model. This can be done with the sensitivity analysis. Some of the parameters like time step, grid size, theta value and manning's number were changed and the results were compared with observed ones. There are many other parameters like number of iterations, transport coefficients, ramp up time, etc that can be checked for sensitivity and better outcome in simulation.

- With the updates in HEC-RAS software in the future, the sediment transport model set up in the study shall be simulated with gated structure and compared with the results obtained in this research and also with the results obtained from physical model. The accuracy of the alternative method adopted in this model shall be evaluated.

- A three dimensional model shall be set up for the same physical model used in this study. The computation time and amount of details obtained from it shall be compared with the results obtained here. The hydraulics and pattern of bed changes shall also be compared. Based on the similarity of results and level of details required by users, applicability of two models can be evaluated. Advantages of a 2D models shall be highlighted based on the comparison.

- The terrain and bed elevation in HEC-RAS seems to be updated with time step. However, it is not clear if the updated bed change is used in the computation in every time step. This has to be confirmed. If it is not the case, the total simulation time can be divided into a number of time steps and model could be run in small intervals. The bed elevation obtained from one time step can be used as an input terrain in the other time step to see the change in results. This is recommended because in a real physical model, the flow changes with the change in bed elevations.

- One difficulty faced in this study is repetitive set up of model for calibration and simulation which takes a lot of time. This can be automated using a tool such as Python. Automation of HEC-RAS can save time as well as make simulation efficient.

9 Conclusion

The research aimed to demonstrate the hydraulic and sediment transport capability of HEC-RAS 2D in a river channel and its bend. Based on the simulation and the qualitative and quantitative analysis done in the study to meet the objectives, it can be concluded that the current version of HEC-RAS 6.2 is capable of simulating the river channel flow hydraulically and also the two dimensional sediment transport in some cases. The results indicate that a 2D numerical model like HEC-RAS can be used to get a fair estimate and visual representation of the bed change and bed load sediment transport for planning purposes. In contrast to a 3D model that requires a higher computation requirement and simulation time, the model used in this study can handle the simulation pretty well and in less computation time from around 5 hours to 30 hours depending on the level of details required by the user. Some of the numerical model results have been verified successfully using the existing physical model results. The study also shows how a good two dimensional model can be set up and how different features in the software can be combined to set up the required simulation environment.

The study presents a two dimensional numerical simulation of bed load transport of a physical model. The simulation has been performed for different cases : without bypass channel, with bypass channel and a gated structure, with modified bypass inlet and with guide walls and bypass. The hydraulic simulation carried out in these model satisfies reasonably with the observed water surface elevation at eight control points set up in the physical model. The model was considered to be good because the observed and simulated hydraulic results show good correlation with each other.

Similarly, bed load transport simulation in the numerical model satisfies well with the physical model when no external structures are used in the model. The result shows similar erosion and deposition pattern in both the observed and simulated models. Limitation in the current version of the software seems to be the main reason for some deviations in simulated results for models with bypass channel. With a proper functioning gated structure in the bypass channel, these differences in the observed results could be reduced to a great extent. As the model was run with certain discharge through the bypass in physical model, a workaround method has been adopted in this study using some existing features in HEC-RAS. The results obtained from this alternative confirms well with the hydraulic results. There are some differences in the simulated result. But it can be observed with the increase in discharge through the bypass and with the installation of guide walls, the sediment inflow to the bypass channel increases too. This shows that the model can perform very well with some improvements or with the release of updated versions.

The model has to be studied further to see if any further improvements can be made. Proper use of this 2D model can save a lot of time, money and resources. The models verified in this study can be used further to make any changes before it can be made in the physical model to save time and effort.

10   References

Alejandro Sanchez, S. G. (2020). *HEC-RAS Two-Dimensional Sediment Transport User's Manual*. Hydrologic Engineering Center (CEIWR-HEC).

Ammar, R., Kazpard, V., Wazne, M., El Samrani, A. G., Amacha, N., Saad, Z., and Chou, L. (2015). Reservoir sediments: a sink or source of chemicals at the surface water-groundwater interface. *Environmental monitoring and assessment*, 187(9):1–20.

Annandale, G. W. (2016). Extending the life of reservoirs : sustainable sediment management for dams and run-of-river hydropower.

Auel, C. and Boes, R. M. (2011). Sediment bypass tunnel design–hydraulic model tests. *Proc. Hydro*.

Bhandari, M., Nyaupane, N., Mote, S. R., Kalra, A., and Ahmad, S. (2017). 2d unsteady flow routing and flood inundation mapping for lower region of brazos river watershed. In *World Environmental and Water Resources Congress 2017*, pages 292–303.

Brown, L. R. and Wolf, E. C. (1984). Soil Erosion: Quiet Crisis in the World Economy. Worldwatch Paper 60.

Brunner, G., Savant, G., and Heath, R. (2020). Modeler Application Guidance for Steady versus Unsteady, and 1D versus 2D versus 3D Hydraulic Modeling. *US Army Corps of Engineers. Retrieved from https://www. hec. usace. army. mil/publications/TrainingDocuments/TD-41. pdf.*

Brunner, G. W. (2022a). *HEC-RAS 2D User's Manual*. US Army Corps of Engineers.

Brunner, G. W. (2022b). *HEC-RAS Hydraulic Reference Manual*. US Army Corps of Engineers.

Brunner, G. W. and Gibson, S. (2005). Sediment transport modeling in hec ras. In *Impacts of Global Climate Change*, pages 1–12.

Chang, H. (1998). Generalized computer program: Users' manual for FLUVIAL-12: Mathematical model for erodible channels. *San Diego*.

Chang, H. H. (1984). Modeling of river channel changes. *Journal of Hydraulic Engineering*, 110(2):157–172.

Chanson, H. (2004). *Hydraulics of open channel flow*. Elsevier.

Chaudhary, H. P., Isaac, N., Tayade, S. B., and Bhosekar, V. V. (2019). Integrated 1D and 2D numerical model simulations for flushing of sediment from reservoirs. *ISH Journal of Hydraulic Engineering*, 25(1):19–27.

Chien, N. (1954). Meyer-peter formula for bed-load transport and einstein bed-load function. mrd sediment ser., 7, 32 pp. *Univ. of Calif.-Berkeley, and The Missouri River Division, US Army Corps of Eng., Berkeley, Calif.*

Damte, F., G_Mariam, B., Ayana, M. T., Lohani, T. K., Dhiman, G., and Shabaz, M. (2021). Computing the sediment and ensuing its erosive activities using hec-ras to surmise the flooding in kulfo river in southern ethiopia. *World Journal of Engineering*.

Day, T. (1980). A study of the transport of graded sediments, rep. *IT190*, 10.

Ghimire, S., Singh, U., and Bhattarai, P. (2021). Generation of a Suspended Sediment Rating Curve of a Himalayan River based on a Long-term Data: A case study of Kabeli River. *Proceedings of 10th IOE Graduate Conference*, page 1110 1118.

Gibson, S., Sánchez, A., Piper, S., and Brunner, G. (2017). New one-dimensional sediment features in hec-ras 5.0 and 5.1. In *World Environmental and Water Resources Congress 2017*, pages 192–206.

Hamrick, J. M. (1992). A Three-Dimensional Environmental Fluid Dynamics Computer Code: Theoretical and Computational Aspects.

Hassanzadeh, Y. (2012). Hydraulics of Sediment Transport. In *Hydrodynamics-Theory and Model*. IntechOpen.

Holly, F., Yang, J., Schwarz, P., Schaefer, J., Hsu, S., and Einhellig, R. (1990). Numerical Simulation of Unsteady Water and Sediment Movement in Multiply Connected Networks of Mobile-Bed Channels. *IIHR Report*, (343).

Holly Jr, F. and Rahuel, J.-L. (1990). New Numerical/Physical Framework for Mobile-Bed Modelling: Part 1: Numerical and Physical Principles. *Journal of hydraulic research*, 28(4):401–416.

Hunziker, R. P. and Jaeggi, M. N. R. (2002). Grain Sorting Processes. *Journal of Hydraulic Engineering*, 128(12):1060–1068.

Hussain, K. and Shahab, M. (2020). Sustainable Sediment Management in a Reservoir Through Flushing Using HEC-RAS model: Case Study of Thakot Hydropower Project (D-3) on the Indus River. *Water Supply*, 20(2):448–458.

Icold, C. (2021). *Mathematical Modelling of Sediment Transport and Deposition in Reservoirs-Guidelines and Case Studies/Modélisation Mathématique du Transport et des Dépôts de Sédiments dans les Réservoirs-Lignes Directrices et Études de Cas*, volume 140. CRC Press.

Jia, Y. and Wang, S. S. (1999). Numerical Model for Channel Flow and Morphological Change Studies. *Journal of Hydraulic Engineering*, 125(9):924–933.

J.Tu, G. H. Y. and C.Liu (2007). *Computional Fluid Dynamic: A Practical Approach*.

Julien, P. Y. (2010). *Erosion and Sedimentation*. Cambridge university press.

Karim, M. F. and Kennedy, J. F. (1982). *IALLUVIAL: A computer-based flow-and sediment-routing model for alluvial streams and its application to the Missouri river*. Iowa Institute of Hydraulic Research, University of Iowa.

Koch, F. and Flokstra, C. (1981). Bed level computations for curved alluvial channels. xix congr. *Int. Assoc. Hydr. Res., New Delhi, India.*

Kondolf, G. M., Gao, Y., Annandale, G. W., Morris, G. L., Jiang, E., Zhang, J., Cao, Y., Carling, P., Fu, K., Guo, Q., et al. (2014). Sustainable sediment management in reservoirs and regulated rivers: Experiences from five continents. *Earth's Future*, 2(5):256–280.

Kovacs, A. and Parker, G. (1994). A new vectorial bedload formulation and its application to the time evolution of straight river channels. *Journal of fluid Mechanics*, 267:153–183.

Krishnappan, B. (1981). User's manual: Unsteady, non-uniform, mobile boundary flow model—mobed. *Hydraulic Division, National Water Research Institute, CCIW, Burlington, Ontario.*

Kuriqi, A., Kocileri, G., and Ardiclioglu, M. (2020). Potential of meyer-peter and müller approach for estimation of bed-load sediment transport under different hydraulic regimes. *Modeling Earth Systems and Environment*, 5:1–9.

Lee, M., Park, G., Park, C., and Kim, C. (2020). Improvement of Grid Independence Test for Computational Fluid Dynamics Model of Building Based on Grid Resolution. *Advances in Civil Engineering*, 2020:1–11.

Lysne, D. K., Glover, B., Støle, H., and Tesaker, E. (2003). *Hydraulic design*. Norwegian University of Science and Technology.

Meyer-Peter, E. and Müller, R. (1948). Formulas for Bed-Load Transport. In *IAHSR 2nd meeting, Stockholm, appendix 2*. IAHR.

Molinas, A. and Yang, C. T. (1986). *Computer program user's manual for GSTARS (generalized stream tube model for alluvial river simulation)*. US Department of Interior, Bureau of Reclamation, Engineering and Research . . . .

Morris, G. L. and Fan, J. (1998). *Reservoir Sedimentation Handbook*. McGraw-Hill Book Co., New York.

Nyaupane, N., Thakur, B., Kalra, A., and Ahmad, S. (2018). Evaluating future flood scenarios using CMIP5 climate projections. *Water*, 10(12):1866.

Olsen, N. R. and Skoglund, M. (1994). Three-Dimensional Numerical Modeling of Water and Sediment Flow in a Sand Trap. *Journal of hydraulic research*, 32(6):833–844.

Olsen, N. R. B. (2007). Numerical Modelling and Hydraulics. *Department of Environment and Hydraulics Engineering, the Norwegian University of Science and Technology.*

Papanicolaou, A., Bdour, A., and Wicklein, E. (2004). A numerical model for the study of sediment transport in steep mountain streams. *J. Hydraul. Res*, 42(4):357–366.

Papanicolaou, A. T. N., Elhakeem, M., Krallis, G., Prakash, S., and Edinger, J. (2008). Sediment Transport Modeling Review—current and Future Developments. *Journal of hydraulic engineering*, 134(1):1–14.

Parker, G., Seminara, G., and Solari, L. (2003). Bed load at low shields stress on arbitrarily sloping beds: Alternative entrainment formulation. *Water resources research*, 39(7).

Paudel, K. (2010). *Role of sediment in the design and management of irrigation canals : Sunsari Morang Irrigation Scheme, Nepal*. PhD thesis, Wageningen University. WU thesis 4933.

Proffitt, G. and Sutherland, A. (1983). Transport of non-uniform sediments. *Journal of Hydraulic Research*, 21(1):33–43.

Ren, M.-E. and Shi, Y.-L. (1986). Sediment discharge of the yellow river (china) and its effect on the sedimentation of the bohai and the yellow sea. *Continental Shelf Research*, 6(6):785–810.

Roache, P. J. (1997). Quantification of Uncertainty in Computational Fluid Dynamics. *Annual Review of Fluid Mechanics*, 29(1):123–160.

Shelley, J., Gibson, S., and Williams, A. (2015). Unsteady flow and sediment modeling in a large reservoir using hec-ras 5.0. In *Federal Interagency Sediment Conference*.

Shields, A. (1936). Anwendung der aehnlichkeitsmechanik und der turbulenzforschung auf die geschiebebewegung. *PhD Thesis Technical University Berlin*.

Song, S., Schmalz, B., and Fohrer, N. (2015). Simulation, quantification and comparison of in-channel and floodplain sediment processes in a lowland area – A case study of the Upper Stör catchment in northern Germany. *Ecological Indicators*, 57:118–127.

Song, Y. and Haidvogel, D. (1994). A semi-implicit ocean circulation model using a generalized topography-following coordinate system. *Journal of Computational Physics*, 115(1):228–244.

Spasojevic, M. and Holly, F. (1994). Three-dimensional numerical simulation of mobile-bed hydrodynamics. contract rep. Technical report, HL-94-2, US Army Engineer Waterways Experiment Station, Vicksburg, Miss.

Spasojevic, M. and Holly, F. M. (1990). *MOBED2: Numerical simulation of two-dimensional mobile-bed processes*. Number 344. Iowa Institute of Hydraulic Research, The University of Iowa.

Thakur, B., Parajuli, R., Kalra, A., Ahmad, S., and Gupta, R. (2017). Coupling hec-ras and hec-hms in precipitation runoff modelling and evaluating flood plain inundation map. In *World Environmental and Water Resources Congress 2017*, pages 240–251.

Thapa, B. S., Dahlhaug, O. G., and Thapa, B. (2015). Sediment erosion in hydro turbines and its effect on the flow around guide vanes of Francis turbine. *Renewable and Sustainable Energy Reviews*, 49:1100–1113.

Thomas, W. A. and Prasuhn, A. L. (1977). Mathematical modeling of scour and deposition. *Journal of the Hydraulics Division*, 103(8):851–863.

Tigrek, S. and Aras, T. (2011). *Reservoir sediment management*. CRC Press.

Van Rijn, L. C. (1984). Sediment transport: bed load transport. *Journal of Hydraulic Engineering - ASCE*, 110(10):1431–1456.

Van Rijn, L. C. and Tan, G. (1985). Sutrench-model: two-dimensional vertical mathematical model for sedimentation in dredged channels and trenches by currents and waves. *Rijkswaterstaat communications*.

Van Rijn, L. C., Walstra, D.-J. R., and Van Ormondt, M. (2007). Unified View of Sediment Transport by Currents and Waves. IV: Application of Morphodynamic Model. *Journal of Hydraulic Engineering*, 133(7):776–793.

Vincenzo Casulli (2008). A high-resolution wetting and drying algorithm for free-surface hydrodynamics Vincenzo. *International Journal for Numerical Methods in Fluids*, 60(August 2008).

Wallingford, H. (1990). Sediment Transport- the Ackers and White theory updated (SR 237).

Wang, H.-W., Kondolf, M., Tullos, D., and Kuo, W.-C. (2018). Sediment management in taiwan's reservoirs and barriers to implementation. *Water*, 10(8).

Wilcock, P. R. and Crowe, J. C. (2003). Surface-based transport model for mixed-size sediment. *Journal of hydraulic engineering*, 129(2):120–128.

Williams, G. P. (1970). *Flume Width and Water Depth Effects in Sediment-Transport Experiments*. US Government Printing Office.

Wong, M. and Parker, G. (2006). Reanalysis and Correction of Bed-Load Relation of Meyer-Peter and Müller Using Their Own Database. *Journal of Hydraulic Engineering*, 132(11):1159–1168.

Woodward, J. and Foster, I. A. N. (1997). controls , processes and problems Linked references are available on JSTOR for this article : Transfer in River Catchments :. *Geographical association*, 82(4):353–376.

Wu, W. (2007). *Computational river dynamics*. Crc Press.

Yang, C. T. (1973). Incipient motion and sediment transport. *Journal of the hydraulics division*, 99(10):1679–1704.

Yang, C. T. and Stall, J. B. (1974). Unit Stream Power for Sediment Transport in Natural Rivers. *Ill Univ Water Resour Cent Res Rep*, (88).

NTNU

M.Sc. THESIS IN HYDRAULIC ENGINEERING

Candidate: **Mr. Rajeev Shrestha**

Title: **2D numerical modeling of sediment diversion in a river bend**

1. Background

Hydropower is one of the major renewable sources of energy. It is considered as the green battery which can be utilized without over exploiting the nonrenewable components of environment. However, there are many problems that require proper planning and attention for efficient operation of hydropower plants (HPP). One of such problems is sedimentation. Sediments carried by river channels pose problems to both run of river as well as storage type hydropower schemes. Excess sediments result in instability of channel, reduction in flood capacity due to infilling, channel aggradation, bank erosion, reduction in power generation from HPP etc. If sediment can be bypassed before it reaches the reservoir or the intake, it can greatly reduce many technical and economic problems. One solution to this problem could be installation of sediment bypass tunnel in a channel bend.

A laboratory experiment has been conducted at NTNU to check the efficiency of a sediment bypass tunnel in a river bend. Flushing operations can be very expensive, and it is therefore important to know the efficiency beforehand. Hence, the physical model has been operated at different discharges with varying flow passing through the sediment bypass tunnel. Operation and modification of a physical model can be expensive and time consuming. Similar modifications can be done in a numerical model before a permanent change is made to the prototype.

This thesis will contribute to a better understanding of how the 2D numerical modelling of sediment transport can be done for a river channel and its bends. Calibration and validation shall be done using data obtained from the physical model. HEC-RAS has been selected as the 2D modelling software because it is free for all and has a good user base. New 2D sediment transport feature in HEC-RAS makes it more attractive to the hydraulic engineers. Proper use of this feature can result in saving lots of time, effort, and money.

2. Work description

The thesis shall cover, though not necessarily be limited to the main tasks listed below.
The candidate must collect available documents such as reports, relevant studies and maps.
Based on the available documentation the following shall be carried out:

1. Literature review on sediment diversion from channels.
2. Literature review of 2D sediment transport.
3. Literature review on HEC-RAS 2D
4. Short description of the experiments and the data available.
5. Setting up the grid for the study case in a HEC-RAS 2D model.
6. Exploit useful features in HEC-RAS 2D for required modifications.
7. Run the numerical model and compare it with the data obtained from physical model.
8. Documentation of the numerical results compared to the experiments.
9. Conclusions

10 Proposals for future work.
11 Presentation.

The literature review should outline the previous contributions on the topics mentioned in 1. and 2.

3 Supervision

Professor Nils Rüther will be the main supervisor. PhD candidate Diwash L. Maskey will be co-supervisors. The supervisors shall assist the candidate and make relevant information available.

Discussion with and input from other research or engineering staff at NTNU or other institutions are recommended. Significant inputs from others shall be referenced in a convenient manner.

The research and engineering work carried out by the candidate in connection with this thesis shall remain within an educational context. The candidate and the supervisors are free to introduce assumptions and limitations which may be considered unrealistic or inappropriate in a contract research or a professional/commercial context.
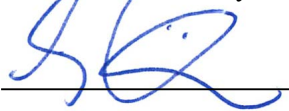
4 Report format and submission

The report should be written with a text editing software. Figures, tables and photos shall be of high quality. The report format shall be in the style of scientific reports and must contain a summary, a table of content, and a list of references.

The report shall be submitted electronically in B5-format .pdf-file in Blackboard, and three paper copies should be handed in to the institute. Supplementary working files such as spreadsheets, numerical models, program scripts, figures and pictures shall be uploaded to MS Teams. The summary shall not exceed 450 words. The Master's thesis should be submitted within 24th of June 2022.

The candidate shall present the work at a MSc. seminar towards the end of the master period. The presentation shall be given with the use of powerpoint or similar presentation tools. The data and format for the MSc. seminar will be announced during the semester.

Trondheim, 10. January 2022

Nils Rüther
Professor
Department of Civil and Environmental Engineering
NTNU

A Appendix

This section some of the data, figures and calculation tables used in this study. As the master's thesis was done with data being used in a PhD study, all the data could not be presented in the annex section.

A.1 Input Data for Simulation

A.1.1 Terrain Files for Comparison

Figure A.1 shows the scanned files from physical model that were used for comparison of simulated results from numerical model.
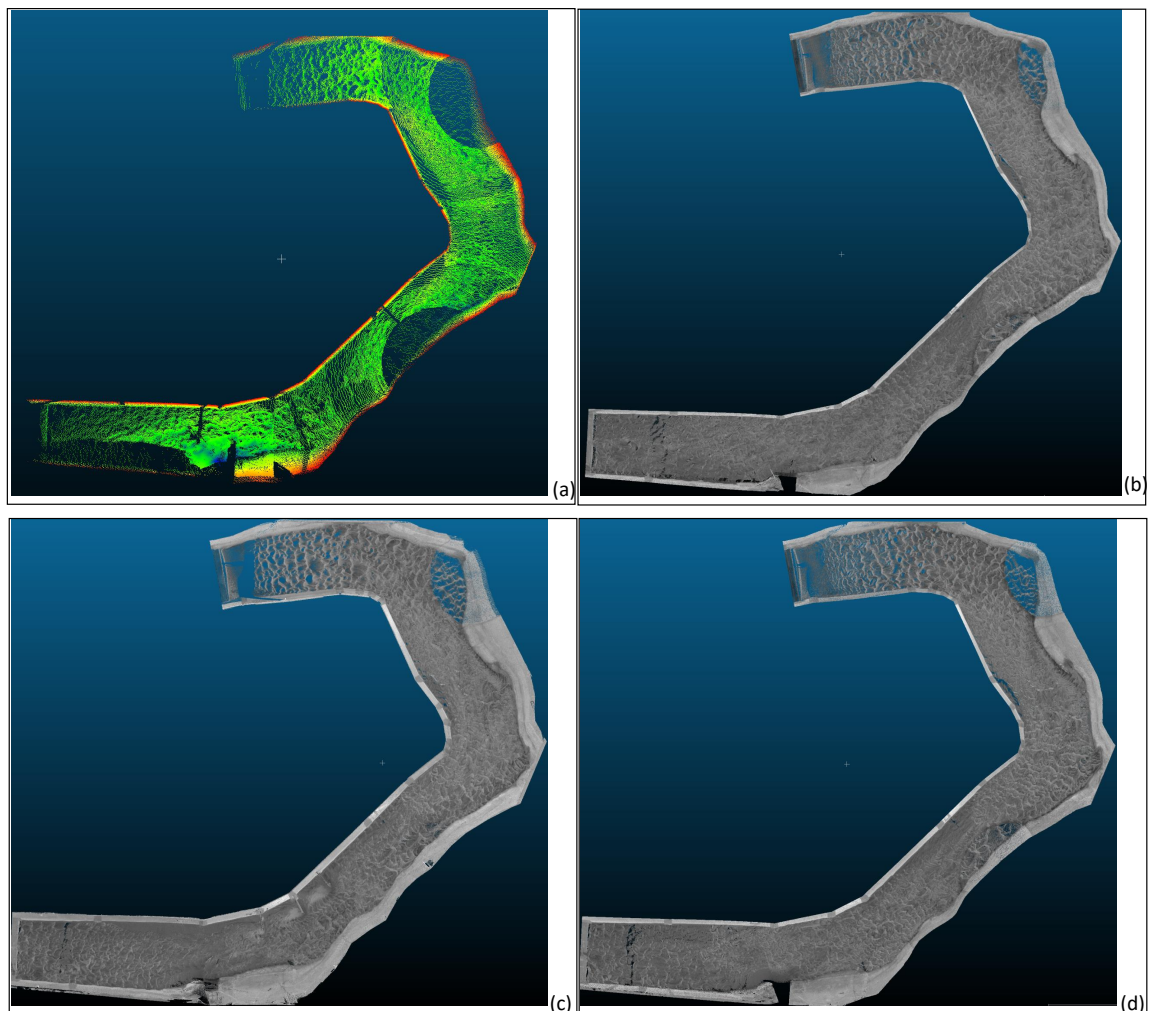
Figure A.1: Observed terrain data after sediment transport test in lab (a). Terrain file for the main channel (b). Terrain file for 15% diversion through bypass (c). Terrain file for guide walls and 15% diversion through bypass (d). Terrain file for 30% diversion

A.2 Hydraulic Calibration

A.2.1 Grid Optimization Test

The Table A.1 shows water surface elevation at eight control points on different grid sizes.

Table A.1: Results from grid optimization test

Sensor Numbers	Observed	Grid 0.05	Grid 0.075	Grid 0.1	Grid 0.15	Grid 0.2
1	0.359	0.360	0.357	0.356	0.356	0.357
2	0.331	0.340	0.338	0.339	0.336	0.335
3	0.335	0.340	0.339	0.339	0.337	0.337
4	0.326	0.339	0.337	0.337	0.334	0.332
5	0.321	0.330	0.330	0.330	0.328	0.326
6	0.316	0.320	0.319	0.319	0.317	0.315
7	0.315	0.311	0.310	0.310	0.311	0.311
8	0.308	0.310	0.309	0.309	0.309	0.308

A.2.2 Grid independence test

Table A.2 shows the calculation done to check the indepencence of results from grid.

Table A.2: Grid Independence Test

Sensor Numbers	0.05 - 0.075	0.075-0.1	0.1-0.15	0.15-0.2
1	-0.003	-0.001	0.000	0.001
2	-0.002	0.001	-0.002	-0.001
3	-0.001	0.000	-0.002	-0.001
4	-0.002	0.000	-0.003	-0.002
5	0.001	0.000	-0.002	-0.002
6	-0.001	0.000	-0.002	-0.002
7	-0.001	0.000	0.000	0.000
8	-0.001	-0.001	0.000	0.000

Table A.3 shows the absolute difference of the simulated results compared to the observed values.

Table A.3: Absolute difference from the observed values

Sensor Numbers	Grid size			
	0.050	0.075	0.1	0.15
1	0.000	0.002	0.003	0.003
2	0.009	0.007	0.008	0.006
3	0.005	0.004	0.004	0.002
4	0.013	0.011	0.011	0.008
5	0.008	0.009	0.008	0.006
6	0.004	0.003	0.003	0.001
7	0.004	0.005	0.004	0.004
8	0.002	0.001	0.001	0.001
	0.045	0.042	0.043	0.031

A.2.3   Hydraulic Calibration using manning's n

Tables A.4 and A.5 shows the water surface elevations obtained for different manning number with the gird size of 0.1m for terrain before and after sediment transport tests respectively.

Table A.4: Hydraulic optimization using manning n for terrain before sediment transport

| Observed WSE	Manning's n with grid size of 0.1m					
	0.01	0.009	0.008	0.007	0.006	0.005
0.359	0.356	0.354	0.355	0.356	0.358	0.361
0.331	0.339	0.337	0.337	0.335	0.334	0.334
0.335	0.339	0.338	0.337	0.336	0.335	0.333
0.326	0.337	0.336	0.336	0.336	0.335	0.335
0.321	0.330	0.328	0.329	0.328	0.328	0.327
0.316	0.319	0.318	0.318	0.317	0.317	0.317
0.315	0.310	0.309	0.308	0.307	0.306	0.305
0.308	0.309	0.309	0.309	0.309	0.308	0.308

Table A.5: Hydraulic optimization using manning n for terrain after sediment transport

Sensor Numbers	Manning's n with grid size of 0.1m			
	0.02	0.01	0.009	0.008
1	0.365	0.351	0.3496	0.3485
2	0.3488	0.335	0.335	0.33
3	0.349	0.335	0.335	0.335
4	0.34	0.33	0.33	0.33
5	0.335	0.325	0.325	0.325
6	0.335	0.325	0.325	0.325
7	0.33	0.3205	0.3205	0.3205
8	0.308	0.3075	0.307	0.3065

A.3   Sediment Transport Modelling

A.3.1   Bed Gradation

Figure A.2 shows the gradation of bed material used as erodible bed in all the simulations.
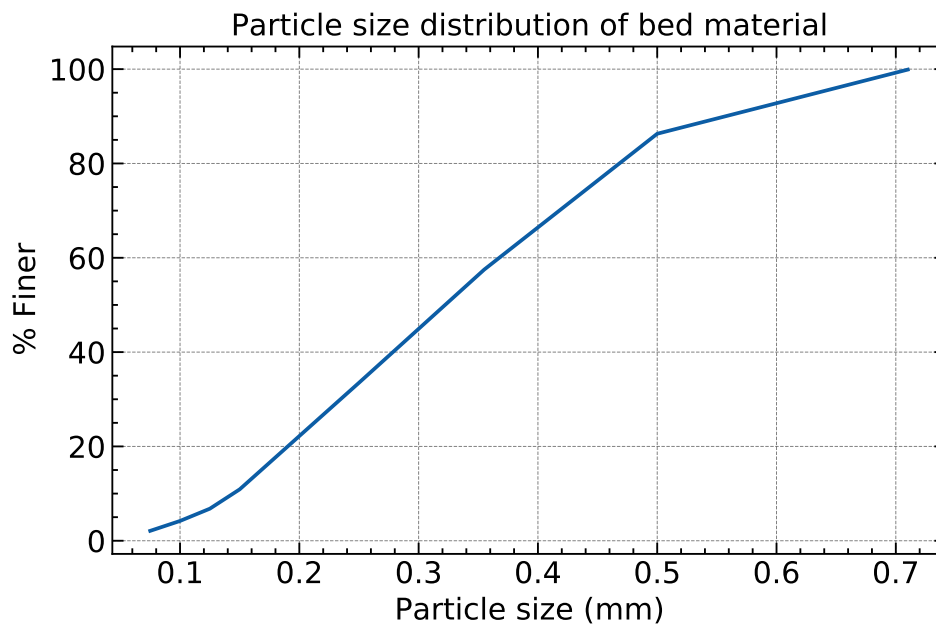
Figure A.2: Particle size distribution of bed material

A.3.2 Hydraulic Simulation for model with 15% diversion

Table A.6 shows the values of water surface elevations at different sensors obtained from physical and simulated models for the model with 15% diversion.

Table A.6: Hydraulic simulation and comparison of water levels between observed and simulated models (15% diversion through bypass)

Sn	Observed (m)	Simulated (m)
1	0.361	0.35
2	0.321	0.321
3	0.325	0.319
4	0.321	0.309
5	0.313	0.306
6	0.32	0.308
7	0.315	0.306
8	0.301	0.301

A.3.3   Hydraulic Simulation for model with 15% diversion and guide walls

Table A.7 shows the values of water surface elevations at different sensors obtained from physical and simulated models for the model with 15% diversion and guide walls.

Table A.7: Water surface elevation: observed vs simulated (15% Bypass through SBT) with guide walls

Sensor Number	Observed	Simulated
1	0.361	0.351
2	0.321	0.324
3	0.325	0.325
4	0.321	0.313
5	0.313	0.305
6	0.32	0.307
7	0.315	0.305
8	0.301	0.301

A.3.4   Hydraulic Simulation for model with 30% diversion

Table A.8 shows the values of water surface elevations at different sensors obtained from physical and simulated models for the model with 30% diversion.

Table A.8: Hydraulic simulation and comparison of water levels between observed and simulated models (30% diversion through bypass)

Sn	Observed (m)	Simulated (m)
1	0.357	0.353
2	0.32	0.32
3	0.32	0.32
4	0.315	0.306
5	0.309	0.307
6	0.315	0.307
7	0.31	0.3
8	0.295	0.295